

Brunel University London
Department of Civil and Environmental Engineering

Behaviour and design of cold-formed
stainless steel hollow section structural
components in fire

By

Asif Mohammed

Submitted in part fulfilment of the requirements for the degree of Doctor of Philosophy
in Civil and Environmental Engineering of Brunel University London, London, October
2019

Declaration of originality

I declare that this thesis behaviour and design of cold-formed stainless steel hollow section structural components in fire entirely my own work and that wherever published or unpublished work was used, it is appropriately acknowledged and referenced.

Copyright Declaration

The copyright of this thesis rests with the author, Asif Mohammed and is made available under Creative Commons Attribution Non-Commercial No Derivatives licence. Researchers are free to copy, distribute or transmit the thesis on the condition that they attribute it, that they do not use it for commercial purposes, and they do not alter, transform or build upon it. For any reuse or redistribution, researchers must make clear to others the license terms of this work.

Abstract

The focus of this thesis is on the behaviour and design of cold-formed stainless steel hollow section structural components in fire conditions. Currently, codified methods for fire design of stainless steel structures are based largely upon those for carbon steel structures. The main aim of this research study was to develop safe, reliable and efficient design methods for stainless steel structural elements that are in line with the observed actual response of the stainless steel structures at elevated temperatures.

An extensive numerical modelling programme was conducted to investigate the behaviour of cold-formed stainless steel columns and beam-columns in fire conditions. The finite element models were rigorously validated against existing test data provided in the literature. The validated models were subsequently utilised to perform a series of parametric studies that allowed the evaluation of key parameters on the structural response of columns and beam-columns at elevated temperatures to be carried out.

It is demonstrated that, due to the existing differences in the material behaviour between carbon steel and stainless steel, it is not possible to utilise the same design formulae for the member stability calculations, as proposed in the existing codified design methods. Furthermore, the results indicate that the existing design formulae to predict the resistance of column and beam-column members are not on the safe side in fire conditions, and improvements and amendments are necessary.

Based on the comparisons between the resistance predictions from the numerical data and the codified design methods for cold-formed stainless steel tubular columns and beam-columns, new modified design rules have been proposed in this thesis. For columns, this included revised flexural buckling curves for square, rectangular and circular hollow sections of austenitic, duplex and ferritic stainless steel grades. The proposed buckling curves were shown to offer significant improvements over the existing buckling curves and comply with the required reliability levels for design at fire conditions. For beam-columns, new combined loading interaction factors were proposed, which in combination with the proposed flexural buckling curves allow the determination of the member

resistance with high degree of predictive accuracy. Overall, these proposed revisions were shown to lead to a more accurate and reliable determination of resistance of stainless steel columns and beam-columns at elevated temperatures, enabling a more efficient use of the material in structural applications.

List of publications

This PhD research project has led to the list of the following journal paper and conference papers.

Journal papers:

- **Mohammed A.** and Afshan S. (2019). Numerical modelling and fire design of stainless steel hollow section columns. *Thin walled-structures*. **144**,1-13.
- **Mohammed A.** and Afshan S. (Submitted). Modelling and design of stainless steel hollow section beam-columns in fire. *Thin walled-structures*.

International conference papers:

- **Mohammed A.** and Afshan S. (2019). Numerical modelling and design of stainless steel square and rectangular hollow section columns in fire. *Proceedings of the 9th International conference on Steel and Aluminium Structures*, Bradford, United Kingdom. 3rd -5th July 2019.
- **Mohammed A.** and Afshan S. (2019). Behaviour and design of stainless steel tubular beam-columns members in fire. *Proceedings of the 3rd International conference on Structural Safety under Fire and Blast Loading*, London, United Kingdom. 2nd - 4th September 2019.
- **Mohammed A.** and Afshan S. (2019). Buckling of circular hollow section stainless steel columns in fire. *Proceedings of the 6th International conference on Stability and Ductility of Steel Structures*, Prague, Czech Republic. 10th -12th September 2019.

National conference papers, presentation and poster:

- **Mohammed A.** (2019). Stainless steel members in fire. Young Researchers' Conference. The Institution of Structural Engineers. IStructE Headquarters, London, UK. 13th March 2019.
- **Mohammed A.** (2019). Behaviour and design of stainless steel member in fire. Structures in Fire Forum. The Institution of Structural Engineers. IStructE Headquarters, London, UK. 9th April 2019.

- **Mohammed A.** (2019). Behaviour and design of stainless steel tubular member in fire. Civil and Environmental Research Conference. Brunel University London. 3rd May 2019.
- **Mohammed A.** (2019). Behaviour and design of stainless steel column in fire. Research student poster conference. Brunel University London. June 4-5th 2019.

Acknowledgements

The time spent on this project has been interesting, challenging, enlightening and enjoyable in almost equal measures. This has been mainly due to the support, friendship, encouragement and guidance that I have been fortunate to receive from many people whom I will endeavour to acknowledge herein.

This work was carried under the supervision of Dr Sheida Afshan, Lecturer in Structural Engineering formerly at Brunel University London and now at the University of Southampton. I am extremely grateful for her expert guidance and advice throughout the duration of the project.

I would like to acknowledge the financial support for the project provided by the Engineering and Physical Sciences Research Council (EPSRC). In addition, I would like to thank all staff members at Brunel University London who supported me when I needed, particularly Dr Katherine Ann Cashell.

Whilst at Brunel University London, I have been fortunate to have some amazing colleagues, most notably Dr Mustesin Ali Khan, Alaa Alisawi, Amy Louise Flynn, Rand Al-Janabi, Umar Amin, Musab Rabei, Keith Adams, Hongtao Zhang and Fatima Ali whose friendship and company have been proven to be invaluable. Further afield, I am grateful to my friends in elsewhere for their loyalty and support throughout my PhD, particularly Habib Ali, Uzayr Butt, Zamina Zishan, Zainab Himdan and Dr Naveed Rahman. I leave Brunel safe in knowledge that these friendships come with me.

Finally, I would like to express my sincere thanks and deepest gratitude to my parents for their continuous support and unconditional love throughout my undergraduate and postgraduate studies. I would like to thank my siblings who patiently and constantly supported me in the best possible way throughout my life.

Contents

Abstract.....	iv
List of publications	vi
Acknowledgements.....	viii
Contents	ix
List of Figures.....	xii
List of Tables	xvi
Notations.....	xviii
Chapter 1 Introduction.....	1
1.1 Background and motivation	1
1.2 Introduction to fire safety.....	4
1.3 Stainless steel in construction	5
1.4 Lifecycle costs of stainless steel	6
1.5 Research Aims and Objectives.....	8
1.5.1 Aims.....	8
1.5.2 Research Objectives.....	8
1.6 Thesis outline	9
Chapter 2 Literature review.....	11
2.1 Introduction.....	11
2.2 Stainless steel	11
2.2.1 Categories of stainless steel	12
2.2.2 Mechanical properties comparison of stainless steel and carbon steel.....	13
2.2.3 Thermal properties	18
2.2.4 Poisson ratio.....	22
2.2.5 Material modelling at elevated temperatures.....	23
2.2.6 Laboratory fire testing	27
2.2.7 Structural stainless steel design standards	29
2.2.8 Fire resistance design.....	30
2.3 Buckling of structural members	31
2.3.1 Columns	32
2.3.2 Beam	38
2.3.3 Beam-columns	40
2.4 Numerical modelling.....	42
2.4.1 Element type	43

2.4.2	Material modelling.....	43
2.4.3	Geometric imperfections.....	44
2.4.4	Residual stresses	45
2.4.5	Analysis technique solution	45
2.5	Concluding remarks	45
Chapter 3	Numerical modelling and validation of elements	47
3.1	Introduction	47
3.2	Test results from literature	48
3.2.1	Brief description of column test programmes.....	48
3.2.2	Brief description of beam-column test programmes.....	50
3.3	Development of numerical models	53
3.3.1	Element type	54
3.3.2	Mesh.....	55
3.3.3	Material modelling.....	56
3.3.4	Initial geometric imperfections	60
3.3.5	Residual stresses	62
3.3.6	Boundary conditions, constraint and loading	63
3.3.7	Heat transfer model.....	64
3.3.8	Analysis technique	67
3.4	Validation of numerical models	68
3.4.1	SHS, RHS and CHS column member validation.....	68
3.4.2	SHS, RHS and CHS beam-column member validation.....	75
3.5	Concluding remarks	85
Chapter 4	Fire design of stainless steel hollow section columns	86
4.1	Introduction	86
4.2	Parametric study	86
4.3	Fire resistance design	92
4.3.1	EN 1993-1-2 (2005).....	92
4.3.2	Lopes et al. (2010)	98
4.3.3	Design Manual for Structural Stainless Steel Design (2017)	99
4.4	Analysis of results and design guidance proposal.....	100
4.4.1	Comparison with EN 1993-1-2 and Design Manual for Structural Stainless Steel methods.....	100
4.4.2	Extension of Lopes et al. method for tubular columns	109
4.5	Reliability analysis	115
4.6	Worked example	117
4.7	Concluding remarks	119

Chapter 5	Fire design of stainless steel hollow section beam-columns	120
5.1	Introduction	120
5.2	Design rules for beam-column members in fire.....	120
5.2.1	EN 1993-1-4 - room temperature design	121
5.2.2	EN 1993-1-2 - elevated temperature design	123
5.3	Proposed design method	125
5.3.1	Combined axial load and bending moment interaction equations.....	125
5.3.2	Derivation of combined loading interaction factors	126
5.4	Comparison of predicted resistances with proposed and codified methods ..	141
5.4.1	Analysis and Discussion of results	141
5.4.2	Reliability analysis.....	148
5.5	Concluding remarks	149
Chapter 6	Conclusion and suggestion for further work.....	151
6.1	Conclusion	151
6.1.1	Numerical modelling and validation of elements	151
6.1.2	Fire design of stainless steel hollow section columns	152
6.1.3	Fire design of stainless steel hollow section beam-columns	153
6.2	Suggestion for further work.....	155
References.....		158

List of Figures

Figure 1.1: Stainless steel columns, Seven World Trade Centre, New York. (SCI, 2017)	6
Figure 1.2: Helix Bridge, Singapore (SCI, 2017)	6
Figure 2.1: Comparison of stainless steel and carbon steel stress-strain curves from 0 to 0.75% strain, DMSS (2017) and EN 1993-1-2 (2005)	14
Figure 2.2: Complete range of stainless steel and carbon steel stress-strain curves, DMSS (2017) and EN 1993-1-2 (2005)	15
Figure 2.3: Comparison of stainless steel and carbon steel stiffness retention factors... ..	19
Figure 2.4: Comparison of stainless steel and carbon steel 0.2% proof strength retention factors.....	19
Figure 2.5: Comparison of thermal expansion of stainless steel and carbon steel	20
Figure 2.6: Comparison of stainless steel and carbon steel specific heat comparison ...	21
Figure 2.7: Comparison of stainless steel and carbon steel thermal conductivity	22
Figure 2.8: EN 1993-1-2 (2005) stainless steel stress-strain relationship at elevated temperatures.....	24
Figure 2.9: Stainless steel stress-strain behaviour at elevated temperature Gardner (2010) model	27
Figure 2.10: Systematic representation of general cases of structural elements	31
Figure 2.11: Instability buckling modes of axially loaded columns.....	32
Figure 2.12: Four behaviour classes of cross-section as defined by Eurocode 3 EN 1993-1-1 (2005).	34
Figure 2.13: Von Karman's Effective Width concept for a simply supported plate	36
Figure 2.14: Structural behaviour of beams.....	39
Figure 2.15: Systematic loading and support conditions of beam-column members.....	41
Figure 3.1: Major and minor axis for a RHS	51
Figure 3.2: Mesh sensitivity SHS 120×120×5.....	55
Figure 3.3: Finer mesh to coarser mesh.....	56
Figure 3.4: Typical (a) global and (b) local buckling mode shapes for a SHS.....	61
Figure 3.5: Test vs FE axial displacement responses for SHS 80×80×3-2500 column. Test from Tondini et al. (2013).....	71
Figure 3.6: Test vs FE axial displacement responses for SHS 80×80×3-2500 column. Test from Tondini et al. (2013).....	71
Figure 3.7: Test and FE failure modes for SHS 80×80×3-3000 column. Test from Tondini et al. (2013).....	72
Figure 3.8: Test and FE load vs mid-height lateral deflection curves for CHS 76.3×3 column. Test from Zhao et al. (2016a)	73

Figure 3.9: Test and FE load vs mid-height lateral deflection curves for CHS 60.5×2.8 column. Test from Zhao et al. (2016a)	73
Figure 3.10: Test and FE load vs mid-height lateral deflection curves for CHS 88.9×2.6-1650 column. Test from Buchanan et al. (2018)	73
Figure 3.11: Test and FE load vs mid-height lateral deflection curves for CHS 106×3-3080 column. Test from Buchanan et al. (2018)	74
Figure 3.12: Test and FE failure modes for CHS 106×3-3080 column. Test from Buchanan et al. (2018)	74
Figure 3.13: Test and FE load vs mid-height lateral deflection curves for SHS 60×60×3, $e_y=10\text{mm}$ beam-column member. Test from Zhao et al. (2016b).....	76
Figure 3.14: Test and FE load vs mid-height lateral deflection curves for CHS 60.5×2.8, $e_y=15\text{mm}$ beam-column member. Test from Zhao et al. (2016a).....	77
Figure 3.15: Test and FE load vs mid-height lateral deflection curves for CHS 60.5×2.8, $e_y=40\text{mm}$ beam-column member. Test from Zhao et al. (2016a).....	77
Figure 3.16: Test and FE load vs mid-height lateral deflection curves for CHS 76.3×3, $e_y=20\text{mm}$ beam-column member. Test from Zhao et al. (2016a).....	77
Figure 3.17: Test and FE load vs mid-height lateral deflection curves for CHS 76.3×3, $e_y=95\text{mm}$ beam-column member. Test from Zhao et al. (2016a).....	78
Figure 3.18: Test and FE failure mode of SHS 100x100x5 (left image) stub column and RHS 150x100x8, $e_z=50\text{mm}$ beam-column, minor axis failure mode (right image). Test from Zhao et al. (2015a)	78
Figure 3.19: Test and FE failure mode beam-columns SHS 60x60x3, $e_z=10\text{mm}$. Test from Zhao et al. (2016b).....	78
Figure 3.20: Comparison of test vs FE axial displacement responses for SHS 120×120×4-3300, $e_y=13.2\text{mm}$, beam-column member in fire. Test from Fan et al. (2016).....	81
Figure 3.21: Test and FE failure modes for SHS 120×120×4-3300, $e_y=13.2\text{mm}$ beam-column. Test from Fan et al. (2016)	81
Figure 3.22: Test and FE load vs axial displacement curves for RHS 120×60×3.6-360, $e_z=10\text{mm}$, $\theta=400^\circ\text{C}$, beam-column member. Test from Pauli et al. (2012).....	83
Figure 3.23: Test and FE load vs axial displacement curves for RHS 120×60×3.6-1840, $e_z=10\text{mm}$, $\theta=400^\circ\text{C}$, beam-column member. Test from Pauli et al. (2012).....	83
Figure 3.24: Test and FE failure mode of S355 stub beam-column RHS 120x60x3.6, $e_z=10\text{mm}$, $\theta=400^\circ\text{C}$. Test from Pauli et al. (2012).....	83
Figure 3.25: Test and FE failure mode of S355 beam-column member level, RHS 120x60x3.6- $e_z=50\text{mm}$, $\theta=400^\circ\text{C}$. Test from Pauli et al. (2012).....	84
Figure 4.1: Typical stress-strain curves for austenitic, duplex and ferritic stainless steel. (SCI, 2017).....	88
Figure 4.2: Reduction in modulus of elasticity for austenitic, duplex and ferritic at temperature θ . (SCI, 2017)	88
Figure 4.3: Reduction in 0.2% proof strength for austenitic, duplex and ferritic at temperature θ . (SCI, 2017)	89
Figure 4.4: Reduction in strength at 2% total strain for austenitic, duplex and ferritic at temperature θ . (SCI, 2017)	90

Figure 4.5: Schematic representation of strength parameters.....	95
Figure 4.6: Comparison of FE results with the EN 1993-1-2 (2005) buckling curve for (a) austenitic, (b) duplex and (c) ferritic SHS and RHS columns, with fully effective and slender cross-sections.	102
Figure 4.7: Comparison of FE results with the EN 1993-1-2 (2005) buckling curve for (a) austenitic, (b) duplex and (c) ferritic CHS columns, with fully effective and slender cross-sections.....	104
Figure 4.8: Comparison of FE results with the Design Manual for Structural Stainless Steel (DMSS) (2017) buckling curves for (a) austenitic, (b) duplex and (c) ferritic SHS and RHS columns for fully effective and slender cross-sections.	105
Figure 4.9: Comparison of FE results with the Design Manual for Structural Stainless Steel (DMSS) (2017) buckling curves for (a) austenitic, (b) duplex and (c) ferritic CHS columns for fully effective and slender cross-sections.....	107
Figure 4.10: Comparison of FE results with the proposed buckling curves for (a) austenitic, (b) duplex and (c) ferritic SHS and RHS columns for fully effective and slender cross-sections.	112
Figure 4.11: Comparison of FE results with the proposed buckling curves for (a) austenitic, (b) duplex and (c) ferritic CHS columns for fully effective and slender cross-sections.....	113
Figure 4.12: Comparisons of predicted capacities from EN 1993-1-2 (2005) and proposed methods for stainless steel SHS/RHS.	114
Figure 4.13: Comparisons of predicted capacities from EN 1993-1-2 (2005) and proposed methods for stainless steel CHS.....	115
Figure 4.14: Schematic representation of the reliability criteria set out by Kruppa (1999)	116
Figure 5.1: Examples of numerically derived k factors for RHS beam-columns ($n=0.2$ at $\theta=200^{\circ}\text{C}$).....	130
Figure 5.2: Examples of numerically derived k factors for CHS beam-columns ($n=0.2$ at $\theta=200^{\circ}\text{C}$).....	131
Figure 5.3: Comparison between FE and proposed derived curves for RHS minor axis at $\theta=200^{\circ}\text{C}$ interaction factors.	133
Figure 5.4: Comparison between FE and proposed derived curves for RHS major axis at $\theta=200^{\circ}\text{C}$ interaction factors.	134
Figure 5.5: Comparison between FE and proposed derived curves for CHS at $\theta=200^{\circ}\text{C}$ interaction factors.	135
Figure 5.6: RHS minor axis beam-column design interaction curves $\theta=200^{\circ}\text{C}$ for varying member slenderness.	138
Figure 5.7: RHS major axis beam-column design interaction curves $\theta=200^{\circ}\text{C}$ for varying member slenderness.	139
Figure 5.8: CHS beam-column design interaction curves $\theta=200^{\circ}\text{C}$ for varying member slendernesses.....	141
Figure 5.9: Axial load and moment interaction diagram for θ	143

Figure 5.10: Comparison of RHS FE results ($N_{u,FE,\theta}$) with EN 1993-1-2 (2005) predicted strength ($N_{u,pred,\theta}$) for (a) Austenitic, (b) Duplex and (c) Ferritic.	144
Figure 5.11: Comparison of CHS FE results ($N_{u,FE,\theta}$) with EN 1993-1-2 (2005) predicted strength ($N_{u,pred,\theta}$) for (a) Austenitic, (b) Duplex and (c) Ferritic.	145
Figure 5.12: Comparison of RHS FE results ($N_{u,FE,\theta}$) with proposed predicted strength ($N_{u,pred,\theta}$) for (a) Austenitic, (b) Duplex and (c) Ferritic.	146
Figure 5.13: Comparison of CHS FE results ($N_{u,FE,\theta}$) with proposed predicted strength ($N_{u,pred,\theta}$) for (a) Austenitic, (b) Duplex and (c) Ferritic.	147

List of Tables

Table 2.1: Nominal values of yield strength and ultimate strength material properties (SCI, 2017).....	13
Table 2.2: Variation of Poisson ratio of stainless steel with temperature (Deng and Murakawa, 2006).....	23
Table 2.3: Material modelling expressions for stainless steel at elevated temperature ..	24
Table 3.1: Summary of the elevated temperature SHS and RHS column tests	49
Table 3.2: Summary of the room temperature CHS column tests	49
Table 3.3: Summary of stainless steel SHS and RHS stub column and beam-column tests	52
Table 3.4: Summary of stainless steel SHS and RHS column and beam-column member tests	52
Table 3.5: Summary of stainless steel CHS beam-column member tests	53
Table 3.6: Summary of the elevated temperature SHS beam-column tests.....	53
Table 3.7: Summary of elevated temperature carbon steel RHS column and beam-column tests	53
Table 3.8: Comparison of test and FE critical temperature θ_{crit} for SHS/RHS columns	72
Table 3.9: Comparison of test and FE ultimate load N_u and displacement at ultimate load δ_u for CHS columns	75
Table 3.10: Comparison of SHS and RHS stainless steel stub column and beam-column test and	79
Table 3.11: Comparison of SHS and RHS stainless steel beam-column members test and FE results	79
Table 3.12: Comparison of CHS stainless steel beam-column member test and FE.....	80
Table 3.13: Comparison of SHS stainless steel beam-column member in fire	82
Table 3.14: Comparison of RHS S355 carbon steel beam-column test and FE results at elevated temperature	84
Table 4.1: Summary of parametric study variables	93
Table 4.2: Room temperature material properties adopted in the parametric models....	94
Table 4.3: Typical imperfection and limiting slenderness values. EN 1993-1-4 (2006).	97
Table 4.4: Comparison between FE and predicted resistances.....	108
Table 4.5: Proposed β and η parameters for cold-formed SHS, RHS and CHS columns.	110
Table 4.6: Summary of the reliability assessment results.....	117
Table 5.1: Summary of the parametric study variables.	128
Table 5.2: Room temperature material properties adopted in the parametric models..	128

Table 5.3: Proposed interaction factors for different cross-sections, material grades and elevated temperatures.	136
Table 5.4: Comparison of stainless steel RHS and CHS beam-column FE results with predicted resistances.	148
Table 5.5: Summary of reliability assessment results.....	149

Notations

A	Cross-sectional area of an element
A_{eff}	Effective cross-sectional area
b	Width of a cross-section
COV	Coefficient of variation
E	Young's modulus
E_{θ}	Elastic modulus at temperature θ
$E_{0.2}$	Tangent modulus at 0.2% proof strength
σ	Stress
σ_{cr}	Elastic buckling stress
$\sigma_{\text{cr,p}}$	Elastic buckling stress for plate elements
$\sigma_{\text{cr,c}}$	Elastic buckling stress for CHS
$\sigma_{0.2}$	0.2% proof strength
$\sigma_{0.2,\theta}$	0.2% proof strength at temperature θ
$\sigma_{1.0}$	1.0% proof strength
$\sigma_{2.0,\theta}$	effective yield strength based at 2% total strain at temperature θ
σ_u	Ultimate strength
f_y	nominal or design yield strength

h	height of a cross-section
SS	Stainless steel
$k_{p,\theta}$	reduction factor for the proportional limit at stainless steel temperature θ
$k_{0.2p,\theta}$	reduction factor for the 0.2% proof strength at stainless steel temperature θ
$k_{2,\theta}$	is the strength reduction factor for the 2% total strain at temperature θ
$k_{y,\theta}$	is the strength reduction factor for the effective yield strength at temperature θ
$k_{E,\theta}$	is the slope of linear elastic range at temperature θ
L	is the length of a member
n	is the strain hardening parameter
$N_{b,fi,t,rd}$	design buckling resistance at time t of a compression member
SHS	square hollow section
RHS	rectangular hollow section
CHS	circular hollow section
r_i	internal radius of curvature
t	thickness of the cross-section
α	imperfection factor
$\gamma_{M,fi}$	partial safety factor
ε	parameter used to determine cross-section classification
ε_θ	strain at temperature

$\varepsilon_{0.2p}$	total strain at 0.2% proof strength $\sigma_{0.2}$
$\varepsilon_{1.0p}$	total strain at 1.0% proof strength $\sigma_{1.0}$
ε_{nom}	engineering strain
ε_{pl}^{\ln}	logarithmic plastic strain
$\varepsilon_{u,\theta}$	ultimate strain at temperature θ
θ	temperature
σ	stress
σ_{θ}	stress at temperature θ
σ_{nom}	engineering stress
σ_{true}	true stress
$\bar{\lambda}$	non-dimensional slenderness at room temperature
$\bar{\lambda}_{\theta}$	non-dimensional slenderness at temperature θ
φ_{θ}	parameter used to calculate χ_{fi}
χ_{fi}	reduction factor for the flexural buckling in fire conditions
ω_0	local imperfection amplitude
ω_g	measured global imperfection amplitude
e	eccentricity
I	second moment of area
k_{σ}	Buckling coefficient

M	Moment
N	Axial force
t	thickness of the cross-section
v	Poisson's ratio

Chapter 1 Introduction

1.1 Background and motivation

Fire has always been one of the main concerns in design of civil engineering structures as it is life threatening and can cause risks to occupants. As a result, fire-resistant design is a major requirement for any new and existing developments. Common deaths associated with fire are from inhaling toxic fumes such as carbon dioxide and monoxide. Elevated temperatures can lead to a reduction in the strength and stability of structures causing them to collapse. Therefore, to protect structures from collapsing, fire design guidance and regulations should be followed by structural engineers to ensure that occupants have enough time to leave the building and minimise the spread of the fire. This research study is primarily focused on evaluating the fire resistance of stainless steel structures to ensure safe and efficient designs in fire.

Structural fire engineering design of stainless steel has tended to receive little attention; however, an understanding of how these structures behaves in fire is paramount (Gardner, 2007). The major part of design guidelines is to provide stability for load bearing functions of a structure, to prevent any premature failure for a certain time, and to enable fire fighters to operate. In addition, environmental issues in the construction industry have become high on the public agenda, especially when fire occurs in buildings which have hazardous materials, leading to toxic fumes and run off water used by fire fighters, which can cause damage to the environment.

The expense of fire protection varies from scheme to scheme, in the type of fire resistance required, and the size and type of structure/element, but for multi-storey buildings, fire protection tends to cost around 20% to 30% of the total cost of a steel frame (Ala-Outinen and Oksanen, 1997; Wang, 1998). However, cost saving can be made by reducing the thickness of fire protection; total elimination of fire protection has far more substantial economic incentives. This can lead towards a decrease in construction costs and the time period of construction as well as more utilisation of interior spaces for a better working environment.

Nevertheless, a main weakness of metallic structures is their susceptibility to fire, which induces a reduction in the stiffness and strength of the material. In comparison with other materials, such as timber and reinforced concrete structures, the strength of metallic structures decreases rapidly when subjected to fire, largely because metallic materials tend to heat up quickly. An increase in risk from this effect can lead to extreme damage, such as property loss and, more importantly, human life if suitable design consideration are not taken into account.

For the last four decades, steel has become a major dominant material for buildings, bridges, towers and other structures. The subject of steel structure research in fire has grown due to a number of global catastrophes, such as the collapse of the World Trade Centre (WTC) in New York in September 2001 and more recently the fire at Grenfell Tower in London in June 2017. Research into the behaviour of steel structures at high temperatures and development of design guidelines have had rapid growth in recent years. General background information related to the behaviour of steel structures at elevated temperature and guidance on design for fire safety may be found in Buchanan (2002) and Wang (2005). In addition, advanced understanding in this area has evolved, in particular, from observations and subsequent analyses from full fire tests at Cardington (Lennon and

Moore, 2003), performed in the mid-90s. On the other hand, stainless steel structures in fire have received little attention, principally due to the relatively limited use in structural engineering applications to date.

The determination of the fire resistance of a structural element is a complicated process due to many variables involved, such as temperature development of the component, fire growth and duration, interaction between building elements, alterations in material properties and the influence of mechanical loads on the structural system. Owing to the expense and impracticality of generating comprehensive data on the behaviour of stainless steel structures during experimentation in fire, numerical modelling has become the most economic method to simulate the behaviour of structures in fire (Ng and Gardner, 2007). The finite element (FE) package, ABAQUS (2016), is able to simulate the nonlinear response of structures in fire and is employed throughout this study.

The mechanical and thermal properties of stainless steel differ from those of carbon steel due to variation in chemical composition between the materials. Ala-Outinen and Oksanen (1997) stated that due to high levels of nickel and chromium, stainless steel can considerably improve the heat resistance of the material. A comparison of these properties for austenitic, duplex and ferritic stainless steel with structural carbon steel is presented herein – the austenitic grade being the most widely used in structural applications in the construction industry (Gardner, 2005).

The primary motivation of this work is to develop sustainable design guidance for stainless steel structural members at elevated temperature, focusing on the element behaviour and fire design. The advantage of this is to enable and ensure that structural engineers and designer can utilise the actual material strength due to cold-forming and prevail the use of stainless steel in the construction industry.

1.2 Introduction to fire safety

The common aims for fire safety in buildings are:

- All buildings must meet certain functional requirements covering means of escape, internal fire spread, external fire spread, access and facilities for the fire service.
- Ensure the load resistance of a buildings to be adequate for a specified period of time under fire conditions.
- Reduce the probability of death and injury to people.

Structural Fire Engineers are usually concerned with ensuring adequate load bearing capacity for steel members and assemblies in fire. This is achieved by preventing structural components from excessively heating up and therefore having a reduction in stiffness and strength. However, there are additional complex structural forms which require specific treatment, and the structural fire design codes include provision for these methods in order for structural engineers not to stifle innovative design.

There are two options for achieving fire resistance, known as active and passive measures (Lennon et al., 2007). Active measures of fire protection include use of sprinklers, automatic detection, smoke barriers, and fire alarm systems, which can improve property protection and more importantly save human life. Although it is quite efficient in some situations, active fire systems cannot be relied on because they can be destroyed during high temperatures or explosion. Hence, passive measures of fire protection and compartmentation of the structure are used to control the effects of a fire once ignition has occurred. Passive fire protection includes traditional construction material such as concrete and brickwork and more recently insulation is provided by spray or fire board protection or both. Passive fire protection is the primary element of the overall safety

strategy to minimise the consequences in the event of a fire. In principle, designers are concerned with determining the amount of fire protection needed to satisfy the required fire resistance for each steel member. Some steel members which support boundary walls and compartments may need special considerations.

The determination of the resistance of a structural element under fire conditions is a complex process due to the numerous variables involved, such as alterations in the material properties, fire development and duration, temperature development of the member, interaction between the building components and elements, and the influence of the mechanical loads on the structural system. Hence, the standard fire test method offers a practically modest solution to an otherwise complex problem, it is moderately time-consuming and costly. Due to a rapid increase in technology and computer power, numerical modelling has become cost-effective method to simulate the behaviour of structural elements and structures in fire conditions. The finite element packages which are used for advanced fire engineering methods, such as ABAQUS, are able to simulate nonlinear response of structural members and structures in fire.

1.3 Stainless steel in construction

The uses of stainless steel in the construction industry is increasing rapidly, yet its utilisation as a primary structural material remains relatively limited, with the leading application being of a specialist or prestigious nature. Figures 1.1 and 1.2 show examples of structures that have made use of stainless steel. Figure 1.1 shows stainless steel columns on the One World Trade Centre in New York, which, completed in 2014, is one of the modern structural applications for high rise structures. Figure 1.2 illustrates the Helix Bridge in Singapore, which features the use of circular hollow tubular trusses.



Figure 1.1: Stainless steel columns, Seven World Trade Centre, New York. (SCI, 2017)



Figure 1.2: Helix Bridge, Singapore (SCI, 2017)

Numerous other examples of structural and architectural applications of stainless steel have been given by Baddoo (2008), Baddoo (2013) and Gardner (2019). Extensive specialist use of stainless steel is made for masonry support, wall ties, shear connectors and wind posts. Other areas include stainless steel bars, which are used for reinforcing concrete structures, providing a longer life span greater than 100 years and decreasing concrete cover, hence providing significant economic benefits (International Stainless Steel Forum, 2013).

1.4 Lifecycle costs of stainless steel

There is growing knowledge that life cycle (or whole life) costs, not just initial cost, must be measured when choosing materials. Rossi (2012) showed that using a corrosion resistant material in order to avoid future maintenance, downtime and replacement can be

a more cost effective solution, even though the initial material costs are higher. Life cycle costs take account of:

- Initial costs
- Maintenance costs
- Diversion from landfills and recycled content
- Service life and environment

The initial material expense of a structural stainless steel members is significantly higher than that of an equivalent structural carbon steel member, varying on the grade of stainless steel. Though, there can be initial expense savings related with eliminating corrosion resistant coatings. Using high strength stainless steel may possibly decrease material requirements by reducing section size and whole structure weight which decreases initial costs. Furthermore, removing the need for component replacement due to corrosion or coating maintenance can lead to significant long-term maintenance cost savings. The outstanding corrosion resistance of stainless steel presents decreased costs and inspection frequency, long service life and reduced maintenance costs.

Stainless steel retains a superior scarp value (i.e. value at the end of a structure's life), even though this is hardly a choosing factor for a structure with a long projected life (for instance over 50 years). Though, because of the superior scarp value, scrap is switched from landfills and recycled into new metal and end-of-life (EOL) recycling rates are very high. Stainless steel manufacturers use as much scrap as is accessible, but the material's overall average 20 to 30 year service life limits scrap availability. Stainless steel is 100% recyclable plus can be indefinitely recycled into new high quality stainless steel. Life cycle assessment uses the traditional accountancy principle of discounted cash flow to decrease all those costs to present values. The discount rate comprises taxes inflation,

bank interest rates, and possibly, a risk factor. This accepts a sensible contrast to be made of the opportunities available and the possible long term advantages of using stainless steel to be measured against other material selections (SCI, 2017).

1.5 Research Aims and Objectives

The following sub-sections provide the aim and objectives of this research study:

1.5.1 Aims

The aim of this research is to develop guidance for the use of stainless steel hollow section members in fire at member level, focusing on the stability and behaviour of primary structural elements such as columns and beam-columns. The obtained findings, comments and conclusion upon the design proposals can be used by structural engineers and researchers interested in employing structural stainless steel square, rectangular and circular hollow sections. The generated results together with the subsequent design recommendations and proposals aim to allow safe accurate, but also economical design guidelines in line with the observed response to potentially contribute to the development of future revisions of stainless steel design specifications. Further to this, as the research on stainless steel is explained and comprehension of the structural performance of stainless steel extends, a more widespread application of stainless steel in the construction industry can be expected, thereby prevailing the material, cost savings.

1.5.2 Research Objectives

In order to achieve the research aim, the objectives are as follows:

- Develop and validate numerical models of stainless steel SHS, RHS and CHS columns and beam-columns against experimental results at room and elevated temperature from literature.

- Implement a parametric study on cold-formed stainless steel columns and beam-column members using numerical models to establish the influence of member slenderness, cross-section at elevated temperature.
- Compare results to existing standards and methods provided in literature.
- To use the FE results to develop a methodology in the form of fire resistant design rules suitable for incorporation into standards that enables stainless steel members to be designed cost effectively and safely in structures.

1.6 Thesis outline

This chapter provides an introduction to fire safety, design guidelines, environmental issues related to stainless steel as a construction material used in structural applications. In addition, it presents the project's aims and objectives.

Chapter 2 offers a review of the literature that is relevant to this research project. The review is intended to give an overview of important topics, with the majority of the literature being introduced and discussed in the relevant chapters.

In Chapter 3, the numerical modelling approaches and principles which are adopted in this thesis are addressed. Subsequently, the developed numerical models are validated against columns and beam-column members at cross-sectional and member level from physical experiments from the literature. The validated numerical models are utilised to verify the proposed buckling curve for columns and design interaction curve for beam column members in the following chapters.

Chapters 4 focuses on the structural response of cold-formed stainless steel square hollow sections (SHS), rectangular hollow sections (RHS) and circular hollow sections (CHS) compression members (columns) in fire. Following the validation of the column

numerical models, parametric studies were undertaken to produce additional structural performance data. Based on the numerically derived data, the accuracy of the current codified design provisions is assessed, and new design methods are proposed. The reliability of the proposal is confirmed by the means of statistical analyses.

Chapters 5 present a study on stainless steel SHS, RHS and CHS beam-columns members in fire. Following the numerical validation on beam-column member in fire conditions presented in chapter 3, parametric studies were undertaken to assess the accuracy of the existing design interaction curves for fire conditions. The methodologies for overcoming the identified shortcomings, and for deriving new beam-column design proposals are then presented. The design proposals are underpinned by a comprehensive numerical simulation programme. The accuracy of the beam-column design proposals are assessed against numerical results. Finally, a reliability analysis is performed on the proposal by the means of statistical analyses.

Finally, Chapter 6 provides a summary of the important findings from the present research project and offers suggestion for further work.

Chapter 2 Literature review

2.1 Introduction

This chapter is divided into broad subject areas and presents a brief overview of the behaviour and design of stainless steel structures in fire conditions. The vital features of stainless steel, comparison with carbon steel, its response to cold-working and elevated temperatures properties and laboratory fire testing is firstly discussed. The development of structural stainless steel design guidance is summarised, with the focus lying on European and UK design guidance. Numerical modelling is discussed with a focus on element type, material modelling, residual stresses, geometric imperfections and analysis technique.

2.2 Stainless steel

The development of stainless steel is commonly attributed to an English metallurgist in 1913, Harry Brearley, who referred to the material as ‘rustless steel’ (Baddoo, 2013) . At a similar time in Germany, it was seen that increasing the chromium content improved the corrosion resistance, in particular when it was a minimum of 10.5% by mass. Between 1911 and 1914 in the United States of America, ferritic stainless steel was developed by Becket and Dantsizen, while martensitic stainless steel was produced by Haynes (Baddoo, 2013). The first austenitic stainless steel was patented by Maurer and Strauss of Krupps in 1912-1913 (Gardner, 2002). Stainless steel is now described as a corrosion resistance iron alloy that contains a minimum of 10.5% chromium. Currently, in a range of structural

and non-structural applications, stainless steel can be cast, cold-formed, hot rolled, forged and additively manufactured for products (Baddoo, 2013).

2.2.1 Categories of stainless steel

As stainless steel is known as iron with a minimum content of chromium, there is a wide range of stainless steel grades available that differ in composition and therefore have different mechanical properties and corrosion resistance. In addition, to iron (Fe) and chromium (Cr) additional alloying elements can contain nickel (Ni), carbon (C), copper (Cu), sulphur (S), nitrogen (N), manganese (Mn), molybdenum (Mo), silicon (Si), phosphorus (P) (Gardner, 2005). Stainless steel can be classified into five different families: austenitic, duplex, ferritic, martensitic and precipitation hardening. Austenitic grades are the most widely used stainless steel and they typically contain chromium content of 17% to 18%, and 8% to 11% nickel content. Ferritic grades have a low initial cost due to their lower chromium content, which is between 10.5% and 18%, and a nickel content of 0% to 2.5% (Design Manual for Structural Stainless Steel (DMSSS), 2017). In addition, ferritic grades tend to have a similar atomic structure to structural carbon steel, leading to a slightly higher proof strength, and are less prone to stress cracking. Traditionally, ferritic grades have been used in construction for plumbing pipework inside industrial buildings and they have moderate corrosion resistance and poor fabrication properties, although they can be strengthened by cold working, but to a more limited degree than austenitic stainless steel. Duplex grades have a mixed microstructure of austenitic and ferritic, which generally have led to better properties such as good wear resistance, high corrosion resistance and higher strength compared to ferritic and austenitic grades. However, the initial cost of duplex is much higher due to the chromium content of 22% to 23% and 4% to 5% of nickel content. Low-cost lean duplex grades, which contain a reduced nickel content but offer high strength, have been developed and

are available, although have a reduction in corrosion resistance (Baddoo, 2013). Martensitic stainless steel have a similar cubic structure as ferritic stainless steels and structural carbon steels, but are less common in construction industry and are used in applications that take advantage of their wear, abrasion resistance and hardness, like surgical instruments, industrial knives, wear plates and turbine blades (Stainless Steel Design Manual, 2017). Precipitation hardening stainless steels, which can achieve high strength through heat treatment, are commonly used in the aerospace industry, although are occasionally used in construction for tension bars, shafts and bolts. Table 2.1 provides the key mechanical properties for hollow section provided in the Design Manual for Structural Stainless Steel (2017).

Table 2.1: Nominal values of yield strength and ultimate strength material properties (SCI, 2017).

Grade	Cold-worked condition				
	f_y (N/mm ²)	f_u (N/mm ²)	f_y (N/mm ²)	f_u (N/mm ²)	
	1.4301	350	600	460	650
	1.4318	220	520	460	650
Austenitic	1.4541	350	600	460	650
	1.4401	350	600	460	650
	1.4571	350	600	460	650

2.2.2 Mechanical properties comparison of stainless steel and carbon steel

The stress-strain characteristics for stainless steel at elevated temperatures are vital to determine the resistance for a structural member at cross-sectional and member level under fire conditions. The stress-strain relationship firstly has to be understood at ambient temperature and then followed by elevated temperature. In addition, comparisons will be made between stainless steel and carbon steel to illustrate the behaviour of these two materials.

The stress-strain response for stainless steel differs from carbon steel in many aspects. The main differences are found in the shape of the stress-strain curve. Figure 2.1

compares the stress-strain characteristics of austenitic, duplex, ferritic and carbon steel (S355) for strains up to 0.75% and Figure 2.2 shows typical range of stress-strain curves. As shown, carbon steel (S355) exhibits linear elastic behaviour up to the yield strength and a plateau before any strain hardening is encountered, whereas stainless steel (austenitic, duplex and ferritic) has a more rounded response with no clearly defined yield point. Stainless steel yield strength is generally defined as a proof stress at an offset permanent strain, conventionally the 0.2% strain. In terms of ductility, austenitic stainless steel has a strain fracture between 40% - 60% nearly twice as much as carbon steel, whereas duplex has approximately 40% - 50% and ferritic around 15% - 30%.

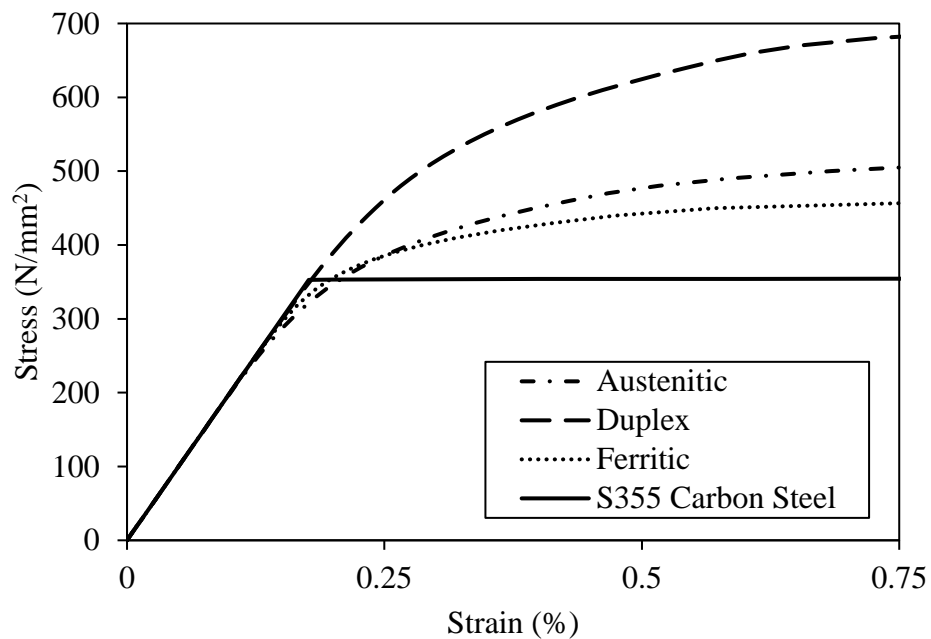


Figure 2.1: Comparison of stainless steel and carbon steel stress-strain curves from 0 to 0.75% strain, DMSS (2017) and EN 1993-1-2 (2005)

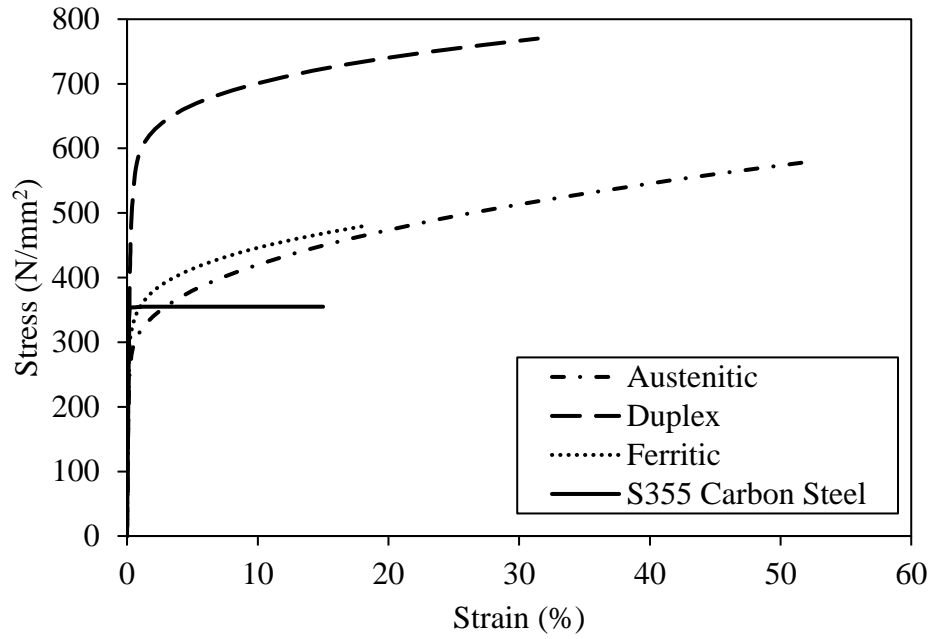


Figure 2.2: Complete range of stainless steel and carbon steel stress-strain curves, DMSS (2017) and EN 1993-1-2 (2005)

The stress-strain behaviour for stainless steel is found to be anisotropic, when upon loading, the material aligned transverse to the rolling direction exhibits different stress-strain response compared to the material loaded longitudinally to the rolling direction and shows higher strain hardening. Thus, high yield stress values are typically obtained from coupon specimens that are cut in the transverse direction (Cruise, 2007). In addition, the material response is also different when subjected to tensile and compressive loading types, leading to asymmetric stress-strain curves for compression and tension. The degree of non-linearity, anisotropy and asymmetry depends on the grade of stainless steel, heat treatment processes and the level of cold-work induced during forming process (Gardner, 2005).

Ramberg and Osgood (1943) developed a material model to describe the stress-strain response of aluminium alloys, given by Equation (2.1).

$$\varepsilon = \frac{\sigma}{E} + K \left(\frac{\sigma}{E} \right)^n \quad (2.1)$$

where ϵ and σ are the engineering strain and stress, respectively, E is the material Young's modulus, and K and n are model constants.

Ramberg and Osgood (1943) noted the applicability of the model, which is similar to aluminium alloys also shows a highly nonlinear stress-strain response. This expression was later modified by Hill (1944) as given by Equation (2.2).

$$\epsilon = \frac{\sigma}{E} + c \left(\frac{\sigma}{R_p} \right)^n \quad (2.2)$$

Where R_p and c , are the proof stress and the corresponding offset plastic strain, and n is the strain hardening coefficient, (which defines the curvature of the stress-strain response a higher n value denotes a sharper curve). Equation (2.2) is typically adopted with R_p set to the 0.2% proof stress ($\sigma_{0.2}$), resulting in the traditional form of the Ramberg-Osgood expression provided in Equation (2.3).

$$\epsilon = \frac{\sigma}{E} + 0.002 \left(\frac{\sigma}{\sigma_{0.2}} \right)^n \quad (2.3)$$

The strain hardening exponent n is commonly determined using the 0.05% or the 0.01% proof stress points and the 0.2% proof stress (Rasmussen and Hancock, 1993; Rasmussen, 2003). When Equation (2.3) is applied to stainless steel, it provides a good agreement of stress-strain behaviour below the material 0.2% proof stress and at higher strains it was found to overestimate the material strength. In order to achieve better representation of the stress-strain behaviour, Mirambell and Real (2000) proposed a two stage stress-strain model for stainless steel. The first stage, Equation (2.3) was adopted up to the 0.2% proof stress. This was followed by the second stage, where a modified Ramberg-Osgood expression which included stresses which go beyond 0.2% proof stress up to the ultimate tensile stress, as given in Equation (2.4) was proposed. The origin of the second curve

was defined at 0.2% proof stress, with continuity of both gradient and magnitude at the transition point maintained.

$$\varepsilon = \frac{(\sigma - \sigma_{0.2})}{E_{0.2}} + \left(\varepsilon_u - \varepsilon_{t,0.2} - \frac{\sigma_u - \sigma_{0.2}}{E_{0.2}} \right) \left(\frac{\sigma - \sigma_{0.2}}{\sigma_u - \sigma_{0.2}} \right)^m + \varepsilon_{t,0.2} \quad \text{for } \sigma \geq \sigma_{0.2} \quad (2.4)$$

where $E_{0.2}$ is the tangent modulus at $\sigma_{0.2}$ change point, ε_u is the strain at the ultimate tensile stress, and m is an additional strain hardening exponent beyond the 0.2% proof stress and $\varepsilon_{t,0.2}$ is the total strain at 0.2% proof stress. The tangent modulus can be calculated from Equation (2.5).

$$E_{0.2} = \frac{\sigma_{0.2}E}{\sigma_{0.2} + 0.002nE} \quad (2.5)$$

In addition, Mirambell and Real (2000) suggested that the strain hardening exponent n to be extracted from the 0.05% and 0.2% proof stresses, based upon previous work by Rasmussen and Hancock (1993). Rasmussen (2003) extended the material model by deriving expressions for the additional strain hardening exponent m , the ultimate tensile strength (σ_u) and the strain at the ultimate tensile strength (ε_u) based on experimental data, as given by Equations (2.6), (2.7) and (2.8), respectively.

$$m = 1 + 3.5 \frac{\sigma_{0.2}}{\sigma_u} \quad (2.6)$$

$$\frac{\sigma_{0.2}}{\sigma_u} = \frac{0.2 + 185(\sigma_{0.2}/E_0)}{1 - 0.0375(n - 5)} \quad (2.7)$$

$$\varepsilon_u = 1 - \frac{\sigma_{0.2}}{\sigma_u} \quad (2.8)$$

This two-stage model was found to be limited, owing to its applicability to describe the tensile stress-strain behaviour only, which included dependency on parameters such as the ultimate tensile stress (σ_u) and the corresponding strain (ε_u). In compression, these parameters do not exist, due to absence of the necking phenomena. (Gardner and Ashraf, 2006) proposed that the 1% proof stress ($\sigma_{1.0}$) and its corresponding total strain ($\varepsilon_{t,1.0}$) to

be used in place of the ultimate tensile stress (ϵ_u, σ_u), as described by Equation (2.9), with Equation (2.3) used for stresses below the 0.2% proof stress.

$$\epsilon = \frac{(\sigma - \sigma_{0.2})}{E_{0.2}} + \left(\epsilon_{t1.0} - \epsilon_{t0.2} - \frac{\sigma_{1.0} - \sigma_{0.2}}{E_{0.2}} \right) \left(\frac{\sigma - \sigma_{0.2}}{\sigma_{1.0} - \sigma_{0.2}} \right)^{n'_{0.2,1.0}} + \epsilon_{t0.2} \quad \text{for } \sigma_{0.2} < \sigma \leq \sigma_u \quad (2.9)$$

Stainless steel cold-formed hollow sections are generally manufactured by cold rolling, where flat sheet material is formed into a circular section, seam welded closed and subsequently deformed into the required tubular section by means of a dies. During fabrication, plastic deformations are encountered, causing strength enhancements to the stainless steel material, which is notably found in the corner regions of the section. Studies on cold working have been undertaken on tensile coupons test and a series of models for predicting strength enhancements in the corner regions has been proposed by Gardner and Nethercot (2004), Ashraf et al.(2005), Cruise and Gardner (2008) and Rossi et al. (2012). It has been experimentally (Cruise and Gardner (2008) and numerically (Gardner and Nethercot, 2004; Ashraf et al., 2006) verified that the corner strength enhancements are not restricted only in the curved edges of the section, but also extends in the flat regions by a distance approximateley equivalent to two times the cross-section thickness.

2.2.3 Thermal properties

The material characteristics of stainless steel at ambient and elevated temperature differ from carbon steel due to the difference in chemical composition and the physical and thermal properties between the two materials. The variation of stiffness, strength, thermal expansion, specific heat and thermal conductivity with temperature will be discussed herein firstly, followed by material models at elevated temperatures. Research on stainless steel material stiffness and strength at elevated temperatures has been conducted. These studies have shown that stainless steel provide better retention of stiffness and

strength at elevated temperatures compared to carbon steel, as illustrated in Figure 2.3 and 2.4.

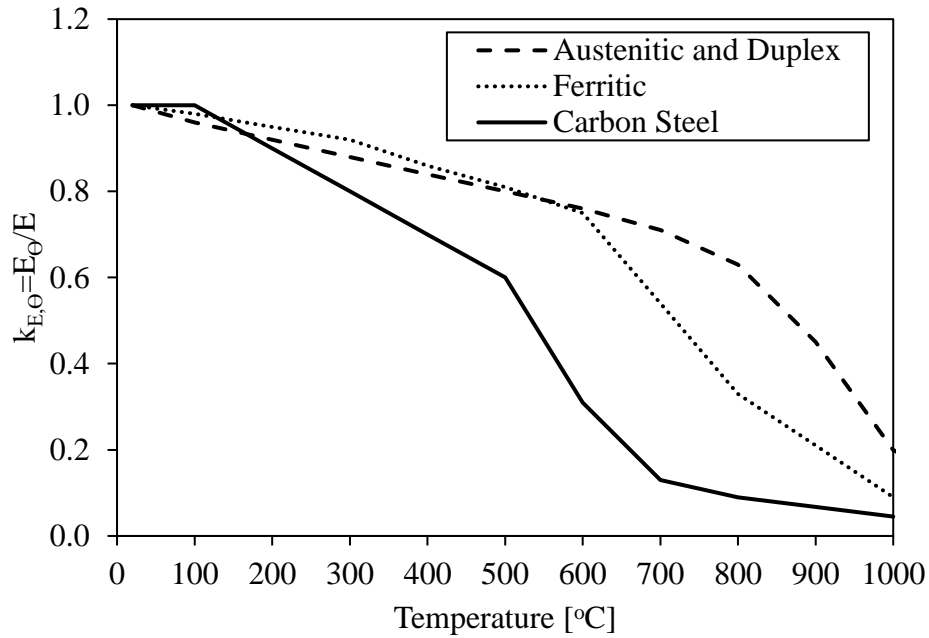


Figure 2.3: Comparison of stainless steel and carbon steel stiffness retention factors

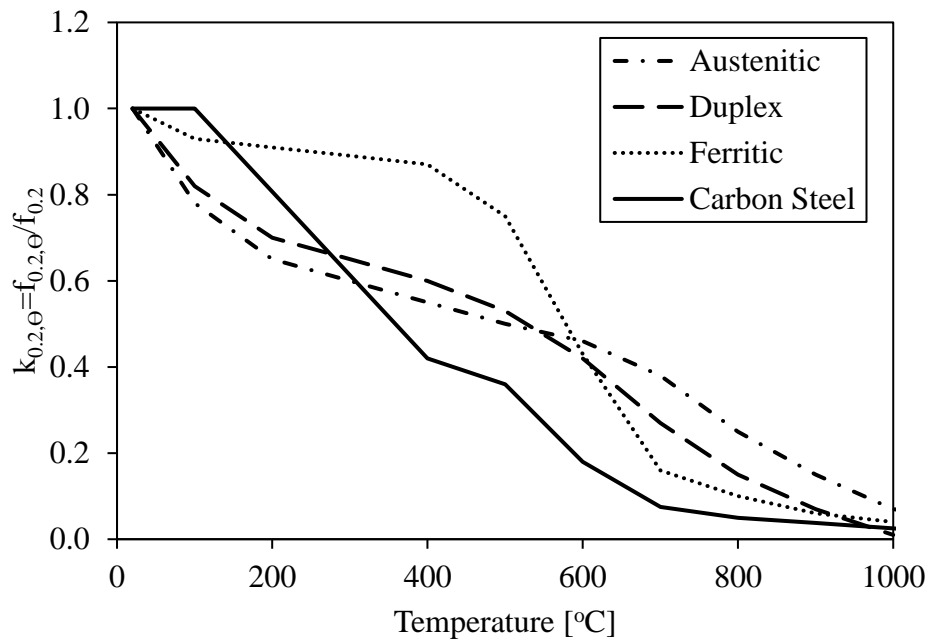


Figure 2.4: Comparison of stainless steel and carbon steel 0.2% proof strength retention factors

Stainless steel has higher thermal expansion than carbon steel as shown in Figure 2.5. The thermal elongation (expansion) of austenitic stainless steel can be determined as shown in Equation (2.10), where L is the length at 20°C, ΔL is the temperature induced expansion

and, θ is the steel temperature ($^{\circ}\text{C}$). Numerical analysis was carried out by Gardner & Ng (2006) at elevated temperature on restrained beam and columns to investigate the thermal expansion of the stainless steel. It was found that stainless steel offers better fire performance for low levels of axial restraint, due to the superior retention in strength and stiffness, whereas for high levels of axial restraint the additional forces induced, due to the restrained thermal expansion, become more detrimental for stainless steel members (Gardner, 2007).

$$\frac{\Delta L}{L} = \frac{(16 + 4.79 \times 10^{-3}\theta - 1.243 \times 10^{-6}\theta^2) \times (\theta - 20)}{10^6} \quad (2.10)$$

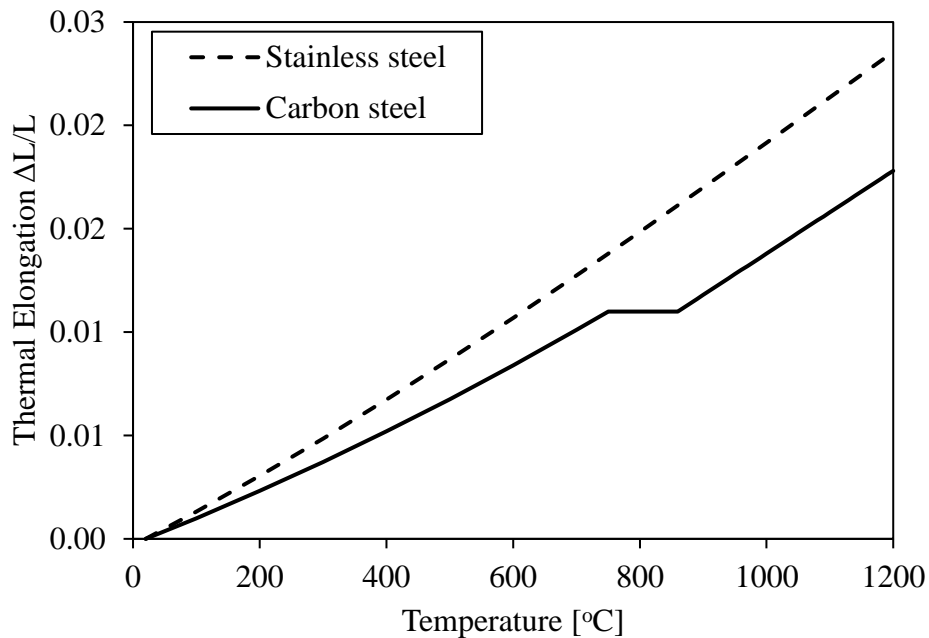


Figure 2.5: Comparison of thermal expansion of stainless steel and carbon steel

Specific heat is known as the amount of heat energy per unit mass required to increase the temperature by one degree. Stainless steel specific heat shows a steady increase with a rise in temperature, while carbon steel develops a discontinuity in the region of 723°C , owing to the phase change in material around this temperature, as shown in Figure 2.6. Averagely, the specific heat of carbon steel is approximately $600 \text{ J/kg } ^{\circ}\text{C}$, whereas stainless steel is around $550 \text{ J/kg } ^{\circ}\text{C}$. The higher the specific heat of a material, the slower

the temperature of the material tends to heat up. The specific heat C (J/kg°C) of stainless steel may be determined from Equation (2.11) for austenitic and duplex grades and Equation (2.12) for ferritic grade (EN 1993-1-2, 2005 and DMSS, 2017), where θ is the steel temperature (°C).

$$C = 450 + 0.28 \times \theta - 2.91 \times 10^{-4} \theta^2 + 1.34 \times 10^{-7} \theta^3 \quad (\text{J/kg}^\circ\text{C}) \quad (2.11)$$

$$C = 450 + 0.26 \times \theta \quad (\text{J/kg}^\circ\text{C}) \quad (2.12)$$

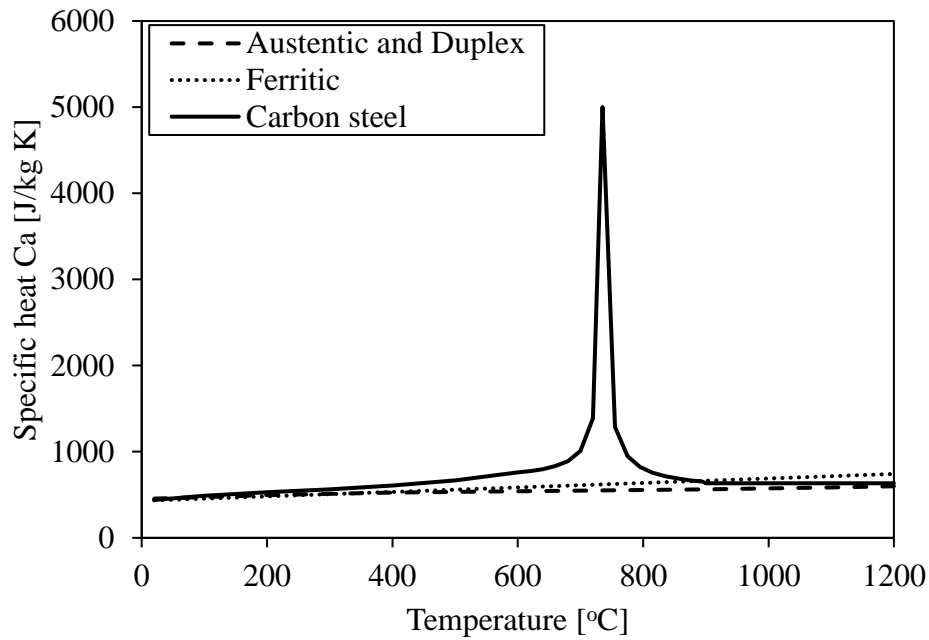


Figure 2.6: Comparison of stainless steel and carbon steel specific heat comparison

The thermal conductivity of stainless steel is different to carbon steel as illustrated in Figure 2.7. The lower thermal conductivity of stainless steel gives growth to more localised temperature development in the material. The thermal conductivity can be determined from Equation (2.13) for austenitic and duplex grades and Equation (2.14) for ferritic grades, as provided in EN 1993-1-2 (2005) and Design manual for structural stainless steel (DMSS, 2017).

$$\lambda = 14.6 + 1.27 \times 10^{-2} \theta \quad \text{W/m}^\circ\text{C} \quad (2.13)$$

$$\lambda = 20.4 + 2.28 \times 10^{-2} \theta - 1.54 \times 10^{-5} \theta^2 \quad \text{W/m}^\circ\text{C} \quad (2.14)$$

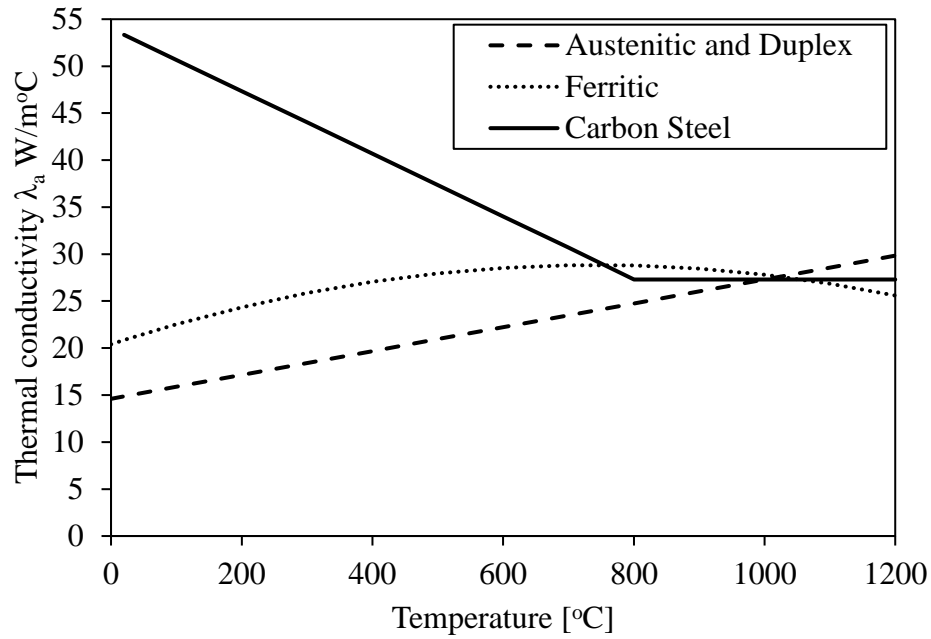


Figure 2.7: Comparison of stainless steel and carbon steel thermal conductivity

2.2.4 Poisson ratio

When a material is under tensile loading, it tends to become long and thin and when it's under compressive loading, it becomes short and thick. This phenomenon is governed by Poisson's ratio (ν), which is defined as the lateral strain normalised by the longitudinal strain (Cooke, 1988). The Poisson ratio of stainless steel at room temperature normally lies in the range 0.294 - 0.33 and is insensitive to variation in the exact composition of the steel. There have been few measurements of Poisson ratio at elevated temperature which have been reported (Deng and Murakawa, 2006) are reproduced in Table 2.2 and indicate that the value does not significantly change with higher temperatures.

The very gradual increase of Poisson ratio with temperature seen in Table 2.2 is consistent with a value of 0.33 at 800°C reported by Deng and Murakawa (2006). Given this data, 0.3 would seem a reasonable value to be used in any structural analysis in the temperature range 0 °C - 1200 °C.

Table 2.2: Variation of Poisson ratio of stainless steel with temperature (Deng and Murakawa, 2006)

Temperature (°C)	Poisson Ratio
0	0.294
100	0.295
200	0.301
300	0.310
400	0.318
600	0.326
800	0.333
1200	0.339

2.2.5 Material modelling at elevated temperatures

Modelling stainless steel structures under fire conditions requires that the elevated temperature stress-strain response of the material is accurately represented. Guidelines on modelling the stress-strain behaviour of stainless steel at elevated temperatures are provided in EN 1993-1-2 (2005), Chen & Young (2006) and Gardner et al. (2010). In addition, stiffness and strength reduction factors are provided. A review of these material models is provided herein.

EN 1993-1-2 (2005)

EN 1993-1-2 (2005) Annex C provides a nonlinear two stage model, as given in Equations (2.15) and (2.16) and shown in Figure 2.8 to define the stainless steel stress-strain material behaviour at elevated temperatures.

$$\sigma_{\theta} = \frac{E\varepsilon_{\theta}}{1 + a\varepsilon_{\theta}^b} \text{ for } \varepsilon_{\theta} \leq \varepsilon_{c,\theta} \quad (2.15)$$

$$\sigma_{\theta} = \sigma_{0.2,\theta} - e + \left(\frac{d}{c}\right) \sqrt{c^2 - (\varepsilon_{u,\theta} - \varepsilon_{\theta})^2} \text{ for } \varepsilon_{c,\theta} < \varepsilon_{\theta} \leq \varepsilon_{u,\theta} \quad (2.16)$$

where, σ_{θ} and ε_{θ} are the engineering stress and strain at elevated temperature θ , respectively E is the Young's modulus at ambient temperature, $\sigma_{0.2,\theta}$ is the 0.2% proof stress at temperature θ , $\varepsilon_{c,\theta}$ is the total strain at $\sigma_{0.2,\theta}$, $\varepsilon_{u,\theta}$ is the strain at the ultimate tensile stress at temperature θ and a, b, c, d and e are defined in terms of the elevated temperature properties provided in EN 1993-1-2, (2005). Table 2.3 provides the

definitions for each of the parameters and functions required according to EN 1993-1-2 (2005) to form the stainless steel stress-strain curve.

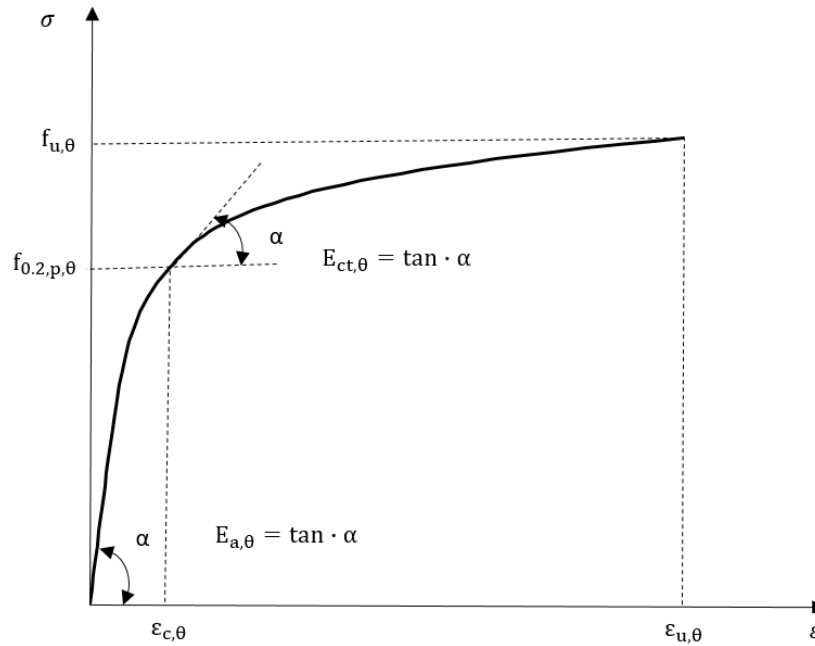


Figure 2.8: EN 1993-1-2 (2005) stainless steel stress-strain relationship at elevated temperatures

Where:

- $f_{u,\theta}$ is tensile strength
- $f_{0.2,\theta}$ is the proof strength
- $E_{a,\theta}$ is the slope of the linear elastic range
- $E_{ct,\theta}$ is the slope at proof strength
- $\epsilon_{c,\theta}$ is the total strain at proof strength
- $\epsilon_{u,\theta}$ is the total strain at proof strength

Table 2.3: Material modelling expressions for stainless steel at elevated temperature

Parameters	$\epsilon_{c,\theta} = \frac{f_{0.2p,\theta}}{E_{a,\theta} + 0.002}$
Functions	
$a = \frac{E_{a,\theta}\epsilon_{c,\theta} - f_{0.2p,\theta}}{f_{0.2p,\theta}\epsilon_{c,\theta}^b}$	$b = \frac{\left(1 - \frac{\epsilon_{c,\theta}E_{ct,\theta}}{f_{0.2p,\theta}}\right)E_{a,\theta}\epsilon_{c,\theta}}{\left(\frac{E_{a,\theta}\epsilon_{c,\theta}}{f_{0.2p,\theta}} - 1\right)f_{0.2p,\theta}}$
$c^2 = (\epsilon_{u,\theta} - \epsilon_{c,\theta})\left(\epsilon_{u,\theta} - \epsilon_{c,\theta} + \frac{e}{E_{ct,\theta}}\right)$	$d^2 = e(\epsilon_{u,\theta} - \epsilon_{c,\theta})E_{ct,\theta} + e^2$
$e = \frac{(f_{u,\theta} - f_{0.2p,\theta})^2}{(\epsilon_{u,\theta} - \epsilon_{c,\theta})E_{ct,\theta} - 2(f_{u,\theta} - f_{0.2p,\theta})}$	

Chen and Young (2006)

Chen and Young (2006) conducted a material testing programme on duplex EN 1.4462 and austenitic EN 1.4301 stainless steel at temperatures ranging from 20°C to 1000°C. A series of equations for predicting the yield strength, Young modulus, ultimate tensile strength and strain at ultimate tensile stress for stainless steel at elevated temperatures were proposed. Furthermore, a stress-strain model was proposed utilising the Ramberg-Osgood model, of the form proposed by Mirambell and Real (2000), which was modified to elevated temperatures as given in Equations (2.17) and (2.18). The proposed stress-strain model showed good agreement when compared to test results.

$$\varepsilon_{\theta} = \frac{\sigma_{\theta}}{E_{\theta}} + 0.002 \left(\frac{\sigma_{\theta}}{\sigma_{0.2,\theta}} \right)^{n_{\theta}} \quad \text{for } \sigma_{\theta} \leq \sigma_{0.2,\theta} \quad (2.17)$$

$$\varepsilon_{\theta} = \frac{(\sigma_{\theta} - \sigma_{0.2,\theta})}{E_{0.2,\theta}} + \varepsilon_{u,\theta} \left(\frac{\sigma_{\theta} - \sigma_{0.2,\theta}}{\sigma_{u,\theta} - \sigma_{0.2,\theta}} \right)^{m'_{\theta}} + \varepsilon_{t0.2,\theta} \quad \text{for } \sigma_{\theta} > \sigma_{0.2,\theta} \quad (2.18)$$

where, σ_{θ} and ε_{θ} are the engineering stress and strain at elevated temperature θ , E_{θ} is the Young's modulus at temperature θ , $\sigma_{0.2,\theta}$ is the 0.2% proof stress at temperature θ , $E_{0.2,\theta}$ is the tangent modulus $\sigma_{0.2,\theta}$ given in Equation (2.19), n_{θ} is the model coefficient given in Equation (2.20), $\varepsilon_{u,\theta}$ is the strain at the ultimate tensile stress at temperature θ , $\sigma_{u,\theta}$ is the ultimate tensile stress at temperature θ , m'_{θ} is the model coefficient given in Equation (2.21) and (2.22), $\varepsilon_{t0.2,\theta}$ is the total strain at 0.2% proof stress at temperature θ and where θ is the temperature.

$$E_{0.2,\theta} = \frac{E}{1 + 0.002n \left(\frac{E}{\sigma_{0.2,\theta}} \right)} \quad (2.19)$$

$$n^{\theta} = 6 + 0.2\sqrt{\theta} \quad (2.20)$$

$$m'^{\theta} = 5.6 - \frac{\theta}{200} \quad \text{for stainless steel EN 1.4462} \quad (2.21)$$

$$m'^{\theta} = 2.3 - \frac{\theta}{200} \quad \text{for stainless steel EN 1.4301} \quad (2.22)$$

Gardner et al. (2010)

Gardner et al. (2010) conducted a material testing programme on stainless steel at elevated temperatures which include austenitic (EN 1.4301, EN 1.4318, EN 1.4401/4, EN 1.4541, EN1.4571), duplex (EN 1.4362, EN 1.4462, EN 1.4162) and Ferritic (EN 1.4003) grades. Eight sets of reduction factors were rationalised on the basis of materials exhibited similar behaviour at elevated temperatures. An accurate stress-strain material model was proposed which is illustrated in Equations (2.23) and (2.24), utilises the stress at 2% total strain, and shown less complex than EN 1993-1-2 (2005) formulations and the model parameters have clear physical significance.

$$\varepsilon_{\theta} = \frac{\sigma_{\theta}}{E_{\theta}} + 0.002 \left(\frac{\sigma_{\theta}}{\sigma_{0.2,\theta}} \right)^{n_{\theta}} \quad \text{for } \sigma_{\theta} \leq \sigma_{0.2,\theta} \quad (2.23)$$

$$\varepsilon_{\theta} = \frac{(\sigma_{\theta} - \sigma_{0.2,\theta})}{E_{0.2,\theta}} + \left(0.02 - \varepsilon_{t,0.2,\theta} - \frac{\sigma_{t2.0,\theta} - \sigma_{0.2,\theta}}{E_{0.2,\theta}} \right) \left(\frac{\sigma_{\theta} - \sigma_{0.2,\theta}}{\sigma_{2.0,\theta} - \sigma_{0.2,\theta}} \right)^{n'_{\theta}} + \varepsilon_{t0.2,\theta} \quad (2.24)$$

for $\sigma_{0.2,\theta} < \sigma_{\theta} \leq \sigma_{u,\theta}$

where n_{θ} and n'_{θ} are model coefficient provided and the rest of the symbols have been previously defined. Figure 2.9 shows the full range stress-strain response curves for temperatures 20°C to 800°C obtained from Gardner et al. (2010) model.

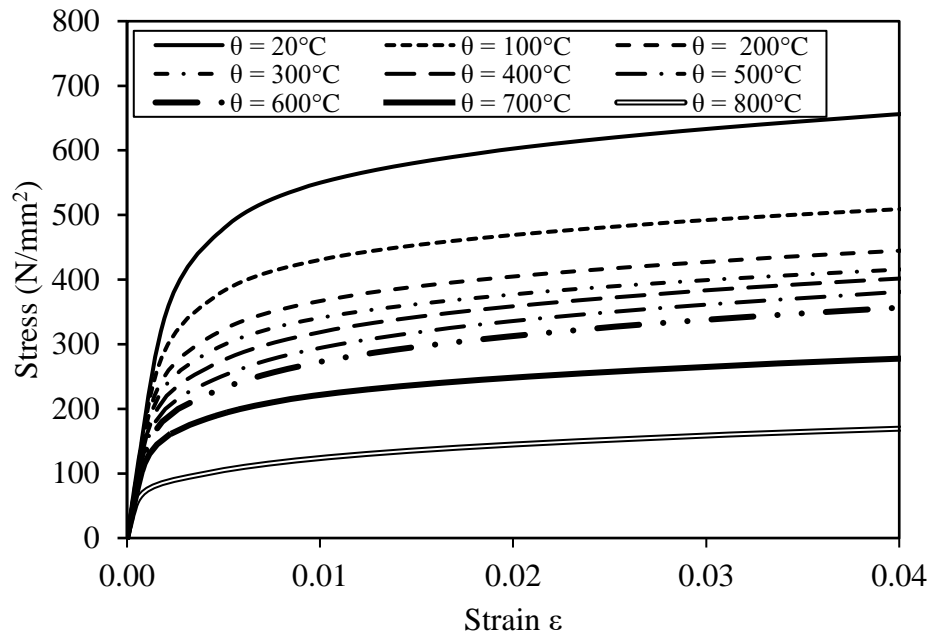


Figure 2.9: Stainless steel stress-strain behaviour at elevated temperature Gardner (2010) model

2.2.6 Laboratory fire testing

The development of efficient codified fire design rules requires high quality laboratory test data. Due to the limited use of stainless steel in buildings and structures, it is unsurprising that the volume of test results for stainless steel structures in fire is currently relatively low, with some areas virtually unexplored such as lateral torsional buckling of stainless steel elements and stainless steel frames and connections under fire conditions. This section contains a brief review of the laboratory tests conducted on stainless steel members in fire.

The early laboratory tests carried out by Ala-Outinen and Oksanen (1997) on stainless steel compression members exposed to fire investigated if austenitic stainless steels column can be used for load-bearing structures without fire protection.

Gardner and Baddoo (2006) presented tests details on unprotected stainless steel beam and columns members in fire. Material testing was conducted on austenitic, duplex and ferritic stainless steel at ambient and elevated temperature using isothermal and

anisothermal methods. The member tests included SHS, RHS and I-sections and all the grades were austenitic EN 1.4301 grade. All tests were conducted using anisothermal conditions, where the specimen is first loaded to a specified load level, and the temperature is then increased until failure, and are described in detail in Chapter 3.

Pauli et al. (2012) performed experimental tests at elevated temperature on S355 SHS, RHS, H and I-sections specimens. This included stub (short) and slender (long) columns and beam-column members. All structural members were made from hot finished sheets which formed into shape at room temperature welded closed. The experiments were performed under isothermal loading conditions of 400, 500 and 700°C and then, once equilibrium had been established at the desired temperature, a mechanical load was applied at a strain rate 0.1%/min, until horizontal displacement increased rapidly and the vertical load could no longer be maintained and are further described in detail in Chapter 3.

SHS and RHS ferritic stainless steel column tests in fire have been reported by Tondini et al. (2013). The sections were fixed at both ends and the series of tests provided an insight into the critical temperatures and failure modes of tubular hollow sections. All tests were conducted anisothermally and are described in detail in Chapter 3.

More recently, Fan et al. (2016) conducted fire tests on unprotected stainless steel columns and beam-column members in fire. Material tests were performed on austenitic stainless steel under isothermal conditions, where the coupon is heated to a specified temperature, which is held constant, followed by a tensile test until failure. All members were SHS and the material grade utilised was austenitic (EN 1.4301). All structural test members were performed under anisothermal method.

2.2.7 Structural stainless steel design standards

In the early 1950s and 1960s, laboratory testing on stainless steel structural members commenced and design rules were put forward. In the past, stainless steel design and guidelines have been based on assumed analogies with respect to carbon steel, with amendments made where required. However, a number of structural stainless steel design guidance has been prepared worldwide. An overview of the design provision for stainless steel codes (European, US, Australia/New Zealand and China) is provided herein.

In the late 1960s, the earliest structural stainless steel standard ‘specification for the design of light gauge cold-formed stainless steel structural members’ was published by the American Iron and Steel Institute (AISI) (Wang and Errara, 1971) (Gardner, 2005). Due to the development of understanding the behaviour of structural stainless steel members and increased in test results, a revised version of the standard was published in 1974 (AISI, 1974) and later in 1991 by the American Society of Civil Engineers (ASCE).

In 1975, the European commission decided to develop an action programme for the field of construction. Within the action programme, the commission established a set of harmonised technical rules for the design of construction work. The commission, with some assistance from the steering committee with representatives from the state, conducted the development of the Eurocodes programme, which was the first generation of the European codes in the late 1980s. The Eurocodes were written under the guidance of CEN (European Committee for Standardisation) and included the design for a widespread range of structures. The materials which are used for structures covered by the design codes are concrete (Eurocode 2), steel (Eurocode 3), composite (Eurocode 4), timber (Eurocode 5), masonry (Eurocode 6) and aluminium (Eurocode 9).

The Euro Inox ‘Design Manual for Structural Stainless Steel’ was produced in 1991 due to an industrial project, which was managed by the UK Steel Construction Institute and later published in 1993 (Euro Inox, 1993). The design manual led towards ENV 1993-1-4 (1996) which was published by European Standards Organisation and later adopted into the full European standard EN 1993-1-4 (2006) and updated as EN 1993-1-4 (2015). The stainless steel design approach consequently adopts the carbon steel approach with revisions where necessary to fit experimental data better (Gardner, 2005); for example, the adoption of new classification limits for cross-section design due to a variety of stress-strain behaviour in EN 1993-1-4 (2015).

The Australian / New Zealand design standard (4673) for cold-formed stainless steel structures was published in 2001 which were developed based upon on the American stainless steel design standards (Rasmussen, 2000). More recently, in 2015, the Chinese CECS (2015) standard for stainless steel structures was published.

2.2.8 Fire resistance design

Currently, there are two structural steel design standards in fire which are used in the UK. These are BS 5950 Part 8 and the fire Eurocodes BS: EN 1991-1-2, BS EN 1993-1-2 and BS EN 1994-1-2. The Eurocode 3 Part 1-2 (EN 1993-1-2, 2005) is used to design stainless steel members in fire, which largely follows the carbon steel design rules, with the main difference being in the material properties provided in Annex C of the Eurocode Part 1-2 (2005) and will be referred to for comparison throughout this study. This section includes an introduction to Eurocode 3 Part 1-2 (EN 1993-1-2, 2005). The European pre-standard ENV 1993-1-4 (1996) was first drafted in 1996. In 1999, the ECCS model (Kruppa et al., 1999) code was prepared for the ECCS technical committee 3 fire safety of steel structures by European fire experts. It was recommended that the format of the design

guidance for stainless steel structural members should follow the carbon steel guidelines, with appropriate change in material properties. The ECCS model code was used to develop a more realistic and economic standard EN 1993-1-2 (2005). EN 1993-1-2 (2005) covers the design of steel structures for the accidental situation of fire exposure, containing methods to determine structural resistances at elevated temperatures.

2.3 Buckling of structural members

Commonly, there are three main types of structural elements (Figure 2.10): columns, beams and beam-columns. A column is a member that transmits, through axial compression, the weight of the structure above to other structural elements. A beam is a member that predominantly resists loads applied laterally on the beam-axis and its mode of deflection is primarily bending. A beam-column member is subjected simultaneously to both axial compression load and bending moments.

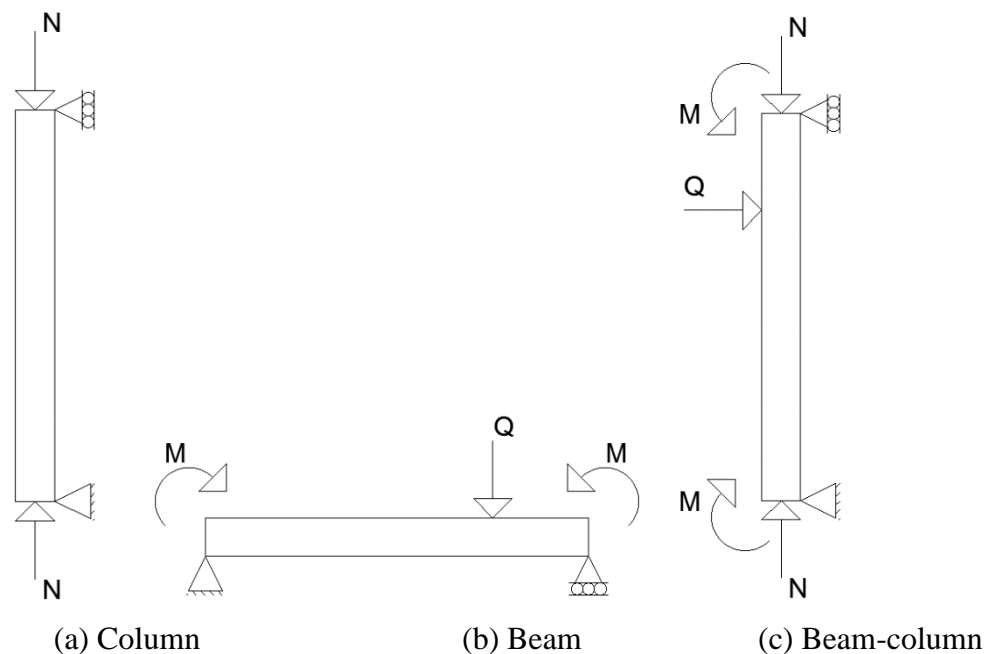
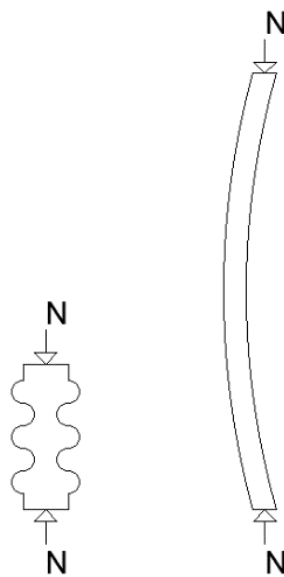


Figure 2.10: Systematic representation of general cases of structural elements

2.3.1 Columns

In columns, there are two crucial modes of instability, local and global as shown in Figure 2.11 or a combination of both. Columns with low level slenderness (i.e. short columns) may fail by cross-section yielding (for low levels cross-section slenderness) or by cross-section local buckling (for high cross-section slenderness). For slender (i.e. long) columns, the failure mode is governed by global buckling as member instability effects dominate.



(a) Local Buckling (b) Global buckling

Figure 2.11: Instability buckling modes of axially loaded columns

2.3.1.1 Local buckling & Element interaction

Local buckling is a failure mode that occurs in metallic cross-sections and is characterised by distortion of the cross-section of the member under compressive stresses. Common structural steel cross-sections, cold-formed or hot-rolled, are composed of interconnected flat plate elements. Due to the high strength to weight ratio, structural metallic sections usually consist of relatively thin plate elements and when under compression, local buckling may occur if the plate to thickness ratio is large. In flat plated cross-sections,

elements are supported along one edge. Examples of outstand elements are the flanges elements in universal beam (UB) or universal column (UC) sections. Elements that are supported along both edges, such as a web of I-sections, are known as internal elements. Outstand and internal elements are also known as unstiffened and stiffened elements, respectively (Knobloch and Fontana, 2006).

Prior to local buckling, the steel plate is under uniform compression. As the stress is increased beyond a critical level, the plate tends to buckle, and significant out-of-plane deformations occur. This does not indicate the ultimate failure of the plate or the cross-section as further loading will result in redistribution of stresses to more stiff regions of the plate or where out-of-plane deformations are less. The stress during this stage becomes non-uniform across the plate element, with maximum stresses close to the supported edges of the plate and minimum stresses in the buckled regions. Increasing the compressive stresses further will eventually cause parts of the plate to reach yield, plasticity will spread, and the ultimate capacity of the plate or cross-section will be reached. Equation (2.25) provide the elastic critical stress level at which local buckling initiates in a rectangular plate, which was originally presented by Bryan (1890).

$$\sigma_{cr} = \frac{\pi^2 E}{12(1 - \nu^2)} \frac{k_{\sigma}}{(b/t)^2} \quad (2.25)$$

where σ_{cr} is the elastic buckling stress, E is the Young's modulus, ν is the poisson's ratio, k_{σ} is the plate buckling coefficient, b is the width of the plate and t is the thickness of the plate.

It is clear from the formula that as the width-to-thickness ratio (b/t) increases, the elastic buckling stress of the plate reduces. The buckling of a plate depends on several factors, which are boundary conditions, plate geometry, stress distribution and element interaction. Boundary conditions of a plate are directly influenced by whether the plate is

an outstand or internal element. In design, all plates in a member are generally assumed to be long as the length of the member is normally significantly greater than the cross-section dimensions. In regard to stress-distribution, a uniform compressive stress across the plate is the most severe in causing local buckling and the buckling factor will be a minimum for this condition.

Set values for buckling coefficient (k_{σ}) can be found in literature such as Bleich (1952), Allen and Bulson (1980), Rhodes (1991) and Galambos (1998). EN 1993-1-5 (2006) provides buckling coefficient values for outstand and internal elements under various stress distributions. Some typical values are given as follows: for outstand and internal elements under uniform compression, k_{σ} is equal to 0.425 and 4.0, respectively. For an internal element under pure bending, k_{σ} is equal to 23.9.

Eurocode 3 applies a cross-section classification in the form of limiting width-to-thickness ratios for individual elements and the classification of the overall cross-section is taken as that of the least favourable of the individual elements. Four discrete behavioural classes of cross-sections, as shown in Figure 2.12 are defined.

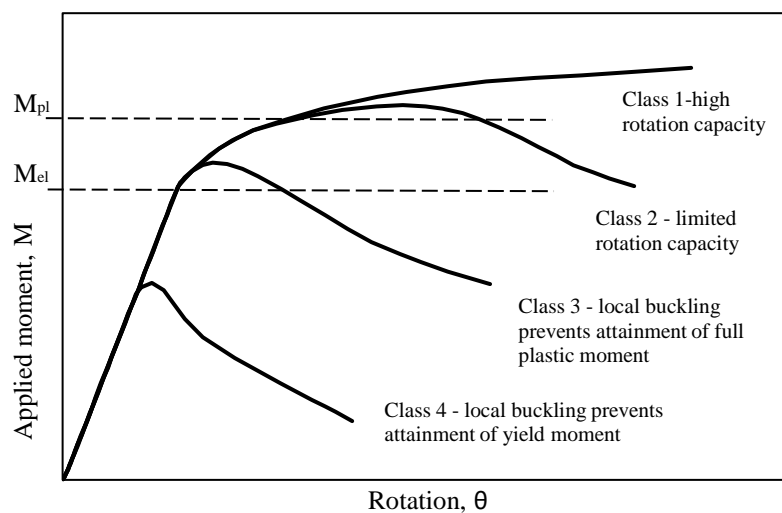


Figure 2.12: Four behaviour classes of cross-section as defined by Eurocode 3 EN 1993-1-1 (2005).

Cross-sections with very high deformation capacity are classified as Class 1. Class 1 cross-sections are fully effective under pure compression and capable of reaching and maintaining their full plastic moment in bending (M_{pl}). Class 2 cross-sections have a somewhat lower deformation capacity but are also fully effective in pure compression and capable of reaching their full plastic moment in bending. Class 3 cross-sections are fully effective in pure compression, but local buckling prevents attainment of the full plastic moment in bending. Bending moment resistance is therefore limited to the yield moment (M_{el}). For Class 4 cross-sections, local buckling occurs in the elastic range. An effective cross-section is therefore defined based on the width-to-thickness ratios of the individual plate elements, and this is used to determine the cross-sectional resistance.

However, the Eurocode 3 cross-section classification framework is best suitable for materials that closely follow an elastic-perfectly plastic stress-strain response such as carbon steels at room temperature (Gardner and Theofanous, 2008). The cross-section classification approach for metallic materials have such as stainless steel, high strength steel and aluminium, becomes unsuitable as these materials a more rounded and non-linear stress-strain response. For Class 4 or slender sections, since local buckling prevents attainment of full cross-sectional strength, this needs to be considered and reduced resistance evaluated. In order to determine the cross-sectional resistance of slender sections, effective width concept is utilised.

The effective width concept is well established and is included in Eurocode 3 (EN 1993-1-5, 2006). The method was first proposed by Von Karman et al. (1932), observing that the majority of the compressive load is carried by the regions of the plate in close vicinity of the edges. In addition, they suggested that the maximum stress acts uniformly over two strips of a simply supported plate and the central region is unstressed. Thus, only a certain proportion of the width is considered effective in resisting the applied compressive

stresses. Von Karman's Effective Width concept for an internal element under pure compression is illustrated in Figure 2.13.

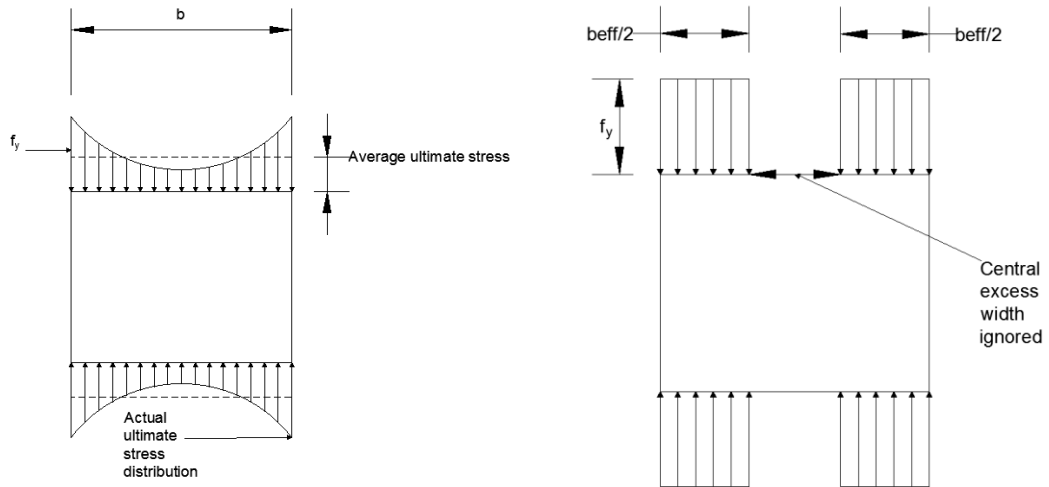


Figure 2.13: Von Karman's Effective Width concept for a simply supported plate

The proposed expression for the maximum stress and effective width is given in Equation (2.26). Where in Figure 2.13 f_y is the yield stress and b_{eff} is the effective width concept defined later on.

$$\frac{\sigma_{max}}{f_y} = \frac{b_{eff}}{b} = \frac{1}{\bar{\lambda}_p} \quad (2.26)$$

where σ_{max} is the maximum stress in a plate, f_y is the yield stress, b_{eff} is the effective width, b is the width of the plate, $\bar{\lambda}_p$ is the generalised plate slenderness. The parameter $\bar{\lambda}_p$ is known as the dimensional plate slenderness parameter defined in Equation (2.27) as follows:

$$\bar{\lambda}_p = \sqrt{\frac{f_y}{\sigma_{cr}}} \quad (2.27)$$

where σ_{cr} is the elastic buckling stress given in Equation (2.25).

Von Karman's effective width Equation (2.26) was based on a perfect plate and the behaviour of actual plates is affected by the existence of residual stresses and geometric

imperfections, which have the tendency to reduce the effective width of a plate from the theoretical value. Successively, Winter (1947) and Winter and Lansing (1950) modified Von Karman's formulation to take account of this and it is now used in EN 1993-1-5 (2006) to account for local buckling in slender plate elements.

As mentioned earlier, elastic critical buckling stress defined in the previous section may be calculated for a cross-section by taking the least critical stress determined for each of the individual plate elements, assuming simply supported edges at junctions with adjacent elements. Though, this explanation can be overly conservative; for some cross-sections, the plate elements are of varying local slenderness and can also be under different stress distributions. The greater this difference in slenderness or flexibility, the effect of element interaction becomes more predominant. For some cross-sections, element interaction is not present; for example, in a square hollow section with uniform thickness and subjected to pure compression, all plate elements buckle simultaneously at the same buckling stress. On the other hand, the same cross-section under bending moment may develop element interaction as the stress distribution is different in the four elements. In order to achieve a more precise assessment of local buckling, element interaction using the elastic buckling stress of the whole cross-section may be considered.

In order to overcome the short comings associated with the cross-section classification approach, alternative design methods, such as the Direct Strength Method (DSM) (Schafer, 2008) and the Continuous Strength Method (CSM) (Gardner, 2008) have been proposed. The direct strength method provides a series of strength curves, for different load instability failure modes, as a function of the cross-section slenderness. The Continuous Strength Method (CSM) is a deformation based design approach, which use the base curve to provide a continuous relationship between the deformation capacity of a cross-section and its slenderness. The deformation capacity is used together with elastic-

linear hardening material model to obtain the predicted load carrying capacity of the cross-section.

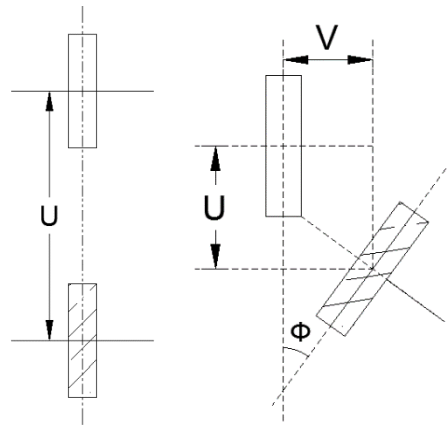
2.3.1.2 Global buckling

In the early eighteen century, van Musschenbroek (1729) documented that column strength is related to its length. Euler (1759) derived the first formula to determine the elastic buckling load. The formula used linear theory based on elastic material behaviour and small deflection approximations for perfect columns. In order to consider the material non-linearity into consideration, efforts made by Shanley (1947) suggested replacing the initial Young's modulus with the tangent modulus in the original Euler Equation, which has led to give better comparison to test results. In contrast the presence of residual stresses and geometric imperfections complicate the problem. In order to overcome this, with the assistance of computational resources, the European Convention for Constructional Steelwork (ECCS) established column design curves on the basis of finite element results (Beer and Schulz, 1970; Sfantesco, 1970; Jacquet, 1970). A number of assumptions were implemented such as a half-sine wave as the deflection shape, assuming $L/1000$ as the initial imperfection, where L is the column length (Beer and Schulz, 1970). A set of five buckling curves were developed and described using the Ayrton-Perry formula, and are currently implemented in EN 1993-1-1 (2014). Those for stainless steel are implemented in EN 1993-1-4 (2015). Only one buckling curve is provide for structural fire design in EN 1993-1-2 (2005). It should be noted that the buckling curves produced are mainly for normal structural carbon steel strength.

2.3.2 Beam

Similar to columns, beams can be prone to local and global buckling. Generally, for beams, the primary global buckling mode is referred to as lateral torsional buckling.

Beams generally show two types of behaviour: in-plane bending and lateral torsional buckling (Figure 2.14). A beam failure mode is generally dependent on the member slenderness and restraint conditions. Figure 2.14 displays the structural behaviour of beam under loading condition, where U is the vertical deflection, V is the lateral deflection and ϕ is the rotation of the member.



(a) Section - In-plane bending (b) Section - Lateral torsional buckling
Figure 2.14: Structural behaviour of beams

2.3.2.1 In-plane behaviour

In the early 19th century, Navier (1826) proposed a fundamental beam theory based on the previous findings of Jacob Bernoulli and Leonard Euler. A vital assumption of beam theory is that plane sections remain plane after bending. Since then, extensive research into the behaviour of beams has been performed; a detailed appraisal of these studies can be found in Timoshenko (1930). The meaning of simple beam theory assumes that no local instability of a beam cross-section will occur.

2.3.2.2 Lateral torsional buckling behaviour

In the late nineteenth century, it was recognised, similar to columns, that the strength of beams is related to the length of the member. Lateral torsional buckling is a combination of flexural buckling and torsional buckling. Flexural buckling represents itself with a

buckling failure of a member in the plane of a principle axis without any rotation of the cross-section, similar to in plane bending. The resistance of flexural buckling is dependent on the flexural rigidity EI , in which E is the Young's modulus and I is the second moment of area of the cross-section relevant to its principal plane. On the other hand, torsional buckling is concerned with the twisting of the member and is related to the torsional stiffness G and J of the member, where G is the torsional rigidity and J is the torsion constant, which is related to the second moment of area.

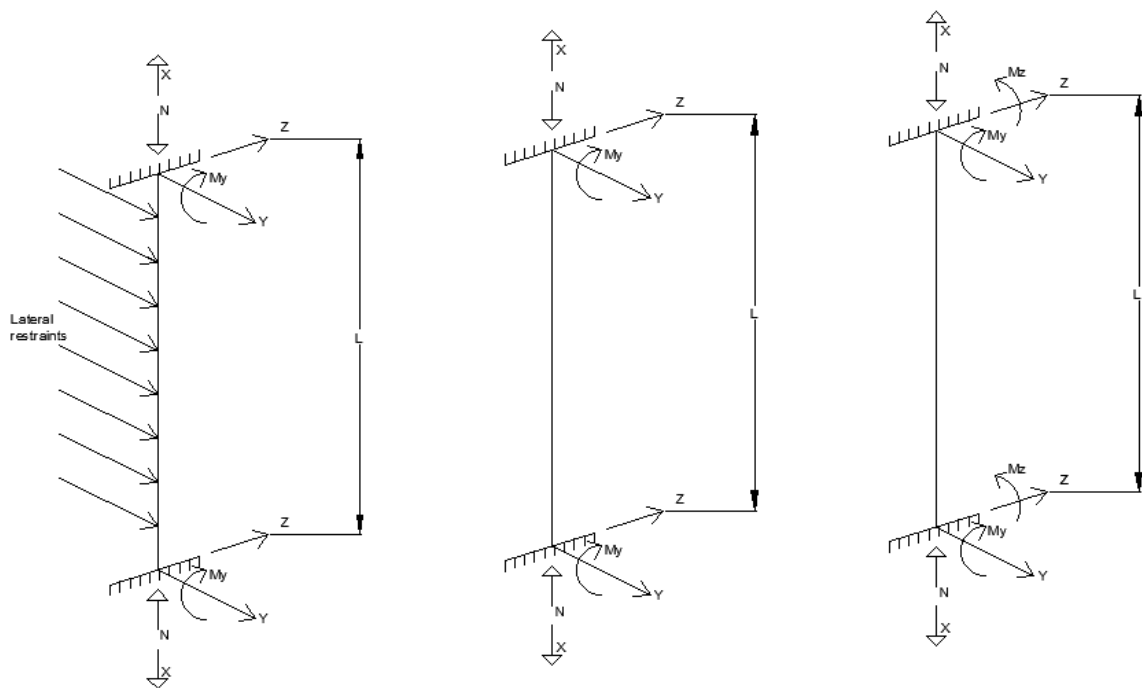
It should be noted that most of the previous research on lateral torsional stability of beams has focused on I-sections (Foster, 2014). Pi and Trahair (1995) and Zhao et al. (1995) investigated the lateral torsional buckling of beams of cold-formed rectangular hollow sections. Test results revealed that existing design rules, which are mainly based on I-sections beams, were conservative and inappropriate when applied to cold-formed rectangular hollow section beams and modifications to design formula were proposed.

2.3.3 Beam-columns

Beam-columns are structural members which combine the features of beam bending and column buckling. Theoretically, all structural members may be regarded as beam-columns, since the common classification of tension, compression and beam members is merely limiting examples of beam-columns. Beam-columns may act in isolation, as in the case of eccentrically loaded compression members with simple end connections, or they may form part of a rigid frame. There are many types of behaviour of isolated beam-columns, such as in plane behaviour, lateral torsional buckling and biaxial bending (Figure 2.15).

In-plane behaviour refers to a beam-column which is under axial compressive force (N) and bending moment about cross-section major axis (M_y) while being restrained against

lateral deflections. Lateral torsional buckling is found in a beam-column which is bent about its stronger principal axis and is not restrained laterally; it may buckle prematurely out of the plane by deflecting laterally and twisting. More generally, a beam-column, which is bent about both principal axes (M_y and M_z), is regarded as biaxial bending, which involves interaction of a beam bending and column buckling (Trahair et al., 2008). The literature on the in-plane behaviour of beam-column is reviewed in the following subsection as this is relevant to this study.



(a) In-plane behaviour (b) Lateral torsional buckling behaviour (c) Biaxial bending behaviour

Figure 2.15: Systematic loading and support conditions of beam-column members.

2.3.3.1 In-plane behaviour

In the late nineteenth century, numerous researchers studied the elastic behaviour of beam-column members and a full description of the solutions is provided by Timoshenko and Gere (1989) for various end conditions. By the early twentieth century, studies on plastic analysis of beam-columns commenced by von Kármán (1908) and von Kármán

(1910). Subsequently, numerous methods have been reported, such as the curvature method (Chen and Atsuta, 1976 and Chen and Atsuta,1977) and the moment method (Cheong Siat Moy, 1974a and Cheong Siat Moy, 1974b), taking into account different loading conditions and cross-sectional shapes. Drastic simplifications and idealisations were made in solving the beam-column problems, which included idealising the material as elastic-perfectly plastic, establishing equilibrium only at mid-height or a number of stations along the length of the beam-column, by idealising the shape of biaxial moment curvature.

In order to provide a practical design method for in-plane beam-columns, further simplifications were developed. Design rules were developed on two conditions, the interaction criteria and first yield criteria. The interaction criteria predicts the ultimate resistance of a beam-column member by axial load and moments (Trahair et al., 2008). More recently, Zhao et al., (2015a); Zhao et al., (2015b); Zhao et al., (2016) investigated stainless steel SHS and RHS sections under combined axial compression and bending experimentally, numerically and analytically. Buchanan (2018) conducted laboratory testing and finite element modelling on stainless steel beam-column CHS at cross-sectional and member level. These will be discussed further in detail in Chapter 3.

2.4 Numerical modelling

Testing members in fire can be time-consuming and highly costly. Numerical modelling has gained an increased usage, when used in parallel with testing by a number of researchers. Validation is first performed and agreements between model results and test results is obtained by selecting suitable representation geometric and material input parameters. This is subsequently followed by a parametric study, to generate further structural performance data. The modelling assumption including the element type,

material modelling, residual stresses, geometric imperfection and the analysis technique which have been used in literature, numerical modelling investigation of stainless steel structures in fire are discussed hereafter. The finite element (FE) package used through this study was ABAQUS (2016).

2.4.1 Element type

Shell elements are used to model stainless steel thin walled structural components. The most common shell element used is the S4R, which has four corner nodes, each having six degrees of freedom with reduced integration and finite membrane strains, which have performed well in previous studies at room temperature and in fire by Gardner and Nethercot (2004), Gardner and Baddoo (2006), Ng and Gardner (2007), Theofanous and Gardner (2009), Theofanous et al. (2009), Foster (2014), Zhao et al. (2015b), Zhao et al. (2016) and Buchanan (2017) for square hollow sections (SHS), rectangular hollow sections (RHS), circular hollow sections (CHS), Elliptical hollow sections (EHS) and I-sections.

A suitable mesh which is able to find accurate results is paramount in numerical modelling. Larger or coarser meshes can provide inadequate results, whilst using a finer mesh can provide precise modelling. Mesh sensitivity analysis are usually performed, as carried out in the numerical models presented in this thesis, to find a suitable mesh size where balance of accuracy and computational efficiency can be achieved.

2.4.2 Material modelling

The FE package ABAQUS used for this study requires that the material properties are defined in terms of true stress and log plastic strain as defined in Equations (2.28) and (2.29), respectively. Firstly, the measured engineering stress and strain curves from tensile coupon data must be represented by the two stage Ramberg-Osgood material

model, and subsequently converted into the true stress-log plastic strain curves, which are then input to ABAQUS.

$$\sigma_{\text{true}} = \sigma_{\text{nom}} (1 + \varepsilon_{\text{nom}}) \quad (2.28)$$

$$\varepsilon_{\text{ln}}^{\text{pl}} = \ln(1 + \varepsilon_{\text{nom}}) - \frac{\sigma_{\text{true}}}{E} \quad (2.29)$$

where σ_{true} and $\varepsilon_{\text{ln}}^{\text{pl}}$ are the true stress and logarithmic plastic strain, respectively. E is the Young's modulus and σ_{nom} and ε_{nom} are the engineering stress and strain, respectively.

2.4.3 Geometric imperfections

Geometric imperfections are found in real stainless-steel members, which significantly affect their structural behaviour. They are introduced during the production, fabrication and handling process. When performing an FE analysis to predict the ultimate load, the model, in general, should include local and global geometric imperfections. Initial local and global imperfection can be incorporated into the FE models in the form of the lowest elastic buckling mode shapes under the correct loading conditions (Gardner and Nethercot 2004; Ashraf et al. 2007 and Zhao et al. 2015b). These buckling mode shapes tend to represent the most unfavourable imperfection patterns and should be determined prior to the non-linear analysis. Generally, during testing, local and global measured imperfection amplitudes are taken and applied into FE models for validation. Alternatively, structural local imperfection amplitude can be determined from predictive models (Dawson and Walker 1972; Gardner and Nethercot 2004) and the global imperfection amplitudes can be assumed as suitable representation value during an imperfection study (Zhao et al., 2015b).

2.4.4 Residual stresses

Residual stresses are encountered during the manufacturing and fabrication process of members. The plastic deformation process introduces bending residual stresses. These bending residual stresses have been studied previously by Cruise and Gardner (2008), and it was concluded that if the coupons are cut from the same tubular member, the effects of the bending residual stresses are present within the measured material properties and do not need be defined separately. In addition, membrane residual stresses can be induced during welding. The differential cooling from the welding has minimum effect on the performance on FE models of cold-formed tubular sections (Gardner and Nethercot, 2004; Ashraf et al., 2007). Hence, residual stresses are not usually explicitly defined in FE models of stainless steel structures (Zhao et al. 2016).

2.4.5 Analysis technique solution

The analysis technique used for thin walled structures is affected by the material and geometric non-linearities. Upon incorporating the local and global imperfections into the FE models, the modified Riks methods has been employed for isothermal conditions to perform the geometrically and materially non-linearity analyses to capture the full load-deformation response of the specimens, including post ultimate path. The static method was used for anisothermal conditions to trace the axial displacement against temperature. These methods are discussed further in Chapters 3, 4 and 5.

2.5 Concluding remarks

The purpose of this literature review was to provide an initial evaluation of the subjects that are being investigated within this thesis, allowing additional literature to be introduced and examined in further detail within the appropriate chapter. In general, research into stainless steel structures in fire conditions has been relatively limited;

however, the currently available stainless steel standards in fire, which have been developed on carbon steel design codes were noted. With the expense of stainless steel being four to six times higher than that of carbon steel, the importance of developing efficient design standards for stainless steel structural elements in fire is paramount and is the focus of this thesis.

Chapter 3 Numerical modelling and validation of elements

3.1 Introduction

In recent years, numerical modelling such as finite element (FE) methods have become valuable to structural engineering research. With respect to structural fire design, FE analysis can provide suitable means of understanding the stability of steel and stainless steel structural members in fire conditions, without performing experimental tests, which can be time consuming and expensive. Furthermore, FE methods allow control of vital test parameters and avoid scatter, which are generally present in test data. However, since analytical and FE methods only provide an approximation of the response of a real life structure, prior to any numerical modelling analysis, at the preliminary stage, validation of the numerical models against relevant test data from literature experiments is vital.

In order to commence towards the numerical modelling investigations in this thesis, a comprehensive numerical validation study was carried out which is presented in this chapter. Firstly, test data were collected where particular attention from the literature test programmes was paid and carefully reviewed. This was followed by the development of the numerical models to the important modelling parameters such as element types, mesh size, material modelling, geometric imperfections, residual stresses, boundary conditions and constraints and analysis techniques procedures. The general purpose finite element (FE) package (ABAQUS, 2016) was employed throughout this study. The validated numerical models described in this chapter are used for the parametric study

investigations carried out in Chapter 4 and 5. The numerical modelling assumptions relevant to the parametric study models are further explained in their respective chapters.

3.2 Test results from literature

The data collected from the literature consisted of cross-section and member level column and beam-column tests. The collected results included both steel and stainless steel materials, isothermal and anisothermal test conditions, and a variety of cross-sectional shapes. In the upcoming sections, a brief description of the test programmes on the columns and beam-columns used for validation is described.

3.2.1 Brief description of column test programmes

Since the focus of this thesis was on stainless steel square (SHS), rectangular (RHS) and circular (CHS) hollow section column and beam-column members in fire, the results of tests on these structural members were sought from literature experimental programmes. For the validation of the SHS and RHS column models, the fire tests carried out by Tondini et al. (2013), Ala-Outinen and Oksanen (1997) and Baddoo and Gardner (2000) were used. For the validation of the CHS column models, where no fire test results from literature were available, the results of room temperature test by Zhao et al. (2016a) and Buchanan et al. (2018) were used.

The key details of the elevated temperature tests on SHS and RHS columns carried out by Tondini et al. (2013), Ala-Outinen and Oksanen (1997) and Baddoo and Gardner (2000), including stainless steel grade, boundary conditions, measured column length (L), applied load and critical temperature (θ_{crit}) are reported in Table 3.1 and those for the room temperature tests on CHS columns performed by and reported in Zhao et al. (2016a) and Buchanan et al. (2018) are presented in Table 3.2, where in addition, the measured ultimate load (N_u) is reported.

Table 3.1: Summary of the elevated temperature SHS and RHS column tests

Specimen reference	Grade	Boundary conditions	L (mm)	Applied load (kN)	θ_{crit} (°C)
SHS 80×80×3 ^a	Ferritic EN 1.4003	Fixed	3000	72	709*
SHS 80×80×3 ^a			2500	78	708*
RHS 120×80×3 ^a			2500	100	705*
SHS 40×40×4-T1 ^b	Austenitic EN 1.4301	Pinned	888.5	45	872
SHS 40×40×4-T2 ^b			888.5	129	579
SHS 40×40×4-T3 ^b			888.0	114	649
SHS 40×40×4-T4 ^b			888.0	95	710
SHS 40×40×4-T5 ^b			888.0	55	832
SHS 40×40×4-T7 ^b			888.5	75	766
RHS 150×100×6 ^c	Austenitic EN 1.4301	Fixed	3400	268	801
RHS 150×75×6 ^c			3400	140	883
RHS 100×75×6 ^c			3400	156	806

Notes:

^a Test reported by Tondini et al. (2013)

^b Test reported by Ala-Outinen and Oksanen (1997)

^c Test reported by Baddoo and Gardner (2000)

* Critical furnace temperature.

Table 3.2: Summary of the room temperature CHS column tests

Specimen reference	Grade	Boundary conditions	L (mm)	N_u (kN)
CHS 60.5×2.8 ^d	Austenitic EN 1.4301	Pinned	1450	90.5
CHS 76.3×3 ^d			1450	146.0
CHS 106×3-550 ^e	Austenitic EN 1.4432	Pinned	554.27	267.0
CHS 106×3-1150 ^e			1154.0	248.8
CHS 106×3-3080 ^e			3083.0	150.8
CHS 88.9×2.6-400 ^e	Duplex EN 1.4462	Pinned	403.9	425.2
CHS 88.9×2.6-1650 ^e			1656.6	243.4
CHS 88.9×2.6-3080 ^e			3082.5	100.5
CHS 80×1.5-700 ^e	Ferritic EN 1.4512	Pinned	698.6	111.1
CHS 80×1.5-900 ^e			899.1	105.8
CHS 80×1.5-1600 ^e			1599.3	77.9

Notes:

^d Test reported by Zhao et al. (2016a)

^e Test reported by Buchanan et al. (2018)

The SHS and RHS columns tested by Tondini et al. (2013) and Ala-Outinen and Oksanen (1997) were formed by cold-forming, where flat sheet material was first made into a circular tube by cold-rolling and closed by seam-welding and then made into the required cross-section size and geometry. For the RHS columns tested by Baddoo and Gardner

(2000), two channel sections, formed by press-braking, were welded tip-to-tip in the longitudinal direction. The CHS columns tested by Zhao et al. (2016a) and Buchanan et al. (2018) were also cold-formed, where the sheet material was cold-rolled into a circular tube and subsequently welded closed.

Anisothermal fire test method was employed for all the SHS and RHS axially loaded members presented in Table 3.1, where the specimens were first loaded at ambient temperature, which was kept constant, and then the temperature was set to increase until the failure was reached at temperature θ_{crit} . The critical temperature θ_{crit} reported in Table 3.1 refers to the specimen temperature at failure for the austenitic columns tested by Ala-Outinen and Oksanen (1997) and Baddoo and Gardner (2000) and the furnace temperature at failure for the ferritic columns tested in Tondini et al. (2013).

3.2.2 Brief description of beam-column test programmes

A number of experimental programmes have been reported on stainless steel SHS, RHS and CHS beam-columns at cross-section level and member level at room temperature by Zhao et al. (2015a, 2016a, 2016b). Two tests on stainless steel SHS beam-column members at elevated temperature were carried out by Fan et al. (2016). Owing to the limited number of stainless steel beam-column tests at elevated temperature, additional test data on carbon steel RHS beam-column members carried out by Pauli et al. (2012) were also employed.

Table 3.3 and 3.4 provide a summary of the cross-section level and member level tests, respectively, on SHS and RHS beam-columns carried out in Zhao et al. (2015a) and Zhao et al. (2016b). Table 3.5 presents the key results of tests on CHS beam-column tests reported in Zhao et al. (2016a). In Tables 3.3 - 3.5, the grade of stainless steel, the boundary conditions, the applied eccentricity (e_y and e_z as explained in Figure 3.1), the

member length (L) and the failure load (N_u) are provided. The tested cross-section in Table 3.3 - 3.5 were formed by cold-rolling production-route as described previously.

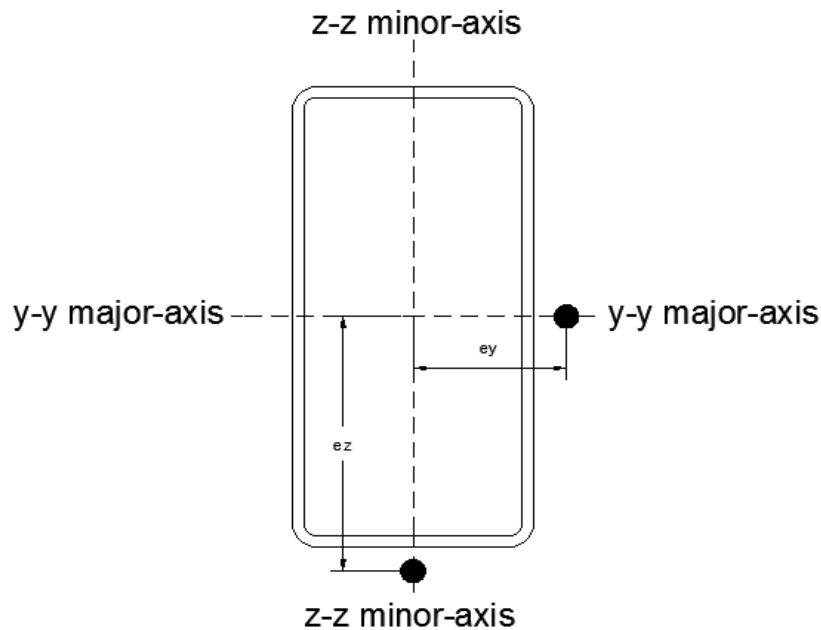


Figure 3.1: Major and minor axis for a RHS

Table 3.6 reports the results of stainless steel SHS beam-column tests performed by Fan et al. (2016); these tests were performed anisothermally. The applied load (N) and the specimen failure temperature θ_{crit} together with other test parameters, as described previously, are presented. Table 3.7 presents the key details and results of the carbon steel RHS beam-column tests reported by Pauli et al. (2012), where an isothermal test approach was employed. The test failure loads (N_u) and the applied isothermal temperature θ together with other test parameters, as described previously, are presented.

Table 3.3: Summary of stainless steel SHS and RHS stub column and beam-column tests

Specimen reference	Grade	Boundary conditions	e_y (mm)	e_z (mm)	L (mm)	N_u (kN)
SHS 100×100×5	Austenitic EN 1.4301	Fixed	0.0	0.0	349.9	1057.0
SHS 120×120×5	Austenitic EN 1.4571		0.0	0.0	399.9	928.4
RHS 150×100×6	Austenitic EN 1.4307		0.0	0.0	450.1	1323.7
RHS 150×100×8	Austenitic EN 1.4404		0.0	0.0	450.0	1825.1
SHS 150×150×8	Duplex EN 1.4162		0.0	0.0	449.8	3257.9
SHS 100×100×5	Austenitic EN 1.4301	Pinned	20.0	0.0	350.0	743.5
			25.0	0.0	350.0	622.2
			50.0	0.0	350.0	472.7
SHS 120×120×5	Austenitic EN 1.4571		10.0	0.0	399.9	793.5
			40.0	0.0	400.0	550.0
			70.0	0.0	400.0	424.0
RHS 150×100×6	Austenitic EN 1.4307		120.0	0.0	399.8	296.1
			45.0	0.0	350.1	825.2
			65.0	0.0	449.8	685.3
			95.0	0.0	450.1	575.7
RHS 150×100×8	Austenitic EN 1.4404	130.0	0.0	450.0	473.4	
		0.0	20.0	450.0	1173.8	
		0.0	50.0	450.2	800.1	
SHS 150×150×8	Duplex EN 1.4162	0.0	75.0	450.0	626.9	
		30.0	0.0	449.8	2186.7	
		55.0	0.0	450.0	1814.9	
		85.0	0.0	450.0	1403.6	
			120.0	0.0	450.1	1186.9

Note: Test reported by Zhao et al. (2015a)

Table 3.4: Summary of stainless steel SHS and RHS column and beam-column member tests

Specimen reference	Grade	Boundary conditions	e_y (mm)	e_z (mm)	L (mm)	N_u (kN)
SHS 60×60×3	Ferritic EN 1.4003	Pinned	10.0	0.0	774.8	199.6
			30.0	0.0	774.8	124.1
			40.0	0.0	774.8	104.7
			80.0	0.0	774.8	65.0
			125.0	0.0	774.8	46.4
RHS 100×40×2			0.0	2.0	674.8	153.2
			0.0	10.0	674.8	106.9
			0.0	30.0	674.8	62.7
			0.0	45.0	674.8	46.3
			0.0	75.0	674.8	32.0

Note: Test reported by Zhao et al. (2016b)

Table 3.5: Summary of stainless steel CHS beam-column member tests

Specimen reference	Grade	Boundary conditions	e_y (mm)	e_z (mm)	L (mm)	N_u (kN)
CHS 60.5×2.8	Austenitic EN 1.4301	Pinned	5.0	0.0	1450.0	18.9
			15.0	0.0	1450.0	25.7
			25.0	0.0	1450.0	29.0
			40.0	0.0	1450.0	34.9
			85.0	0.0	1450.0	43.1
CHS 76.3×3			10.0	0.0	1450.0	16.4
			20.0	0.0	1450.0	19.6
			30.0	0.0	1450.0	22.9
			50.0	0.0	1450.0	26.6
			95.0	0.0	1450.0	34.3

Note: Test reported by Zhao et al. (2016a)

Table 3.6: Summary of the elevated temperature SHS beam-column tests

Specimen reference	Grade	Boundary conditions	L (mm)	e_y (mm)	e_z (mm)	Load (N)	θ_{crit} (°C)
SHS 120×120×4	Austenitic EN 1.4301	Pinned	3300	13.2	0.0	160	700.8
			3300	23.8	0.0	140	665.0

Note: Test reported by Fan et al. (2012)

Table 3.7: Summary of elevated temperature carbon steel RHS column and beam-column tests

Specimen reference	Grade	Boundary conditions	L (mm)	Temperature (°C) θ	e_y (mm)	e_z (mm)	N_u (kN)
RHS 120×60×3.6	Carbon steel S355	Pinned	360	400	0	0	408
			360	400	0	10	280
			360	400	0	50	133
			360	550	0	0	257
			360	550	0	10	205
			360	550	0	50	87
			360	700	0	0	74
			850	550	0	30	96
			1840	400	0	0	242
			1840	400	0	10	139
			1840	400	0	50	73
			1840	550	0	0	186
			1840	550	0	10	111
			1840	550	0	50	49
			1840	700	0	0	71

Note: Test reported by Pauli et al. (2012)

3.3 Development of numerical models

Numerical models of stainless steel columns and beam-columns were developed, which were validated against the selection of collected test data presented in Section 3.2. This section presents the development of the numerical models within this research study.

3.3.1 Element type

In finite element packages, there are a variety of element types which can be utilised and considered for specified applications. Elements are characterised and separated by the number of nodes, degrees of freedom, full and reduced integration, structural point of view (shell, solid, beam and truss) and the formulation. The nodes of an element refer to the nodal degree of freedom which are included in the element domain. The mathematical theory applied for shell elements behaviour corresponds to the formulation of Kirchoff and Mindlin-Reissner for thin and thick shells, respectively. The element stiffness is calculated through specific points which are known as integration points. Full and reduced integration methods correspond to the case that the integration order is the minimum required for the precise integration of strain energy. Shell elements features a three-dimensional idealisation of a solid where the thickness is considered to be smaller compared other dimensions (ABAQUS, 2016).

In thin-walled stainless steel structures where cross-section and member deformations are important, structural sections are better represented using shell elements (Bathe, 2014). Shell elements are utilised throughout this research study to model thin SHS, RHS and CHS structural members. The general-purpose four-noded three-dimensional shell element S4R (ABAQUS, 2016) with reduced integration was used for all the stress analysis models developed herein. For the thermal models, where heat transfer analysis were conducted, the DS4 element, which is compatible with S4R element, were employed. The elements have been utilised for stress analysis and heat transfer analysis of carbon steel and stainless steel structural elements by a number of researchers e.g. Gardner and Nethercot (2004) and Ng and Gardner (2007).

3.3.2 Mesh

Achieving an adequate mesh for a numerical model is an important parameter to achieve precise results. A larger mesh or more known as a coarser mesh can result in insufficient solution; while, these issues can be overcome by using a finer mesh, the disincentive is that it can result in an increase in the computational time to the required complete analysis. In order to find the appropriate mesh element size that captures accurate results but at the same time provides efficient computational time, a mesh sensitivity study was performed for the developed numerical models. Figure 3.2 and 3.3 illustrate an example of a mesh convergence study for the developed numerical models of specimen SHS 120×120×5 stub column tested in Zhao et al. (2015a).

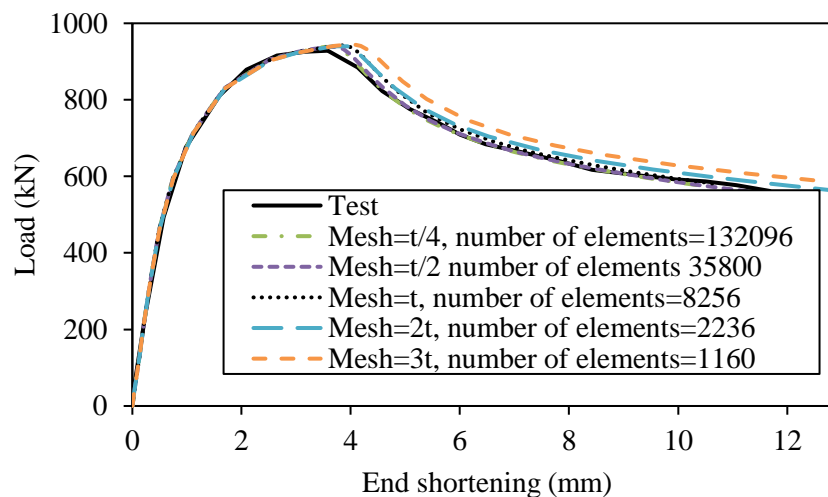


Figure 3.2: Mesh sensitivity SHS 120×120×5

Different element mesh sizes, as a multiple of the cross-section thickness (t) were employed to discretise the model. As expected, the ability of the model to capture the load-displacement response, particularly for the post-buckling region, improved with reducing the element size. However, the prediction accuracy of the ultimate load seemed to be less sensitive to the adopted mesh size. Following the analysis, a mesh size equal to the cross-section thickness (t) for the flat regions and four elements for the curved regions

of the cross-section, provided the best balance between computational time and accuracy, and thus was applied to the numerical models.

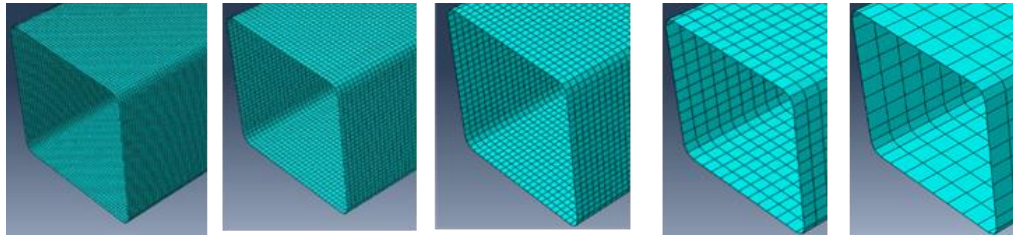


Figure 3.3: Finer mesh to coarser mesh

3.3.3 Material modelling

Modelling the stress-strain response of the material represents one of the main vital aspects of a numerical model. Inaccurate material modelling of a structure or a member can lead towards overshadowing the performance of the refined numerical model. In order to simulate the material behaviour of stainless steel, data from material tests, e.g. tensile coupon test, can be adopted. The material properties which were inserted into the validation numerical models developed in this chapter were based upon the measured stress-strain responses at room and elevated temperatures, which were reported in the test programmes. Since cold-formed stainless steel tubular sections include strength enhancements in their corner regions, different stress-strain response curves were assigned to the regions as described in the following.

In the column test programme by Baddoo and Gardner (2000), the elevated temperature stress (σ_θ)-strain (ϵ_θ) responses for the unformed material sheets from which the channel sections were fabricated by press-braking was measured by conducting isothermal tests at $\theta = 20 - 1000^\circ\text{C}$. Ala-Outinen and Oksanen (1997) performed tensile anisothermal tests on the material belonging to the flat parts of the cold-rolled hollow sections; these were subsequently converted to stress (σ_θ) - strain (ϵ_θ) relationships at discrete temperatures in the range of $\theta = 20 - 900^\circ\text{C}$. For these columns Baddoo and Gardner (2000) and Ala-

Outinen and Oksanen (1997), the measured elevated temperature stress (σ_θ)-strain (ϵ_θ) responses were used to describe the material behaviour for the flat parts of the SHS and RHS columns in the developed validation FE models.

For the case of the SHS and RHS ferritic columns by Tondini et al (2013) in the absence of measured elevated temperature stress-strain responses, the two-stage elevated temperature Ramberg-Osgood material model recommended in the Design Manual for Stainless Steel Structures (2017) as provided by Equations (3.11) and (3.12) was employed to construct full range stress (σ_θ)-strain (ϵ_θ) relationships at temperatures $\theta = 20 - 800$ °C. The reduction factors pertaining to grade EN 1.4003 provided in (DMSS, 2017) together with the room temperature material properties measured in the tests were used. These were used to describe the material behaviour of the flat portions of these columns in the developed FE models.

For the SHS and RHS columns tested by Baddoo and Gardner (2000), Ala-Outinen and Oksanen (1997) and Tondini et al. (2013) of the corner regions of the sections, the enhanced strength, associated with cold-forming effects, was included in the FE models as described hereafter. For the ferritic columns (Tondini et al., 2013), the room temperature corner material properties were measured. For the austenitic columns (Baddoo and Gardner, 2000; Ala-Outinen and Oksanen, 1997), the material properties for the corner regions of the sections were not measured, and hence the strength enhancement predictive equations from Cruise and Gardner (2008) for cold-rolled and press-braked stainless steel sections were employed to determine the room temperature strengths. Equations (3.1) and (3.2) in conjunction with the reduction factors for EN 1.4301 and EN 1.4003 from the Design Manual for Stainless Steel Structures (2017) for material with enhanced cold-formed strength were employed to construct continuous stress (σ_θ) - strain

(ε_θ) relationships to describe the material behaviour of the cold-worked corner regions at elevated temperatures.

$$\varepsilon_\theta = \frac{\sigma_\theta}{E_\theta} + 0.002 \left(\frac{\sigma_\theta}{\sigma_{0.2,\theta}} \right)^{n_\theta} \quad \text{for } \sigma_\theta \leq \sigma_{0.2,\theta} \quad (3.1)$$

$$\varepsilon_\theta = \frac{(\sigma_\theta - \sigma_{0.2,\theta})}{E_{0.2,\theta}} + \left(0.02 - \varepsilon_{0.2,\theta} - \frac{\sigma_{2.0,\theta} - \sigma_{0.2,\theta}}{E_{0.2,\theta}} \right) \left(\frac{\sigma_\theta - \sigma_{0.2,\theta}}{\sigma_{2.0,\theta} - \sigma_{0.2,\theta}} \right)^{n'_\theta} + \varepsilon_{t0.2,\theta} \quad \text{for } \sigma_{0.2,\theta} < \sigma_\theta < \sigma_{u,\theta} \quad (3.2)$$

In Equations (3.1) and (3.2), σ_θ and ε_θ are the engineering stress and strain, respectively, $\sigma_{0.2,\theta}$ is the 0.2% proof stress at temperature θ , $\sigma_{2.0,\theta}$ is the stress at 2.0% total stain at temperature θ , $\sigma_{u,\theta}$ is the ultimate tensile strength at temperature θ , $\varepsilon_{0.2,\theta}$ is the total strain corresponding to $\sigma_{0.2,\theta}$, E_θ and $E_{0.2,\theta}$ are the Young's modulus and the tangent modulus at $\sigma_{0.2,\theta}$ respectively at temperature θ , and n_θ and n'_θ are the exponential coefficients to define the degree of material nonlinearity at temperature θ .

For the room temperature CHS column tests in Zhao et al. (2016a) and Buchanan et al. (2018), reported values from tensile coupon tests on materials cut from the cold-formed sections were used to obtain the stress-strain response of the material, which were directly used in the development of the FE models of the CHS columns.

In the beam-column test programme reported by Zhao et al. (2015a, 2016a, 2016b), tensile coupons tests on specimens extracted from the flat and corner regions of cold-formed SHS/RHS and curved walls of CHS were performed to obtain the engineering stress-strain response of the material. The measured stress-strain curves were incorporated in their respective beam-column FE models. Pauli et al. (2012) and Fan et al. (2016) reported the results of isothermal tensile tests on material extracted from the flat faces of the tested carbon steel and stainless steel beam-column specimens,

respectively. The stress-strain curves for room temperature and elevated temperatures, 100 - 800°C in 100°C intervals were provided, which were employed in the FE models.

In order to simulate the material response into the FE models, ABAQUS requires the engineering stress-strain to be converted to true-stress and logarithmic plastic strain through Equations (3.3) and (3.4). This conversion is paramount since ABAQUS formulations have not been set in terms of engineering stresses (i.e. based on applied load divided by initial cross-section area). The true stress (i.e. based on applied load divided reduced area) is used instead.

$$\sigma_{\text{true}} = \sigma_{\text{nom}} (1 + \varepsilon_{\text{nom}}) \quad (3.3)$$

$$\varepsilon_{\text{ln}}^{\text{pl}} = \ln(1 + \varepsilon_{\text{nom}}) - \frac{\sigma_{\text{true}}}{E} \quad (3.4)$$

where σ_{true} is the true stress, $\varepsilon_{\text{ln}}^{\text{pl}}$ is logarithmic plastic strain, σ_{nom} is the nominal engineering stress, and ε_{nom} is the nominal engineering strain and E is the Young's modulus.

The engineering stress and strain are defined as $\sigma_{\text{nom}} = \frac{F}{A_0}$ and $\varepsilon_{\text{nom}} = \frac{\Delta L}{L_0}$ in which F is the applied force, A_0 is the original cross-sectional area, ΔL is the change in length, which is calculated as $\Delta L = L - L_0$, where L is the new length and L_0 is the original length. If it is assumed that beforehand and after an axial test, there is no transformation in volume, but the area reduces to A then:

$$A \cdot L = A_0 \cdot L_0$$

True stress is defined as:

$$\sigma_{\text{true}} = \frac{F}{A} = \frac{F}{A_0} \cdot \frac{L}{L_0}$$

True strain $\varepsilon_{\text{true}}$ is defined as the sum of engineering strain $c\varepsilon = \frac{cL}{L}$ so that:

$$\varepsilon_{\text{true}} = \int c\varepsilon = \int_{L_0}^{L_1} \frac{cL}{L} = \ln \frac{L_1}{L_0} = \frac{\ln(L_0 + \Delta L)}{L_0} = \ln(1 + \varepsilon_{\text{nom}})$$

The true plastic strain $\varepsilon_{\text{true}}$ defined in Equation (3.4) is purely the plastic part of the true strain, which is obtained by subtracting the elastic part of strain $\frac{\sigma_{\text{true}}}{E}$.

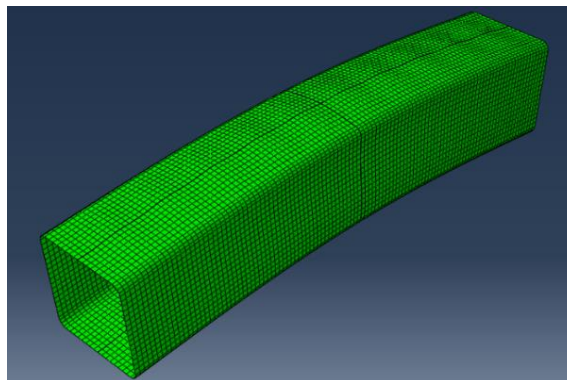
3.3.4 Initial geometric imperfections

Real structural members are not perfectly straight, as they contain geometric imperfections. Initial geometric imperfections are introduced in structural specimens during the production and manufacturing stages but lie within specific tolerances upon delivery. The behaviour of a metallic structural section can be significantly influenced by initial geometric imperfections, affecting their load carrying capacity and mode of failure. Initial geometric imperfections are broken down into local and global imperfections for numerical modelling purposes. Local geometric imperfections have a major influence on the local buckling capacity. Examples include models of short compression members (i.e. stub columns) and laterally restrained beams with in-plane bending response. Global imperfections have a major influence on the member buckling capacity of metallic structural members and need to be considered in numerical models that examine the member behaviour. Examples include models of flexural buckling behaviour of long columns and lateral torsional buckling behaviour of laterally unrestrained beams.

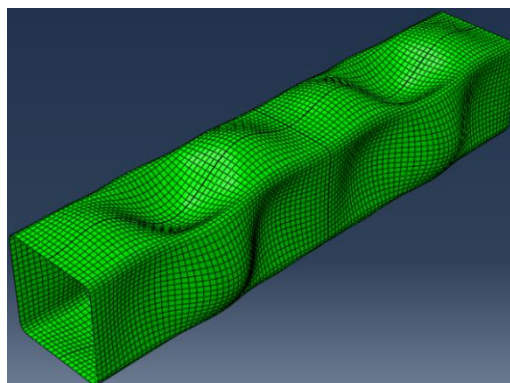
In this research, FE models include initially imperfect geometries corresponding to the most likely instability modes, which for columns and beam-column with thin-walled SHS, RHS and CHS cross-sections can be local, global or both. Suitable buckling eigenmodes extracted from the eigenvalue buckling prediction analysis were selected to represent the local and global imperfection patterns of the modelled columns, as illustrated in Figure 3.4. For the presented validation study, the amplitudes of the global

imperfection (ω_g) were set to the measured values in the tests; except for the elevated temperature tests performed in Ala-Outinen and Oksanen (1997) and Baddoo and Gardner (2000), for which a value of $L/1000$, (L = columns length), gave the closest agreement between the responses from test and FE. In the absence of the measured values, the local imperfection (ω_o) amplitudes were set to a portion of the thickness of the cross-section ($t/10$) for the CHS models, as recommended in Afshan et al. (2019), and those obtained from the modified Dawson and Walker predictive model (Gardner and Nethercot, 2004), as provided by Equation (3.5), for the SHS and RHS columns, where t is the thickness of the cross-section, $\sigma_{0.2}$ is the 0.2% proof stress and σ_{cr} is the plate element buckling stress.

$$\omega_o = 0.023t \frac{\sigma_{0.2}}{\sigma_{cr}} \quad (3.5)$$



(a) Typical global mode



(b) Typical local mode

Figure 3.4: Typical (a) global and (b) local buckling mode shapes for a SHS

3.3.5 Residual stresses

Stresses that exist in steel and stainless steel structural members in their unloaded state are termed as residual stresses. The overall influence of residual stresses on structural response is to encounter pre-mature yielding, leading to a loss in stiffness and reduction in load-bearing capacity. Residual stresses are produced during production of structural members and are related to the non-uniform plastic deformation induced during cold-working of cold-formed sections and the differential cooling observed in hot-rolled and welded sections. The differential cooling of a structural member can result in tensile and compressive residual stresses patterns for parts that cool slowly and quickly, respectively. For structural elements, the effect of residual stresses on the components depends on the slenderness and imperfection sensitivity (Galamboas, 1998). There are various techniques to measure residual stresses which are categorised as destructive and non-destructive methods. Destructive methods, such as hole drilling and sectioning technique, involve the measurement of deformation due to the residual stresses upon removal of the material from the specimen. Sectioning method is the principal destructive technique used for steel, stainless steel and aluminium specimen which involves measuring the released strains on the sectioned strips and converting them to stresses via a stress-strain model (Young and Lui, 2005; Cruise and Gardner, 2008). Non-destructive methods comprise of electron diffraction, ultra-sonic methods, X-ray, neutron and magnetic methods (Cruise, 2007).

There are two main types of residual stresses for tubular section: (i) bending residual stresses, which arise during the plastic deformation phase during the cold-forming of the sheet material required into the section shapes, and (ii) membrane residual stresses, which arise during (seam) welding of the closed section (Gardner, 2002).

In cold-formed stainless steel tubular sections, bending residual stresses are released from coupons which are extracted hollow sections, which curve longitudinally. The bending residual stresses are reintroduced when the coupons are straightened under loading and therefore the influence of bending residual stresses are present in the measured material stress-strain response. On the other hand, membrane residual stresses on cold-formed tubular sections have been investigated (Cruise and Gardner, 2008) and found to be small and therefore safe to disregard. Residual stresses were therefore explicitly introduced into the described models, but their influence was present in the material modelling (Theofanous and Gardner, 2009). The same approach was adopted in the numerical models developed herein.

3.3.6 Boundary conditions, constraint and loading

The modelled columns and beam-column elements had their distinct boundary conditions and loading arrangement adopted in the experimental test programmes. These were carefully replicated in the numerical models by restraining suitable translational and rotational degrees of freedom of the model ends to mimic the experimental conditions. For columns and beam-column models with fixed end boundary conditions, all translational degrees of freedom except axial displacement at the loaded end were restrained (i.e. $u_x \neq 0$, $u_y = 0$ and $u_z = 0$) while all rotational degrees of freedom at both ends were restrained (i.e. $uR_x = 0$, $uR_y = 0$ and $uR_z = 0$). For columns and beam-column models with pinned end boundary conditions, all translational degrees of freedom, except axial displacement at the loaded end were restrained (i.e. $u_x = 0$, $u_y = 0$ and $u_z \neq 0$) with the rotational degrees of freedom restrained at both ends, except that related to the plane of buckling ($uR_x = 0$, $uR_y \neq 0$ and $uR_z = 0$ for buckling about y-y (major) axis and $uR_x = 0$, $uR_y = 0$ and $uR_z \neq 0$ for buckling about z-z (minor) axis).

3.3.7 Heat transfer model

In order to replicate an anisothermal loading condition by numerical modelling, the time-temperature relationship is required. The measured specimen time-temperature data reported was utilised in the numerical models developed for the austenitic EN 1.4301 columns and beam-columns tested in Ala-Outinen and Oksanen (1997), Baddoo and Gardner (2013) and Fan et al. (2016). For the column tests by Tondini et al. (2013), the measured time-temperature data for the specimens was not measured, only the furnace temperature was measured. In order to validate the column, heat transfer analysis was vital to obtain the development of the time-temperature of the test specimen, which is required by the analysis. In structural members thermal analysis can be divided in two main components: the conductive heat transfer in the structural component and the heat transfer from the fire to the exposed surface of the structural member through a combination of convection and radiation mechanisms. In this section, a brief description is provided for modelling the temperature development utilising the heat transfer mechanisms for structural fire design.

Conduction

Conduction is internal energy or heat which is transferred either in a solid or liquid to the cooler part of an object, as a result of temperature gradient. The rate at which this energy is conducted as heat is between two bodies and is a function of temperature difference (also known as temperature gradient). The rate of the internal energy transferred per unit time by conduction can be calculated by the Fourier's law series illustrated in Equation (3.6).

$$\dot{q} = -k\nabla\theta \quad (3.6)$$

where \dot{q} is the heat flux (W/m^2), k is the thermal conductivity of the material (W/mK) and $\nabla\theta$ is the temperature gradient vector. The negative sign in Equation (3.6) represents the fact that heat is transferred in the direction of decreasing temperature.

Convection

The convection heat transfer mechanism occurs mostly in liquids and solid surface through a fluid motion. In addition, it is known as a function of temperature, and although convection will occur at all stages of a fire, it has a major influence at low temperatures where radiation is at its lowest. The rate of convection heat transfer is overseen by Equation (3.7).

$$\dot{h}_{\text{net},c} = \alpha_c(\theta_g - \theta_m) \quad (3.7)$$

where $\dot{h}_{\text{net},c}$ is the net convective heat flux (W/m^2), α_c is the convective heat transfer coefficient ($\text{W}/\text{m}^2\text{K}$), θ_g is the gas temperature in the furnace ($^{\circ}\text{C}$) and θ_m is the surface temperature of the member ($^{\circ}\text{C}$). EN 1991-1-2 (2002) recommends to use $\alpha_c=25 \text{ w}/\text{m}^2\text{K}$ with the standard time-temperature curve, alternative values are provided for hydrocarbon curve ($\alpha_c=50 \text{ w}/\text{m}^2\text{K}$) and parametric curve ($\alpha_c=35 \text{ w}/\text{m}^2\text{K}$).

Radiation

Radiation is the emission of energy in the form of waves or particles, which can be reflected, absorbed and transmitted to a surface. Radiation heat transfer is employed through a resultant emissivity. Emissivity is a dimensionless property that is found in the range of zero and unity, and largely depends on factors such as temperature, emissivity angles and wavelengths. In structural fire design, carbon steel and stainless steel emissivity are recommended as $\epsilon_m=0.7$ and $\epsilon_m=0.4$ in EN 1991-1-2 (2002). Radiation can be expressed as given by Equation (3.8).

$$\dot{h}_{\text{net,r}} = \varphi \varepsilon_m \varepsilon_f \sigma [(\theta_g - 273)^4 - (\theta_m - 273)^4] \quad (3.8)$$

In Equation (3.8), $\dot{h}_{\text{net,r}}$ is the net heat radiative heat flux (W/m^2), φ is the configuration factor used to signify a proportion of incident thermal radiation on the surface, ε_m is the emissivity of the surface, ε_f is the emissivity of the fire, σ represents the Stephan-Boltzmann constant ($=5.67 \times 10^{-8} \text{ W}/\text{m}^2\text{k}^4$), θ_g is the gas temperature in the vicinity of a fire, θ_m is the surface temperature of a structural member.

Heat transfer problem

Under anisothermal state heat conduction, temperature changes with time. The conservation of heat energy as given in Equation (3.9) state that:

$$\rho c \frac{\partial \theta}{\partial t} = -\nabla \dot{q} + Q \quad (3.9)$$

where ρ is the material density, c is the material specific heat, t is the time, and Q is the internal heat generation rate per unit volume. The heat energy conservation equation is the basis for the heat transfer modelling in analysis package such as ABAQUS, which solved, subjected to appropriate boundary conditions, to obtain the temperature distribution. As it is difficult to obtain analytical solutions to Equation (3.9), numerical methods are employed to solve the heat transfer analysis problem.

Heat transfer analysis was performed on ferritic stainless steel columns reported by Tondini et al (2013). Each column had the measured mean furnace temperature applied uniformly to the surface of the specimen with a uniform initial temperature of 20°C . Then, convection, radiation and conduction heat transfer mechanisms were carefully simulated to obtain the temperature rise in the member. Radiation was modelled as surface radiation with using the command *SRADIATE in ABAQUS with the emissivity coefficient taken

as 0.4 from EN 1993-1-2 (2005). Convection was modelled as a film condition using the command *SFILM in ABAQUS with the coefficient for the convective heat transfer taken as 25 W/m²K as specified in EN 1993-1-2 (2005). Other required physical properties for the thermal model included the temperature dependent specific thermal capacity (c), thermal conductivity (λ) and thermal expansion – these were obtained from Clauses 8.4.1, 8.4.2 and 8.4.3, respectively of the Design Manual for Stainless Steel Structures (DMSS) (2017). The results from the heat transfer analysis consisted of the temperature distribution for all the nodes within the three dimensional model, which were stored as a function of time and subsequently read into the stress analysis model as a predefined field.

3.3.8 Analysis technique

The method required for the nonlinear analysis depends on the method of testing, whether the test were performed under isothermal or anisothermal conditions. Isothermal conditions involve a two-step procedure for the analysis. Firstly, a linear buckling analysis (LBA) is performed to obtain the buckling failure modes to be used for the initial geometric imperfections and secondly a nonlinear analysis is performed, as with ambient temperature models but with the elevated temperature material properties for a specific temperature assigned to it, using the Riks method which is employed to solve the geometrically and materially nonlinear of thin-walled structure. The Riks method uses the load and magnitude as an additional unknown parameter by solving load and displacement simultaneously in each iteration by adopting the Newton-Raphson algorithm. The use of the Riks method allows effective solutions to be found for unstable problems at room temperature and elevated temperature (such as post-ultimate response of thin walled structures (Ng and Gardner, 2007) and effectively traces nonlinear unloading paths.

For anisothermal test conditions, LBA was first performed to obtain the buckling failure mode, and nonlinear analysis was undertaken using the general STATIC Newton method in two stages. The first stage involved, applying a constant load at room temperature and at the second stage, the temperature was increased until failure was detected in the column. The time-temperature curves were either extracted from the test measured data or from a prior heat transfer analysis model.

3.4 Validation of numerical models

In this section, the results from the developed FE models for columns and beam-columns are compared to the test results. In order to confirm that the FE models are able to capture the structural behaviour response, the following validation measures were considered:

1. The initial stiffness of the structural member (i.e. comparing the initial linear part of the load-deformation response obtained from test results and numerical results).
2. Ultimate load capacity (i.e. comparing the maximum load achieved in the test results ($N_{u,test}$) and the numerical results ($N_{u,FE}$)).
3. The overall load-deformation response (i.e. comparing the whole test and FE load-deformation response from start of the loading, to the peak load and the unloading behaviour).
4. Failure mode (comparing the shape of both the experimental and the numerical failure mode).

3.4.1 SHS, RHS and CHS column member validation

The modelling procedures described in this chapter were applied to replicate the experimental test responses of the stainless steel columns reported in Table 3.1 and Table 3.2. Two performance criteria for structural members subjected to vertical loads at elevated temperatures, which are related to the magnitude of the vertical contraction (ΔL)

and the vertical contraction rate ($\Delta L/\Delta T$), are specified in EN 1363-1 (2012) to mark their critical failure temperature in fire. According to these criteria, the failure temperature is specified as that at which the vertical contraction and the rate of vertical contraction reach their limiting values – $(\Delta L)_{\text{limit}} = L/100$ (mm) and $(\Delta L/\Delta T)_{\text{limit}} = 3L/1000$ (mm/min), respectively. The failure temperatures of the simulated SHS and RHS columns at elevated temperature (Table 3.1) were specified by applying the EN 1363-1 (2012) criteria explained above, which were compared with the failure test temperatures determined by the same manner. The test and simulation critical temperature θ_{crit} comparison results for the elevated temperature SHS and RHS columns are presented in Table 3.8. The values for the mean and the coefficient of variation (COV) of the FE/test critical temperatures for the modelled austenitic (Ala-Outinen and Oksanen, 1997 and Baddoo and Gardner, 2000) and ferritic (Tondini et al., 2013) stainless steel columns are 0.90 and 0.03 and 1.00 and 0.02, respectively.

Figures 3.5 and 3.6 compare the axial displacement-temperature responses from the tests and FE for the SHS 80×80×3 - 2500 and RHS 150×75×6 columns, respectively, where the solid black line represents the test result and the dash black line represent the FE results. It should be noted that the temperatures in Figures 3.5 and 3.6 refer to the furnace temperature for both the tests and the FE models to enable a like-for-like comparison of the observed and modelled responses. The axial displacement-temperature response of the axially loaded compression members at elevated temperatures begins with an initial shortening when the compressive load is applied at room temperature, which is then followed by increasing axial expansion with the temperature rise. The rate of increase in the axial thermal expansion decreases at high temperatures as the column stiffness reduces and mechanical shortening becomes important. The mechanical shortening is due the combination of axial shortening and the out-of-plane lateral deflection from column

buckling. Finally, the column reaches a limiting point where it starts to contract as the mechanical shortening overtakes the thermal expansion, and the applied compressive load cannot be supported. Since the mechanical shortening of the column is controlled by the tangent stiffness of the material at elevated temperature, which reduces very rapidly, the final stage of the response is rather abrupt. The FE models were capable of accurately replicating these experimentally observed stages of behaviour. An example test and FE failure mode comparison for SHS 80×80×3-3000 column is presented in Figure 3.7, where good agreement between both is shown.

Figures 3.8 to 3.11 depict the test and FE responses in terms of the load versus mid-height lateral deflection curves for the CHS 76.3×3, CHS 60.5×2.8, CHS 88.9×2.1-1650 and CHS 106×3-3080 columns, respectively. The comparison results for the test and FE room temperature CHS columns are presented in Table 3.9, where the FE to test ratios for the ultimate loads N_u and the mid-height lateral deflection at ultimate loads δ_u are reported. The mean and COV of the FE/test are 1.02 and 0.06, respectively for N_u and 0.91 and 0.46, respectively for δ_u . The comparatively higher variation in the FE/test ratios of δ_u was also observed in numerical modelling simulations conducted by Buchanan et al. (2018) and is expected due to the higher variability associated with displacements at ultimate loads of models of these structural members. Figure 3.12 compares the failure modes from test and FE for CHS 106×3-3080 column, which are in good agreement.

Considering the high degree of accuracy obtained in predicting the flexural buckling response of the SHS/RHS columns at elevated temperatures and the CHS columns at room temperature, in terms of the axial displacement-temperature and load-deformation response characteristics as well as the failure modes, the developed numerical modelling procedures described herein are validated and can reliably be adopted for performing numerical parametric investigations.

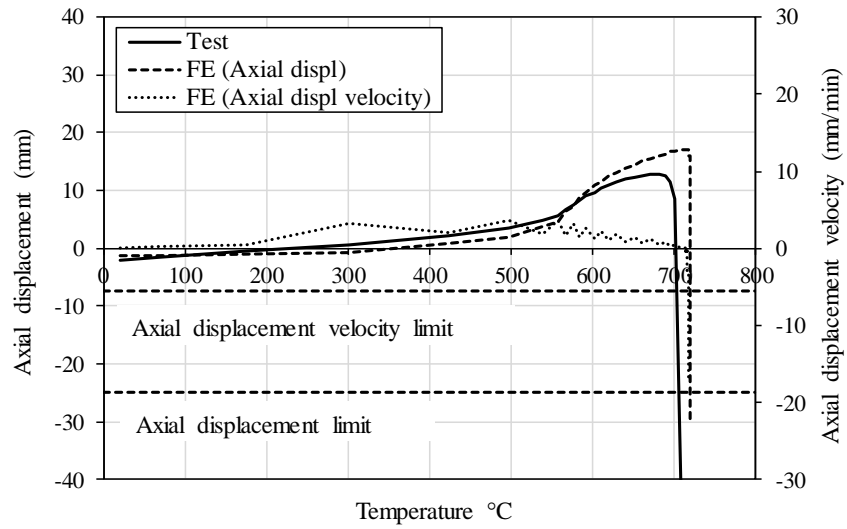


Figure 3.5: Test vs FE axial displacement responses for SHS 80×80×3-2500 column. Test from Tondini et al. (2013)

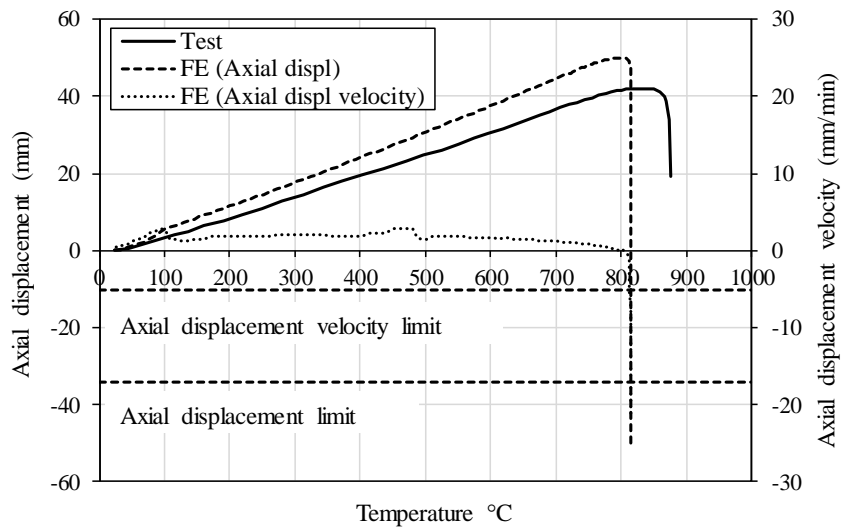


Figure 3.6: Test vs FE axial displacement responses for SHS 80×80×3-2500 column. Test from Tondini et al. (2013)

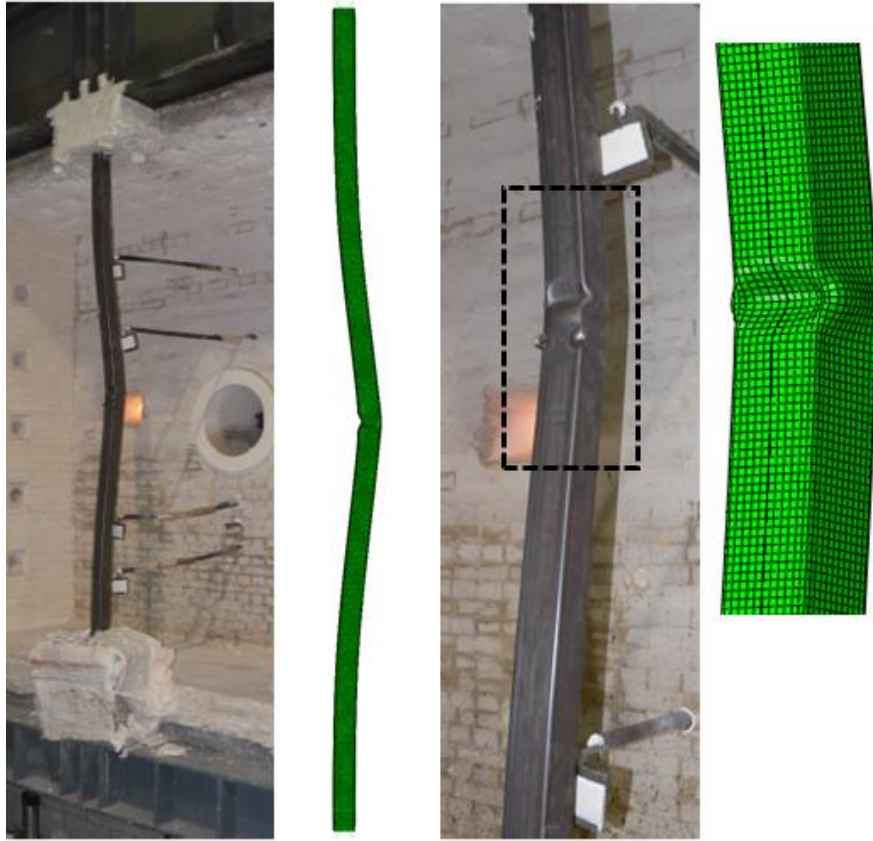


Figure 3.7: Test and FE failure modes for SHS 80×80×3-3000 column. Test from Tondini et al. (2013)

Table 3.8: Comparison of test and FE critical temperature θ_{crit} for SHS/RHS columns

Specimen reference	θ_{crit} (°C)		
	Test	FE	FE/Test
SHS 80×80×3-3000	709	726	1.02
SHS 80×80×3-2500	708	718	1.02
RHS 120×80×3-2500	705	709	1.01
SHS 40×40×4-T1	872	750	0.86
SHS 40×40×4-T2	579	502	0.87
SHS 40×40×4-T3	649	608	0.94
SHS 40×40×4-T4	710	646	0.91
SHS 40×40×4-T5	832	722	0.87
SHS 40×40×4-T7	766	681	0.89
RHS 150×100×6	801	757	0.91
RHS 150×75×6	883	814	0.92
RHS 100×75×6	806	744	0.92
Mean			0.93
COV			0.06

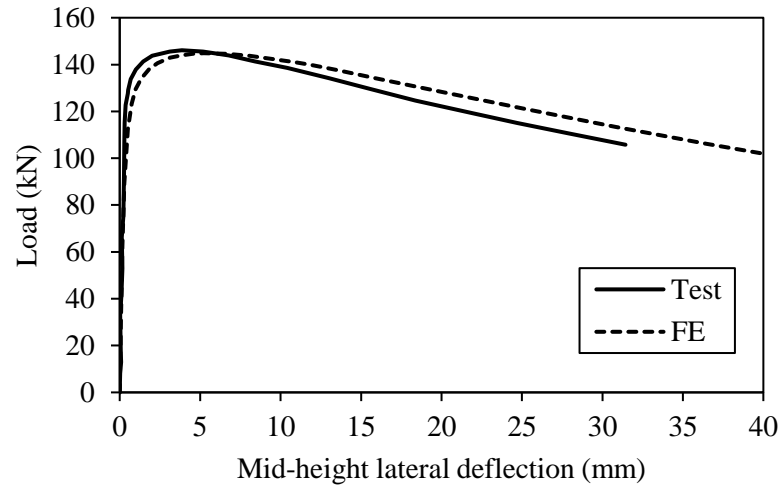


Figure 3.8: Test and FE load vs mid-height lateral deflection curves for CHS 76.3×3 column. Test from Zhao et al. (2016a)

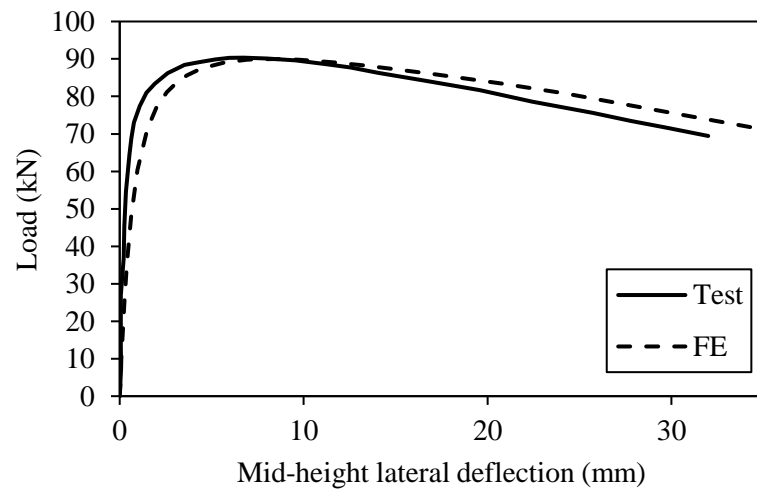


Figure 3.9: Test and FE load vs mid-height lateral deflection curves for CHS 60.5×2.8 column. Test from Zhao et al. (2016a)

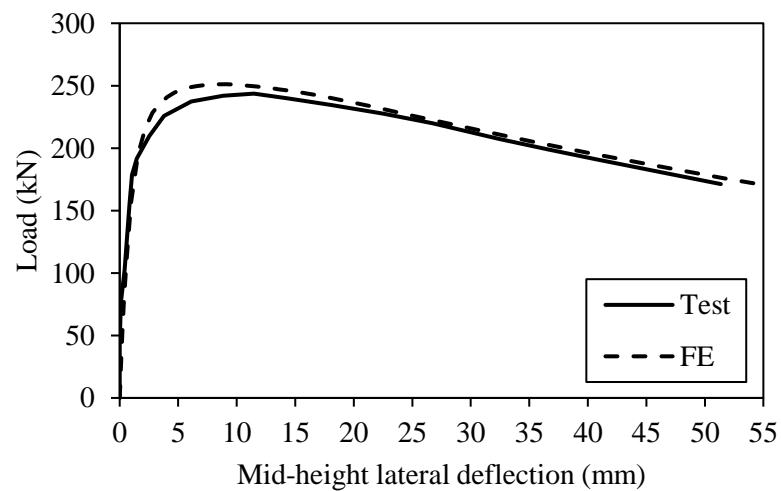


Figure 3.10: Test and FE load vs mid-height lateral deflection curves for CHS 88.9×2.6-1650 column. Test from Buchanan et al. (2018)

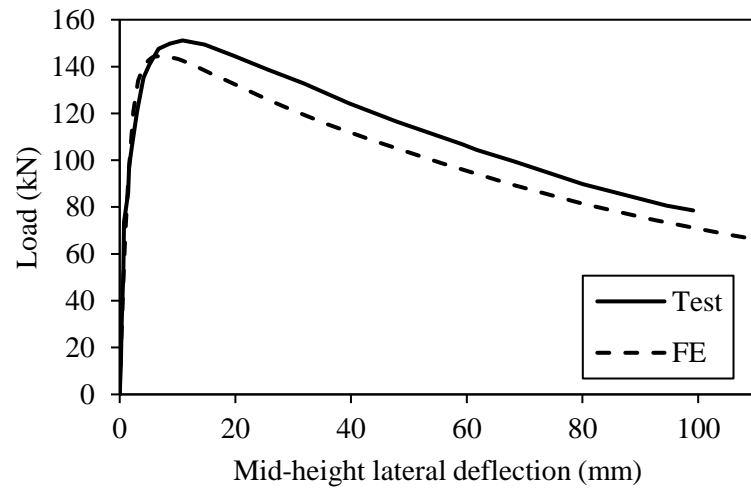


Figure 3.11: Test and FE load vs mid-height lateral deflection curves for CHS 106x3-3080 column. Test from Buchanan et al. (2018)

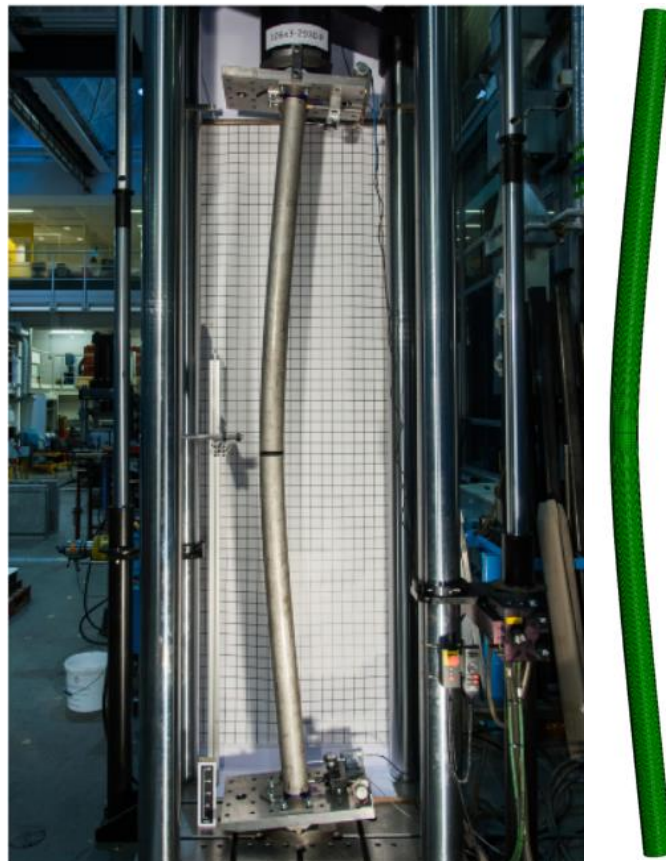


Figure 3.12: Test and FE failure modes for CHS 106x3-3080 column. Test from Buchanan et al. (2018)

Table 3.9: Comparison of test and FE ultimate load N_u and displacement at ultimate load δ_u for CHS columns

Specimen reference	N_u (kN)			δ_u (mm)		
	Test	FE	FE/Test	Test	FE	FE/Test
CHS 60.5×2.8	90.5	89.6	0.99	6.4	10.0	1.56
CHS 76.3×3	146.0	144.7	0.99	4.1	5.4	1.32
CHS 106×3-550	267.0	285.5	1.07	7.7	2.3	0.30
CHS 106×3-1150	248.8	226.6	0.91	3.9	5.7	1.46
CHS 106×3-3080	150.8	144.4	0.96	10.9	6.9	0.63
CHS 88.9×2.6-400	425.2	418.4	0.98	2.9	2.2	0.76
CHS 88.9×2.6-1650	243.4	251.1	1.03	11.5	8.5	0.74
CHS 88.9×2.6-3080	100.5	106.5	1.06	25.8	34.4	1.33
CHS 80×1.5-700	111.1	116.5	1.05	3.3	1.8	0.55
CHS 80×1.5-900	105.8	108.5	1.03	3.8	2.6	0.68
CHS 80×1.5-1600	77.9	87.0	1.12	9.1	6.0	0.66
Mean	1.02					
COV	0.05					

3.4.2 SHS, RHS and CHS beam-column member validation

Due to the limited test data in the literature on stainless steel beam-column member in fire, the numerical models were validated against (1) room temperature tests on SHS/RHS and CHS stainless steel beam-columns reported by Zhao et al. (2015a, 2016a, 2016b) at cross-sectional level and member level, (2) elevated temperature tests on SHS stainless steel beam-columns reported by Fan et al. (2016) and (3) elevated temperature tests on RHS S355 mild strength steel beam-columns reported by Pauli et al. (2012). The same modelling procedures adopted for the stainless steel columns was employed for the beam-column members, reported in Table 3.3 to 3.7 with the addition of an eccentric load, to generate axial load and bending moment as adopted in the tests.

3.4.2.1 Beam-columns test (Zhao et al., 2015a, 2016a, 2016b)

A comparison summary between the ultimate FE failure load ($N_{u,FE}$) and the test ultimate load ($N_{u,test}$). It was shown that for the stainless steel SHS and RHS stub columns and beam-columns the $N_{u,FE}/N_{u,test}$ ratio has a mean value of 1.01 and coefficient of variation

(COV) of 0.04. On the other hand, at member level, the mean and COV of $N_{u,FE}/N_{u,test}$ are 1.02 and COV of 0.02 for SHS and RHS, respectively and 1.02 and COV 0.02 for CHS, respectively. The test and FE load-deformation curves for the typical stainless steel beam-columns at room temperature are depicted in Figures 3.13 to 3.17, where the solid black line represent the test line and the dash black line represent the FE model results, which are in good agreement. Example of failure modes from both test and FE are shown in Figure 3.18 and 3.19, representing the ability of the developed FE models to capture the observed failure responses at both cross-section level and member level. From the overall results, it is concluded that the FE models are capable for predicting the tests results at room temperature for stainless steel beam-column members.

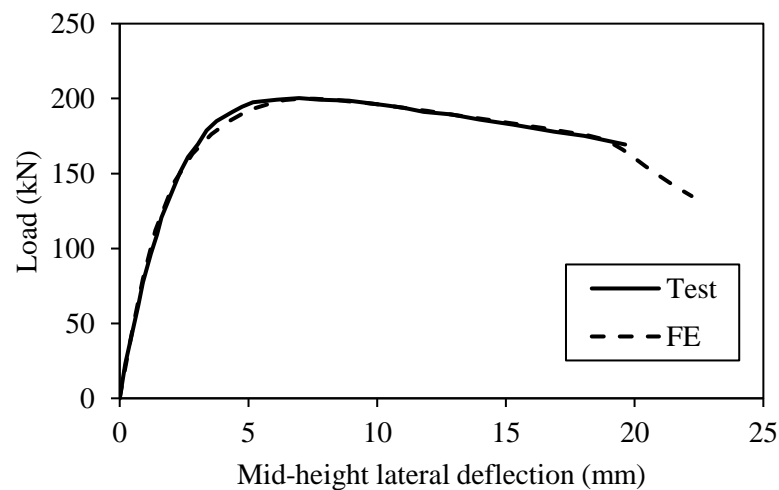


Figure 3.13: Test and FE load vs mid-height lateral deflection curves for SHS 60×60×3, $e_y=10\text{mm}$ beam-column member. Test from Zhao et al. (2016b)

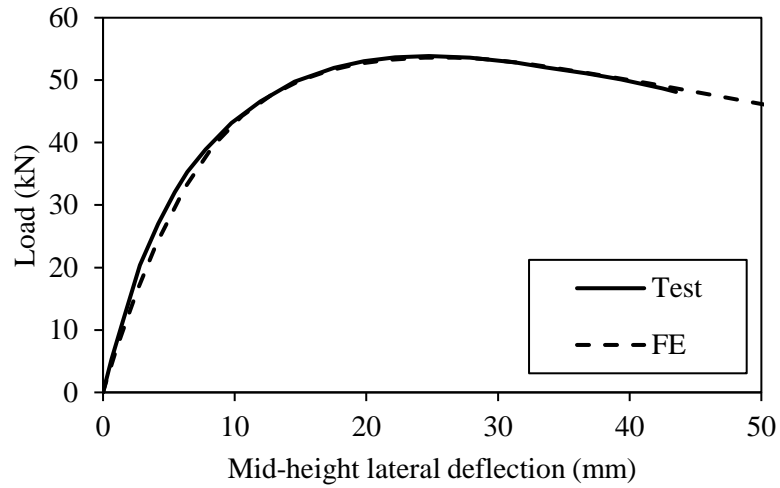


Figure 3.14: Test and FE load vs mid-height lateral deflection curves for CHS 60.5×2.8, $e_y=15\text{mm}$ beam-column member. Test from Zhao et al. (2016a)

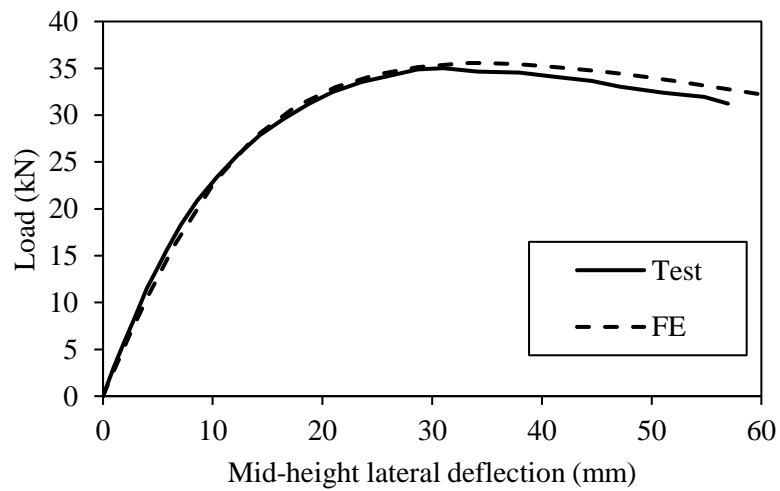


Figure 3.15: Test and FE load vs mid-height lateral deflection curves for CHS 60.5×2.8, $e_y=40\text{mm}$ beam-column member. Test from Zhao et al. (2016a)

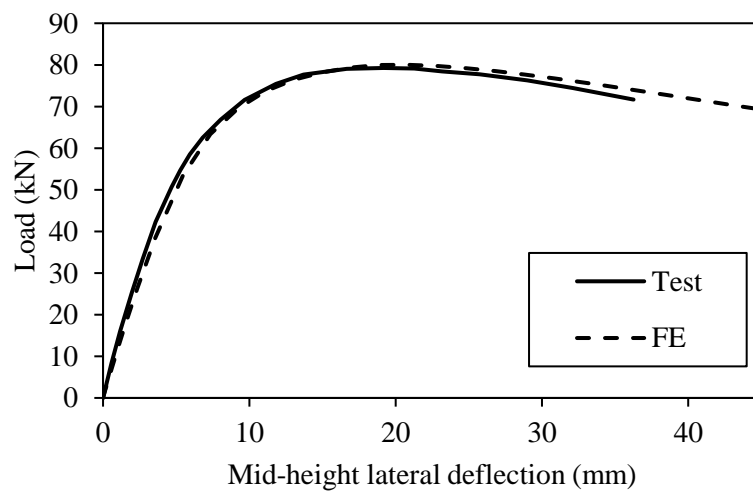


Figure 3.16: Test and FE load vs mid-height lateral deflection curves for CHS 76.3×3, $e_y=20\text{mm}$ beam-column member. Test from Zhao et al. (2016a)

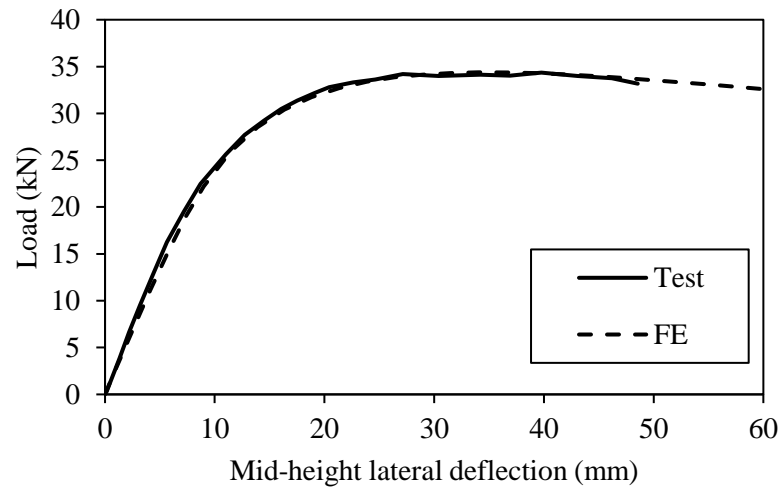


Figure 3.17: Test and FE load vs mid-height lateral deflection curves for CHS 76.3×3, $e_y=95\text{mm}$ beam-column member. Test from Zhao et al. (2016a)

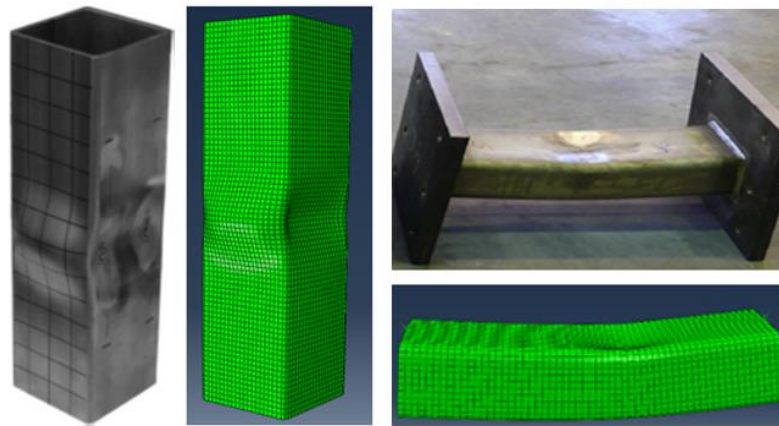


Figure 3.18: Test and FE failure mode of SHS 100×100×5 (left image) stub column and RHS 150×100×8, $e_z=50\text{mm}$ beam-column, minor axis failure mode (right image). Test from Zhao et al. (2015a)



Figure 3.19: Test and FE failure mode beam-columns SHS 60×60×3, $e_z=10\text{mm}$. Test from Zhao et al. (2016b)

Table 3.10: Comparison of SHS and RHS stainless steel stub column and beam-column test and FE results

Specimen reference	e_y (mm)	e_z (mm)	L (mm)	$N_{u,Test}$ (kN)	$N_{u,FE}$ (kN)	$N_{u,FE}/N_{u,test}$
SHS 100×100×5	0.0	0.0	349.9	1057.0	988.1	0.93
SHS 120×120×5	0.0	0.0	399.9	928.4	927.1	1.00
RHS 150×100×6	0.0	0.0	450.1	1323.7	1381.8	1.04
RHS 150×100×8	0.0	0.0	450.0	1825.1	1909.5	1.05
SHS 150×150×8	0.0	0.0	449.8	3257.9	3349.8	1.03
SHS 100×100×5	20.0	0.0	350.0	743.5	665.5	0.90
	25.0	0.0	350.0	622.2	617.6	0.99
	50.0	0.0	350.0	472.7	445.0	0.94
SHS 120×120×5	10.0	0.0	399.9	793.5	784.3	0.99
	40.0	0.0	400.0	550.0	532.6	0.97
	70.0	0.0	400.0	424.0	410.5	0.97
	120.0	0.0	399.8	296.1	277.5	0.94
RHS 150×100×6	45.0	0.0	350.1	825.2	867.5	1.05
	65.0	0.0	449.8	685.3	719.4	1.05
	95.0	0.0	450.1	575.7	607.1	1.05
	130.0	0.0	450.0	473.4	475.4	1.00
RHS 150×100×8	0.0	20.0	450.0	1173.8	1198.7	1.02
	0.0	50.0	450.2	800.1	831.3	1.04
	0.0	75.0	450.0	626.9	654.6	1.04
SHS 150×150×8	30.0	0.0	449.8	2186.7	2243.7	1.03
	55.0	0.0	450.0	1814.9	1793.2	0.99
	85.0	0.0	450.0	1403.6	1442.8	1.03
	120.0	0.0	450.1	1186.9	1159.6	0.98
Mean						1.01
COV						0.04

Table 3.11: Comparison of SHS and RHS stainless steel beam-column members test and FE results

Specimen reference	e_y (mm)	e_z (mm)	L (mm)	$N_{u,Test}$ (kN)	$N_{u,FE}$ (kN)	$N_{u,FE}/N_{u,test}$
SHS 60×60×3	10.0	0.0	774.8	199.6	203.1	1.02
	30.0	0.0	774.8	124.1	126.3	1.02
	40.0	0.0	774.8	104.7	106.7	1.02
	80.0	0.0	774.8	65.0	66.6	1.02
	125.0	0.0	774.8	46.4	47.7	1.03
RHS 100×40×2	0.0	2.0	674.8	153.2	152.3	0.99
	0.0	10.0	674.8	106.9	106.4	1.00
	0.0	30.0	674.8	62.7	63.7	1.02
	0.0	45.0	674.8	46.3	45.6	0.99
	0.0	75.0	674.8	32.0	33.9	1.06
Mean						1.02
COV						0.02

Table 3.12: Comparison of CHS stainless steel beam-column member test and FE

Specimen reference	e_y (mm)	e_z (mm)	L (mm)	$N_{u,Test}$ (kN)	$N_{u,FE}$ (kN)	$N_{u,FE}/N_{u,test}$
CHS 60.5×2.8	5.0	0.0	1450.0	66.3	69.0	1.04
	15.0	0.0	1450.0	53.8	53.7	1.00
	25.0	0.0	1450.0	43.1	43.9	1.02
	40.0	0.0	1450.0	35.0	35.9	1.03
	85.0	0.0	1450.0	23.0	22.7	0.99
CHS 76.3×3	10.0	0.0	1450.0	94.7	99.0	1.05
	20.0	0.0	1450.0	79.4	81.3	1.02
	30.0	0.0	1450.0	66.9	69.3	1.04
	50.0	0.0	1450.0	50.8	52.8	1.04
	95.0	0.0	1450.0	34.3	34.4	1.00
Mean						1.02
COV						0.02

3.4.2.2 Beam-column tests (Fan et al., 2016)

The anisothermal modelling procedures described section 3.3 were utilised to replicate the two austenitic stainless steel beam-column tests reported in Table 3.6. The two failure criteria for axially loaded members in fire explained in section 3.41 to these tests to mark their failure temperature. Figure 3.20 compares the axial displacement-time responses from the tests and FE for the SHS 120×120×4-3300 beam-column, respectively, where the solid black line represents the test result and the dash black line represent the FE results. The overall behaviour of the beam-column member is found similar to the column. In Figure 3.30, it was noted (1) in the early stage of the temperature rise, the axial displacement increases over time as temperature increases, (2) following an increase of axial expansion due temperature increase, the structural element stiffness reduces and the axial shortening, due to a combination of axial load and the out-of-plane deflection from the member buckling. Lastly, the axial shortening surpasses the thermal expansion of the member, and the member contracts, and the load-carrying capacity reduces. A ratio for the critical temperature (θ_{crit} °C) results between the FE and test is provided in Table 3.13 where a mean ratio of 1.01 and COV of 0.01 is achieved. Good agreement between the

test and FE failure modes are captured as displayed in Figure 3.21. From the comparison of the test and numerical results, it is concluded that the described models are capable of replicating the nonlinear behaviour of stainless steel beam-columns member in fire.

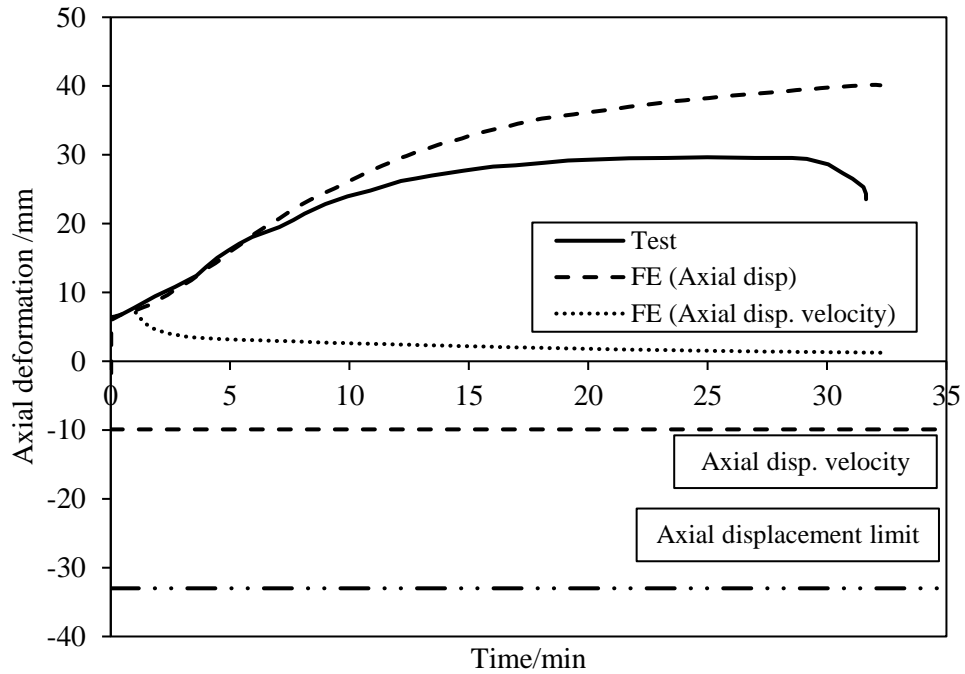


Figure 3.20: Comparison of test vs FE axial displacement responses for SHS 120×120×4-3300, $e_y=13.2\text{mm}$, beam-column member in fire. Test from Fan et al. (2016)

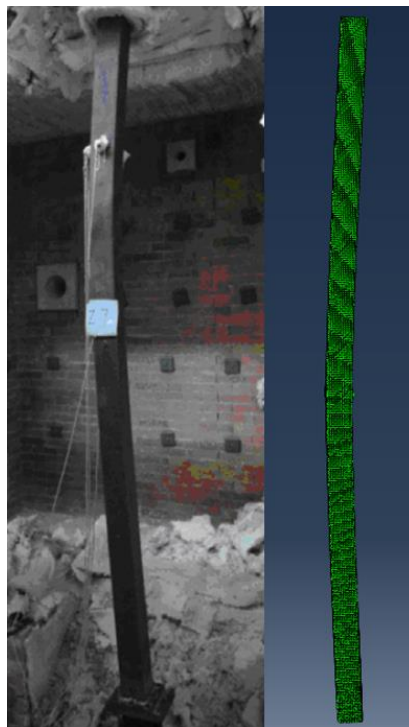


Figure 3.21: Test and FE failure modes for SHS 120×120×4-3300, $e_y=13.2\text{mm}$ beam-column. Test from Fan et al. (2016)

Table 3.13: Comparison of SHS stainless steel beam-column member in fire

Specimen reference	e_y (mm)	e_z (mm)	θ_{crit} (°C)		
			Test	FE	FE/Test
SHS 120×120×4	13.2	0.0	700.8	704.2	1.01
	23.8	0.0	665	676.8	1.02
Mean					1.01
COV					0.01

3.4.2.3 Beam-column tests (Pauli et al., 2012)

The procedures for the development of FE models described in section 3.3 were adopted to validate the tests reported by Pauli et al. (2012). Although these experiments were performed on S355 carbon steel, they are utilised in this research study for validation of the FE models owing to the lack of experimental results for stainless steel beam-column members in fire. The FE model utilised the combination of global imperfection values reported by Pauli et al. (2012) and local imperfection predicted using Equation (3.5). Table 3.14 provides the results by the means of a ratio of FE to test ultimate failure loads ($N_{u,FE}/N_{u,test}$), which shows a good agreement between the test and FE models. The comparison of axial load-deformation response of the test and FE results are displayed in Figures 3.22 to 3.23, where the solid black line represent the test and dash black line represent FE model. The FE models are generally capable of tracing the load-deformation response. Good agreement between the test and FE failure modes are captured as displayed in Figure 3.24 and 3.25. In summary, from results provided in Table 3.14, it is concluded that the finite element models are capable of predicting the ultimate strengths of S355 structural beam-columns sections at elevated temperature.

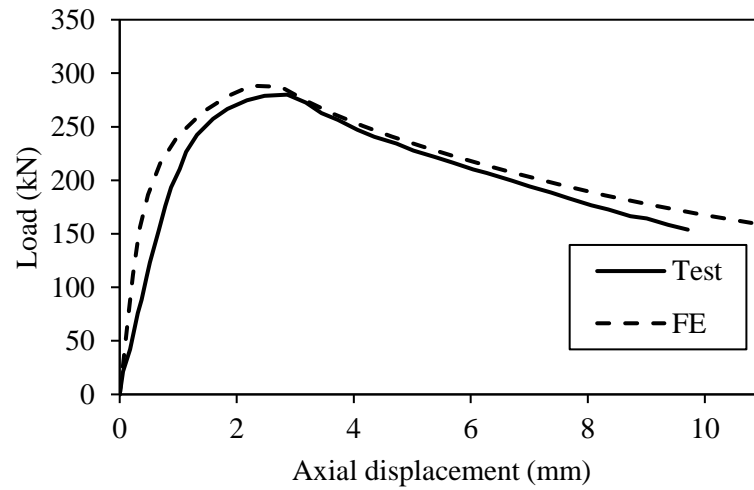


Figure 3.22: Test and FE load vs axial displacement curves for RHS 120×60×3.6-360, $e_z=10\text{mm}$, $\theta=400^\circ\text{C}$, beam-column member. Test from Pauli et al. (2012)

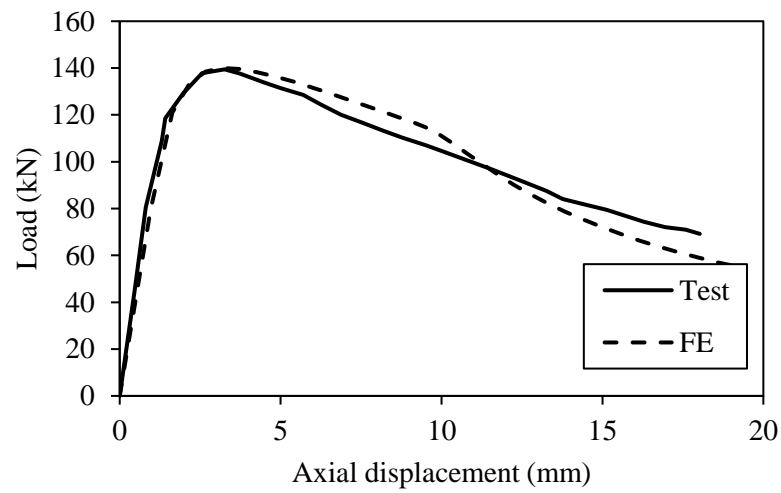


Figure 3.23: Test and FE load vs axial displacement curves for RHS 120×60×3.6-1840, $e_z=10\text{mm}$, $\theta=400^\circ\text{C}$, beam-column member. Test from Pauli et al. (2012)

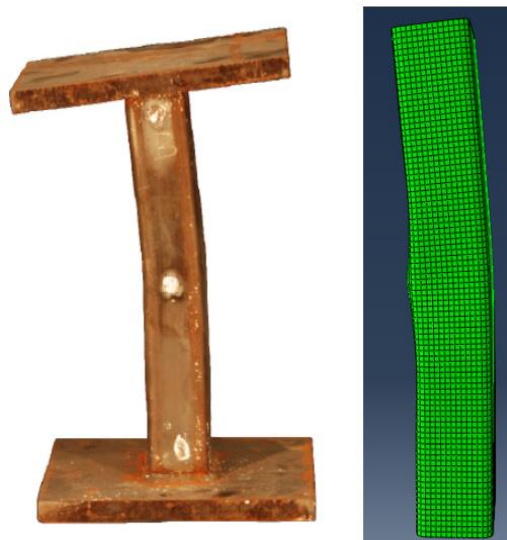


Figure 3.24: Test and FE failure mode of S355 stub beam-column RHS 120×60×3.6, $e_z=10\text{mm}$, $\theta=400^\circ\text{C}$. Test from Pauli et al. (2012)



Figure 3.25: Test and FE failure mode of S355 beam-column member level, RHS 120x60x3.6-
 $e_z=50\text{mm}$, $\theta=400^\circ\text{C}$. Test from Pauli et al. (2012)

Table 3.14: Comparison of RHS S355 carbon steel beam-column test and FE results at elevated temperature

Specimen reference	L (mm)	Temperature ($^\circ\text{C}$) θ	e_y (mm)	e_z (mm)	$N_{u,\text{Test}}$ (kN)	$N_{u,\text{FE}}$ (kN)	$N_{u,\text{FE}}/N_{u,\text{Test}}$
RHS 120x60x3.6	360	400	0.0	0.0	408	413	1.01
	360	400	0.0	10.0	280	288	1.03
	360	400	0.0	50.0	133	148	1.11
	360	550	0.0	0.0	257	240	0.93
	360	550	0.0	10.0	205	179	0.87
	360	550	0.0	50.0	87	92	1.06
	360	700	0.0	0.0	74	77	1.04
	850	550	0.0	30.0	96	102	1.06
	1840	400	0.0	0.0	242	207	0.85
	1840	400	0.0	10.0	139	140	1.01
	1840	400	0.0	50.0	73	75	1.03
	1840	550	0.0	0.0	186	195	1.05
	1840	550	0.0	10.0	111	102	0.92
	1840	550	0.0	50.0	49	54	1.09
	1840	700	0.0	0.0	71	68	0.96
	Mean						
COV							0.07

3.5 Concluding remarks

In this chapter, a comprehensive numerical validation study was carried out, which forms the basis for the numerical parametric investigations carried out in the subsequent chapters. A large pool of experimental test data on column and beam-column structural members at both room and elevated temperatures including both stainless steel and carbon steel were collected from the literature test programmes. The collected test data for SHS, RHS and CHS columns and beam-columns which are the focus of this thesis. The key details of the experimental programmes required as input in the models for the validation of the FE models were presented. The important details of the numerical modelling approach such as the material modelling, geometric imperfections, boundary conditions and analysis steps were explained. In all cases, the results of the numerical models were compared with their corresponding experimental test results. The validated FE models in this chapter are employed for conducting parametric studies on stainless steel columns and beam-columns at elevated temperature in Chapters 4 and 5, the results of which form the basis for the development of the design guidance in Chapters 4 and 5.

Chapter 4 Fire design of stainless steel hollow section columns

4.1 Introduction

This chapter focuses on the design methods for stainless steel tubular columns in fire conditions. Following the validation of the models for stainless steel tubular columns subjected to elevated temperatures in Chapter 3, parametric studies were performed which are presented in this Chapter. Tubular columns of different stainless steel grades, member slenderness, geometric sections, aspect ratios and axis of buckling were modelled. The columns were investigated under four different elevated temperatures. The applicability and accuracy of the design methods recommended in EN 1993-1-2 (2005) and the Design Manual for Stainless Steel Structures (2017) were carefully assessed on the basis of the numerical flexural buckling results generated by the parametric study. New buckling curve formulations for the fire design of cold-formed stainless steel SHS/RHS and CHS columns were subsequently proposed, and their suitability was confirmed by applying the reliability criteria set out by Kruppa (1999). Detailed description of these is provided in the following sections.

4.2 Parametric study

Parametric studies to examine the flexural buckling response of stainless steel columns with square, rectangular and circular hollow cross-section of different grades at elevated temperatures were carried out, the details of which are presented hereafter. For the purpose of the parametric study, the columns were modelled as isothermal testing conditions, in which the stress-strain data corresponding to a given temperature θ were

assigned to the FE models, akin to applying a uniform temperature θ , and the compressive load applied was set to increase until failure was reached similar to the validated models of the room temperature tests. A static Riks method (ABAQUS, 2016) was employed to solve the geometrically and materially nonlinear stress analysis problem from which the load versus deformation response of the columns and their failure loads were determined, which were used to derive buckling curves for their fire design as discussed in Section 4.3. This approach, which has been also adopted in other similar numerical modelling investigations e.g. in Huang and Young (2018) and Lopes et al. (2010), was deemed acceptable, since the developed elevated temperature FE models did not explicitly include the effect of time dependent factors such as creep, i.e. creep effects were only implicitly included in the material properties/reduction factors of the Design Manual for Structural Stainless Steel (2017) derived from anisothermal tests, and as a results both the isothermal and anisothermal modelling approaches would yield very similar results.

The stress-strain response of stainless steels at room temperature differs for austenitic, duplex and ferritic grades due to the chemical composition, production and level of cold-work induced into the materials as illustrated in Figure 4.1 (Afshan et al., 2019). The major difference as shown in Figure 4.1 is austenitic tends to have the highest ductility compared to the other stainless steel grades, duplex has the highest strength due to high chromium content, however has less ductility than austenitic, and ferritic has lowest chromium content compared to austenitic and duplex, which reduces strength and ductility.

Material properties and their response to elevated temperatures form an essential part of structural fire design. The degree of degradation of the mechanical properties with respect to temperature also vary. A comparison of the elevated temperature performance of stainless steel is presented in Figure 4.2 to 4.4; the data is provided in SCI Design Manual

for Structural Stainless Steel (2017) and EN 1993-1-2 (2005) both which are based on the test results reported in Zhao (2000); Gardner and Baddoo (2006); Ala-Outinen (1996); Hoke (1977) and Gardner et al. (2010) from anisothermal and isothermal tests. In Figure 4.2, the reduction in modulus of elasticity ($k_{E,\theta}$) is defined as the elevated temperature initial Young's modulus E_θ , normalised by the initial Young's modulus (E) at room temperature.

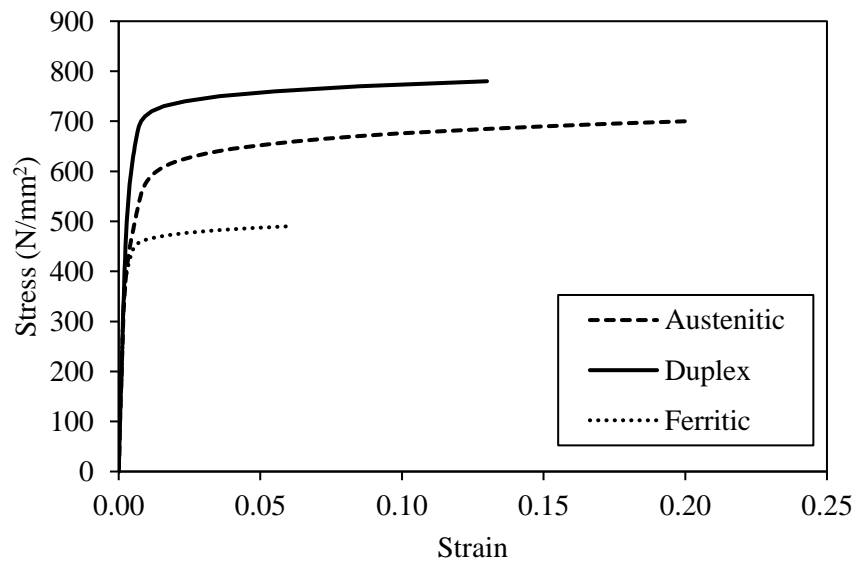


Figure 4.1: Typical stress-strain curves for austenitic, duplex and ferritic stainless steel. (SCI, 2017)

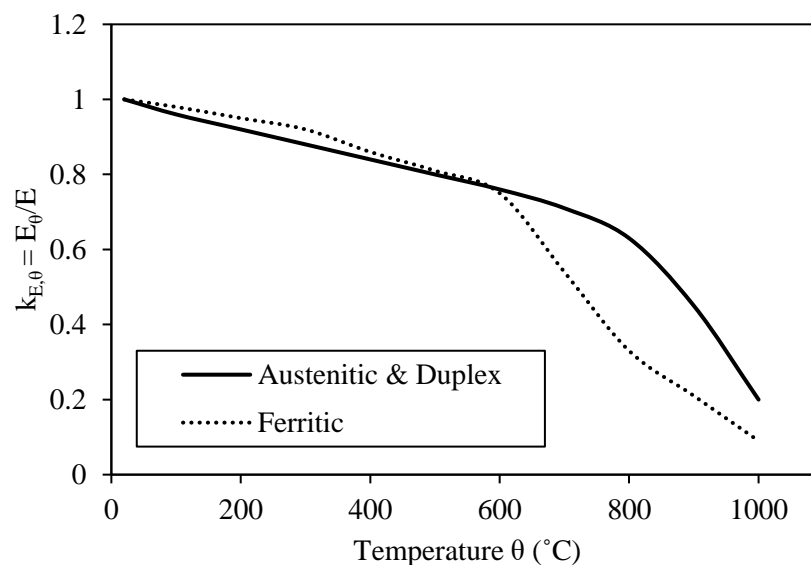


Figure 4.2: Reduction in modulus of elasticity for austenitic, duplex and ferritic at temperature θ . (SCI, 2017)

Strength reduction factors are defined into two distinct categories: $k_{2,\theta}$ is the strength at two percent total strain at temperature $f_{2,\theta}$, which is normalised by the room temperature 0.002 proof strength f_y , whereas $k_{p,0.2,\theta}$ is the strength at 0.002 proof strength $f_{0.2,\theta}$ at temperature, which is normalised by room temperature 0.002 proof strength f_y . The $k_{2,\theta}$ and $k_{p,0.2,\theta}$ strength retention factors for Austenitic I, Duplex II and Ferritic II grades provided in Table 8.1 of the Design Manual for Stainless Steel Structures (2017) are presented in Figures 4.3 and 4.4. In Figure 4.4, it can be seen at low temperatures, austenitic, duplex and ferritic $k_{2,\theta}$ retention factors are substantially greater than unity, and this due to the two percent strain limit at elevated temperature and the significant strain hardening that the material exhibits.

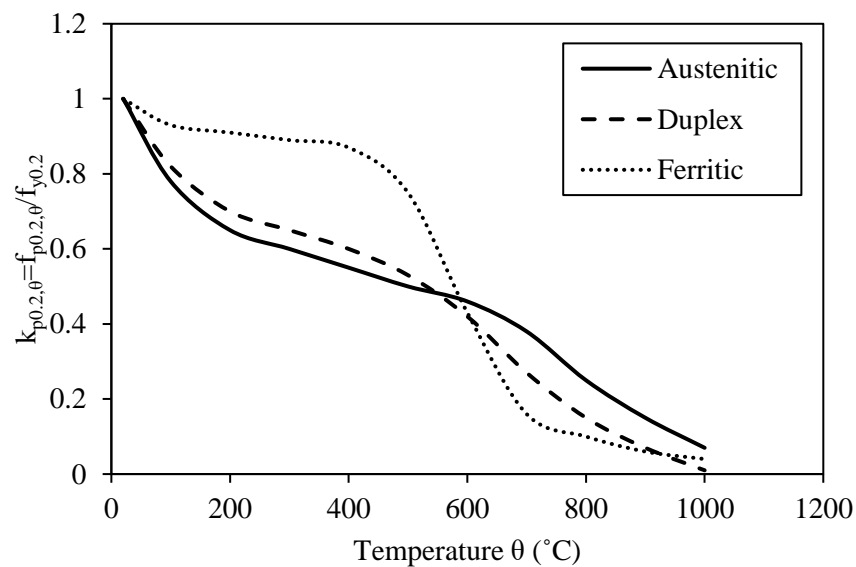


Figure 4.3: Reduction in 0.2% proof strength for austenitic, duplex and ferritic at temperature θ . (SCI, 2017)

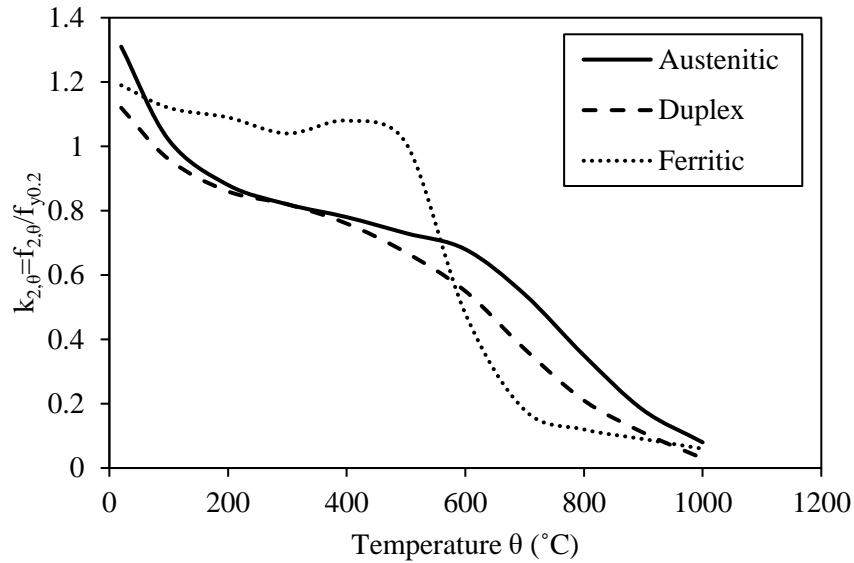


Figure 4.4: Reduction in strength at 2% total strain for austenitic, duplex and ferritic at temperature θ . (SCI, 2017)

Hence, in order to study the effect of the different elevated temperature stress-strain response of the material on the flexural buckling capacity of compression members, the parametric study included austenitic, duplex and ferritic stainless steels. For each stainless steel grades considered, the varied parameters were the elevated temperature member slenderness ($\bar{\lambda}_{\theta}$) for the SHS, RHS and CHS models as well as the aspect ratio of the cross-section (h/b), where h is the section height and b is the section breadth, and the axis of buckling (major and minor) for the RHS models. For each of the cross-section dimensions and member lengths, the columns were modelled with four different temperatures in the range of 200 $^{\circ}C$ to 800 $^{\circ}C$. The end support conditions of the columns were modelled as pinned at both ends, allowing free rotation about the designated member axis of buckling as well as free longitudinal displacement along the column length. All cross-sections were classified as fully effective and slender sections in accordance with the EN 1993-1-2 (2005) and EN 1993-1-4 (2015) limits for classification of cross-sections at both room and elevated temperatures. Table 4.1 outlines the examined parameters for each of the cross-sections. The cross-section slendernesses of the modelled columns, $\bar{\lambda}_p$

and $\bar{\lambda}_c$, are also included in Table 4.1, in which $\bar{\lambda}_p$ is the plate slenderness of the SHS and RHS - as defined by Equation (4.11) and $\bar{\lambda}_c$ is the local slenderness of the CHS - as defined by Equation (4.12). In Equation (4.11), $\sigma_{cr,p}$ is the elastic critical buckling stress of the plate element, $\sigma_{2.0}$ is the stress at 2% total strain, which is the strength parameter used for fire design as discussed in more detail in Section 4.3, b and t are the flat plate width and thickness, respectively, E is the Young's modulus, k_σ is the plate buckling coefficient, set to 4.0 for internal plate elements subjected to uniform compressive stress state and ν stands for the Poisson's ratio taken as 0.3. In Equation (4.12), $\sigma_{cr,c}$ is the elastic critical buckling stress for a circular hollow section, D is the section outer diameter, and all other symbols are as previously defined. In total, 1235 cold-formed stainless steel columns with SHS, RHS and CHS cross-section at elevated temperatures were modelled.

$$\bar{\lambda}_p = \sqrt{\frac{\sigma_{2.0}}{\sigma_{cr,p}}} = \left(\frac{b}{t}\right) \left(\frac{f_2}{E}\right)^{0.5} \left(\frac{12(1-\nu^2)}{\pi^2 k_\sigma}\right)^{0.5} \quad (4.11)$$

$$\bar{\lambda}_c = \sqrt{\frac{\sigma_{2.0}}{\sigma_{cr,c}}} = \left(\frac{\sigma_{2.0} D}{2tE}\right)^{0.5} \left(\sqrt{3(1-\nu^2)}\right)^{0.5} \quad (4.12)$$

The same modelling assumptions as explained in Chapter 3 were adopted in the models of the parametric study with the input parameters taken as those described hereafter. The room temperature material properties recommended by Afshan et al. (2019) for austenitic, duplex and ferritic stainless steel cold-formed SHS, RHS and CHS, presented in Table 4.2, together with the required reduction factors pertaining to Austenitic I, Duplex II and Ferritic II grades provided in Table 8.1 of the Design Manual for Stainless Steel Structures (2017) were employed; these are the most up to date set of reduction factors for stainless steel materials at elevated temperature. The two-stage Ramberg-Osgood material model, Equations (3.11) and (3.12), was used to develop full-range stress-strain relationships for the modelled temperatures. The values for n_0 were taken as the room temperature values

for n provided in Afshan et al. (2019) and the values for $m_{\theta,2}$ were determined using Equation (4.13); these are in accordance with the recommendations in Clause 8.5 of the Design Manual for Stainless Steel Structures (2017).

$$m_{\theta,2}=1+2.8 \frac{\sigma_{0.2,\theta}}{\sigma_{u,\theta}} \quad (4.13)$$

Similar to the validation models, the initial geometric imperfections were introduced as eigenmodes that were scaled to a suitable magnitude. The amplitudes for the global imperfection mode was set equal to the tolerance limit for fabrication, which is specified in EN 1090-2 (2008) as $L/1000$, where L is the member length. For the local imperfection for the SHS and RHS columns, the amplitude was set to $b/200$, where b is the section width and for the CHS columns, the amplitude was set to $0.008D$, where D is the diameter, in accordance with the recommendations in EN 1993-1-5-Annex C (2006). Shell element S4R was selected to discretise the modelled cross-sections; the element mesh size was equal to the thickness of the cross-sections t for the CHS columns and the flat elements of the SHS and RHS columns which had a smaller mesh size of four elements in their corner portions to allow an accurate representation of the curved geometry (Gardner and Nethercot, 2004).

4.3 Fire resistance design

4.3.1 EN 1993-1-2 (2005)

The design of structural elements and assemblies made of stainless steel in fire is covered in EN 1993-1-2 (2005) with similar treatments as carbon steel structures. The response of steel structures in fire is typically accompanied by large deformations, and therefore in fire design, higher strain levels are considered acceptable compared to those at room temperature. For this reason, the strength parameter which the resistance of structural

Table 4.1: Summary of parametric study variables

Section	Grade	Section	h/b	Buckling axis	Temperatures (°C)	$\bar{\lambda}_p$ or $\bar{\lambda}_c$	Classification	$\bar{\lambda}_\theta$
SHS/RHS	Austenitic	SHS 100×100×10	1.0	-	200 °C, 400 °C, 600 °C and 800 °C	0.33	Fully effective	0.1-2.0
		RHS 150×100×14	1.5	Major and Minor		0.34	Fully effective	
		SHS 100×100×5	1.0	-		0.62	Slender	
		RHS 150×100×7	1.5	Major and Minor		0.66	Slender	
	Duplex	SHS 100×100×9	1.0	-		0.38	Fully effective	
		RHS 150×100×14	1.5	Major and Minor		0.36	Fully effective	
		SHS 100×100×5	1.0	-		0.65	Slender	
		RHS 150×100×8	1.5	Major and Minor		0.62	Slender	
	Ferritic	SHS 100×100×9	1.0	-		0.32	Fully effective	
		RHS 150×100×11	1.5	Major and Minor		0.39	Fully effective	
		SHS 100×100×5	1.0	-		0.54	Slender	
		RHS 150×100×7	1.5	Major and Minor		0.58	Slender	
CHS	Austenitic	CHS 100×8	-	-	200 °C, 400 °C, 600 °C and 800 °C	0.18	Fully effective	0.1-2.0
		CHS 100×2	-	-		0.35	Slender	
	Duplex	CHS 100×8	-	-		0.19	Fully effective	
		CHS 100×2	-	-		0.38	Slender	
	Ferritic	CHS 100×8	-	-		0.16	Fully effective	
		CHS 100×2	-	-		0.33	Slender	

Table 4.2: Room temperature material properties adopted in the parametric models.

Grade	Section	E (N/mm ²)	f _{0.2} (N/mm ²)	f ₂ (N/mm ²)	f _u (N/mm ²)	n
Austenitic	SHS/RHS (F), CHS	200000	460	603	700	2.9
Duplex	SHS/RHS (F), CHS	200000	630	706	780	4.8
Ferritic	SHS/RHS (F), CHS	200000	430	490	490	4.6
Austenitic	SHS/RHS (C)	200000	640	838	830	7.1
Duplex	SHS/RHS (C)	200000	800	896	980	6.7
Ferritic	SHS/RHS (C)	200000	560	610	610	6.8

F = Flat face, C = Corner region

members, including columns, in fire is based on EN 1993-1-2 (2005) is the stress at 2% total strain at elevated temperature θ i.e. $f_{2,\theta} = k_{2,\theta} f_y$ for members with fully effective cross-sections (i.e. Class 1, 2 and 3) and the 0.2% proof stress at elevated temperature θ i.e. $f_{0.2,\theta} = k_{0.2,\theta} f_y$ for members with slender cross-section (i.e. Class 4), where f_y is the design yield strength at room temperature and $k_{2,\theta}$ and $k_{0.2,\theta}$ are the reduction factors for $f_{2,\theta}$ and $f_{0.2,\theta}$, respectively. These design strength parameters are also adopted in EN 1993-1-2 (2005) for the fire design of columns made of stainless steels, where the design yield strength at room temperature f_y is taken as the 0.2% proof stress. Figure 4.5 shows the schematic illustration of the definition of these strength parameters. As mentioned previously, EN 1993-1-4 (2006) is the room temperature design for stainless steel elements, however, for stainless steel structural fire design, EN 1993-1-4 (2006) references to EN 1993-1-2 (2005), meaning that the design rules adopted are for carbon steel elements. In this section, the design rules for stainless steel columns at room temperature and elevated temperature are described.

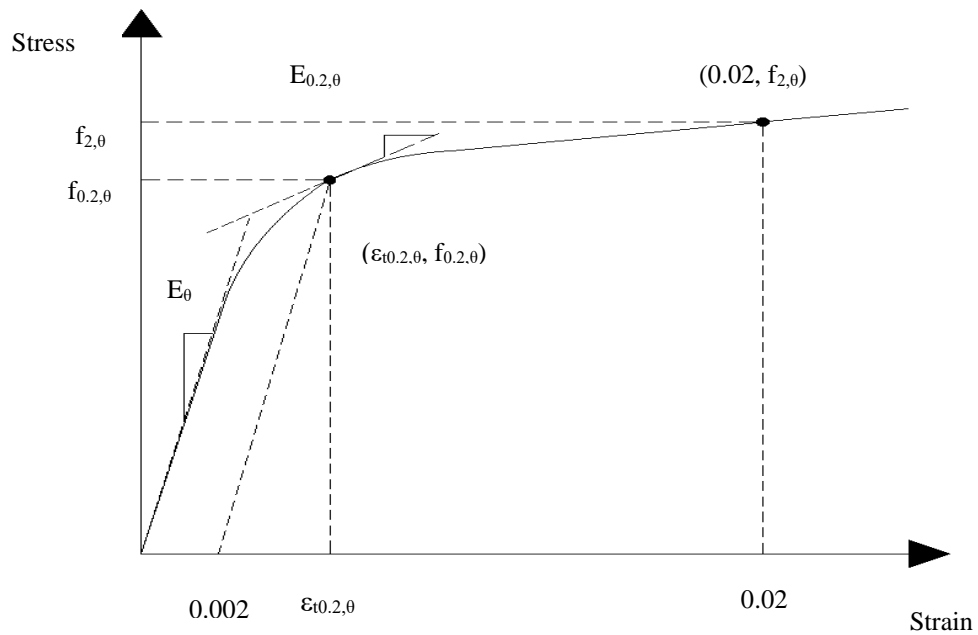


Figure 4.5: Schematic representation of strength parameters.

The classification of stainless steel cross-section at room temperature, according to EN 1993-1-4 (2006) is made using factor ε defined as a function of yield strength and modulus of elasticity as defined in Equation (4.14).

$$\varepsilon = \left(\frac{235}{f_y} \frac{E}{210000} \right)^{0.5} \quad (4.14)$$

Where f_y is the yield strength of the material and E is the modulus of elasticity at room temperature. At room temperature for carbon steel elements the modulus of elasticity is equal to 210000 N/mm² as defined in EN 1993-1-1 (2014), however for stainless steel the modulus of elasticity varies for the type of grade being utilised. This led to the use of a different factor ε for stainless steel as presented Equation (4.14).

In order to design a stainless steel column at member level, EN 1993-1-4 (2006) provides a design procedure for elements subjected to axial compression according to the classification (i.e. for Class 1, 2 and 3), the buckling resistance of stainless steel member ($N_{b,Rd}$) is calculated as follows:

$$N_{b,Rd} = \frac{\chi A f_y}{\gamma_{M1}} \text{ for Class 1, 2 and 3 cross-sections} \quad (4.15)$$

$$N_{b,Rd} = \frac{\chi A_{eff} f_y}{\gamma_{M1}} \text{ for Class 4 cross-sections} \quad (4.16)$$

Where χ is the flexural buckling reduction factor for the relevant buckling mode, A is the cross-sectional area, A_{eff} is the effective area of the effective cross-section, f_y is the yield strength of the material and γ_{M1} is the partial safety factor. EN 1993-1-4 (2006) prescribe the use of partial safety ($\gamma_{M,fi}$) of 1.1, though in this research study, a value of unity is utilised for the partial safety coefficient as the design rules for structural fire design for carbon steel structures is prescribed at unity.

The flexural buckling reduction factor is the minimum between y axis and z axis and is defined by Equation (4.17).

$$\chi_{fi} = \frac{1}{\phi + \sqrt{\phi^2 - \bar{\lambda}^2}} \leq 1 \text{ with } \phi = 0.5[1 + \alpha(\bar{\lambda} + \bar{\lambda}_0) + \bar{\lambda}^2] \quad (4.17)$$

Where the imperfection factor (α) and limiting slenderness ($\bar{\lambda}_0$) are fixed provided in Table 4.3. In order to determine the coefficient ϕ , the non-dimensional slenderness is calculated either using Equation (4.18) for Class 1, 2 and 3 cross-sections or Equation (4.19) for Class 4 cross-sections.

$$\bar{\lambda} = \sqrt{\frac{Af_y}{N_{cr}}} \text{ for Class 1, 2 and 3 cross-sections} \quad (4.18)$$

$$\bar{\lambda} = \sqrt{\frac{A_{eff}f_y}{N_{cr}}} \text{ for Class 4 cross-sections} \quad (4.19)$$

Where N_{cr} is the elastic critical force for the relevant buckling mode.

Table 4.3: Typical imperfection and limiting slenderness values. EN 1993-1-4 (2006).

Buckling mode	Type of member	α	$\bar{\lambda}_0$
Flexural	Cold formed open sections	0.49	0.4
	Hollow sections (welded and seamless)	0.49	0.4
	Welded open sections (major axis)	0.49	0.2
	Welded open sections (minor axis)	0.76	0.2
Torsional and torsional flexural	All members	0.34	0.2

The form of the flexural buckling curves provided in EN 1993-1-2 (2005) for the column design is the same as the flexural buckling curves for room temperature design set out in EN 1993-1-1 (2014) for carbon steel and in EN 1993-1-4 (2015) for stainless steel. The only exceptions are that there is no plateau i.e. $\bar{\lambda}_0 = 0$ and the imperfection factor α is expressed in terms of the yield strength f_y using $\alpha = 0.65\sqrt{235/f_y}$. In addition, the non-dimensional member slenderness at elevated temperature $\bar{\lambda}_\theta$, as defined by Equations (4.20) and (4.21), is employed, in which $\bar{\lambda}$ is the column slenderness at room temperature, $k_{E,\theta}$ is the reduction factor for Young's modulus E_θ at temperature θ and $k_{2,\theta}$ and $k_{0.2,\theta}$ are

as previously defined. The non-dimensional buckling reduction factor χ_{fi} as given by Equation (4.22) is also recommended for stainless steel columns of all cross-section shapes and all temperatures.

$$\bar{\lambda}_{\theta} = \bar{\lambda} \left(\frac{k_{2,\theta}}{k_{E,\theta}} \right)^{0.5} \quad \text{for Class 1, 2 and 3 cross-sections} \quad (4.20)$$

$$\bar{\lambda}_{\theta} = \bar{\lambda} \left(\frac{k_{0,2,\theta}}{k_{E,\theta}} \right)^{0.5} \quad \text{for Class 4 cross-sections} \quad (4.21)$$

$$\chi_{fi} = \frac{1}{\varphi_{\theta} + \sqrt{\varphi_{\theta}^2 - \bar{\lambda}_{\theta}^2}} \quad \text{with } \varphi_{\theta} = \frac{1}{2} [1 + \alpha \bar{\lambda}_{\theta} + \bar{\lambda}_{\theta}^2] \quad (4.22)$$

Finally, the predicted flexural buckling resistance $N_{b,fi,t,Rd}$ of a compression member at time t and experiencing a uniform temperature θ is obtained from Equations (4.23) and (4.24), where A is the cross-sectional area for the gross cross-section, A_{eff} is the cross-sectional area of the effective cross-section, $\gamma_{M,fi}$ is the member resistance partial resistance factor, which is 1.0 as set out in EN 1993-1-2 (2005) and all other symbols are as previously defined.

$$N_{b,fi,t,Rd} = \frac{\chi_{fi} A k_{2,\theta} f_y}{\gamma_{M,fi}} \quad \text{for Class 1, 2 and 3 cross-sections} \quad (4.23)$$

$$N_{b,fi,t,Rd} = \frac{\chi_{fi} A_{eff} k_{0,2,\theta} f_y}{\gamma_{M,fi}} \quad \text{for Class 4 cross-sections} \quad (4.24)$$

4.3.2 Lopes et al. (2010)

Lopes et al. (2010) conducted an extensive parametric numerical modelling investigation on axially loaded columns with welded stainless steel I-section in fire and proposed a modified version of the EN 1993-1-2 (2005) flexural buckling curves. In the proposed buckling curves, (1) the parameter β was introduced in the non-dimensional buckling reduction factor χ_{fi} and φ_{θ} formulations as presented in Equation (4.25) and (2) the imperfection parameter α was defined in terms of temperature θ , as given by Equations

(4.26) and (4.27), which results in temperature dependant buckling curves. For welded I-section columns, β values equal to 1.0 for major axis buckling and 1.5 for minor axis buckling, for all stainless steel grades were proposed. The α values were recommended as equal to 1.3 for austenitic grades - EN 1.4301, EN 1.4401, EN 1.4404, EN 1.4571 and ferritic grade - EN 1.4003 grades and 0.9 for EN 1.4462 grade (Lopes et al., 2010). Using the proposed fire buckling curves and the same definition of $\bar{\lambda}_\theta$ given in Equations (4.20) and (4.21), $N_{b,fi,t,Rd}$ may similarly be obtained from Equations (4.23) and (4.24).

$$\chi_{fi} = \frac{1}{\varphi_\theta + \sqrt{\varphi_\theta^2 - \beta \bar{\lambda}_\theta^2}} \leq 1.0 \text{ with } \varphi_\theta = 0.5 \left[1 + \alpha \bar{\lambda}_\theta + \beta \bar{\lambda}_\theta^2 \right] \quad (4.25)$$

$$\alpha = \eta \sqrt{\frac{235}{f_y} \frac{E}{210000}} \sqrt{\frac{k_{E,\theta}}{k_{2,\theta}}} \text{ for Class 1, 2 and 3 cross-sections} \quad (4.26)$$

$$\alpha = \eta \sqrt{\frac{235}{f_y} \frac{E}{210000}} \sqrt{\frac{k_{E,\theta}}{k_{0.2,\theta}}} \text{ for Class 4 cross-sections} \quad (4.27)$$

4.3.3 Design Manual for Structural Stainless Steel Design (2017)

The method provided in the Design Manual for Structural Stainless Steel (2017) for determination of the flexural buckling resistance uses the same buckling curves as for room temperature, with plateau length $\bar{\lambda}_\theta$ and imperfection factor α as those recommended in Table 6.1 in Design Manual for Structural Stainless Steel (2017), for elevated temperature design. The fire design buckling resistance $N_{b,fi,t,Rd}$ is obtained from Equations (4.28) and (4.29), where A is the cross-sectional area of the gross cross-section, A_{eff} is the cross-sectional area of the effective cross-section, χ_{fi} is as defined in Equation (4.30), where $\bar{\lambda}_\theta$ is given by Equation (4.31). Based on this approach, for all cross-section classes, the flexural buckling resistance of stainless steel columns in fire is determined on the basis of the 0.2% proof stress ($k_{0.2,\theta} f_y$), where $k_{0.2,\theta}$ is the reduction factor for the 0.2%

proof strength and f_y is the design yield strength (taken as the 0.2% proof stress) at room temperature.

$$N_{b,fi,t,Rd} = \frac{\chi_{fi} A k_{0.2,\theta} f_y}{\gamma_{M,fi}} \text{ for Class 1, 2 and 3 cross-sections} \quad (4.28)$$

$$N_{b,fi,t,Rd} = \frac{\chi_{fi} A_{eff} k_{0.2,\theta} f_y}{\gamma_{M,fi}} \text{ for Class 4 cross-sections} \quad (4.29)$$

$$\chi_{fi} = \frac{1}{\phi_{\theta} + \sqrt{\phi_{\theta}^2 - \bar{\lambda}_{\theta}^2}} \leq 1.0 \text{ with } \phi_{\theta} = 0.5 \left[1 + \alpha (\bar{\lambda}_{\theta} - \bar{\lambda}_0) + \bar{\lambda}_{\theta}^2 \right] \quad (4.30)$$

$$\bar{\lambda}_{\theta} = \bar{\lambda} \left(\frac{k_{0.2,\theta}}{k_{E,\theta}} \right)^{0.5} \text{ for all Classes of cross-sections} \quad (4.31)$$

4.4 Analysis of results and design guidance proposal

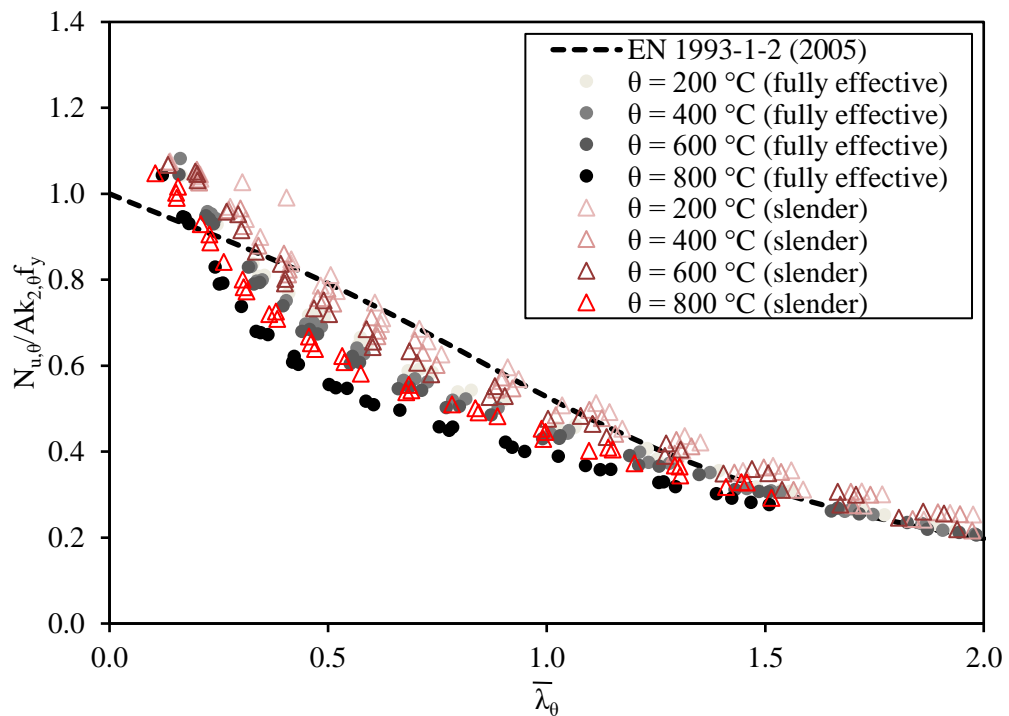
4.4.1 Comparison with EN 1993-1-2 and Design Manual for Structural Stainless Steel methods

The flexural buckling capacities for the parametric models presented in Section 4.2 are compared with the predicted capacities determined using the existing fire design methods presented in Section 4.3 hereafter. Figure 4.6(a)-(c) show the results of SHS and RHS columns, where the FE ultimate loads ($N_{u,\theta}$) normalised by the elevated temperature yield loads of the cross-section ($A k_{2,\theta} f_y$) versus the elevated temperature member slenderness ($\bar{\lambda}_{\theta}$), determined using Equation (4.20) for fully effective section and Equation (4.21) for slender section columns, for the austenitic, duplex and ferritic columns, respectively are plotted. The EN 1993-1-2 (2005) flexural buckling curves is also depicted. Figure 4.7 (a)-(c) show the similar results for CHS columns of austenitic, duplex and ferritic grades, respectively. For the SHS and RHS columns, the room temperature yield strength f_y is taken as the weighted average $f_{0.2,wa}$ value (by area), as described in Equation (4.32), in order to normalise out the strength increases in the corner portions associated with cold-work effects during the production of these cross-sections. In Equation (4.32) $f_{0.2,f}$ and

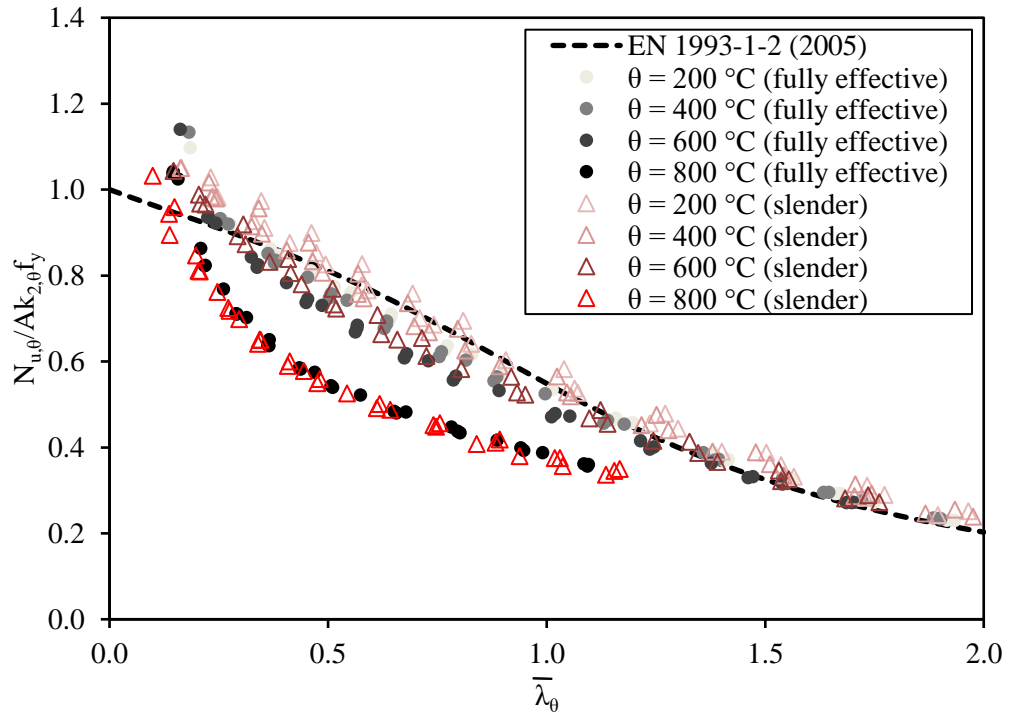
$f_{0.2,c}$ and A_f and A_c are the 0.2% proof stress and the cross-sectional areas for the flat and corner portions of the section, respectively, and A is the total cross-sectional area.

$$f_{0.2,wa} = \frac{f_{0.2,f} A_f + f_{0.2,c} A_c}{A} \quad (4.32)$$

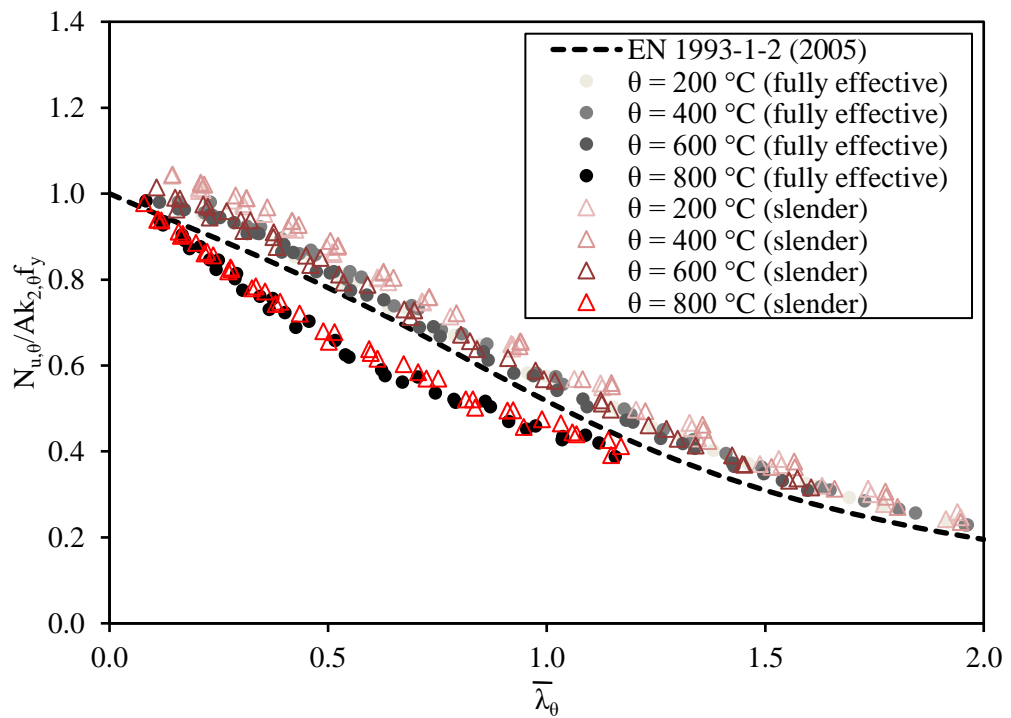
Figure 4.8 (a)-(c) and 4.9 (a)-(c) compares the FE results for the SHS/RHS and CHS columns, respectively with the Design Manual for Structural Stainless Steel (2017) buckling curves, where for the SHS and RHS columns the plateau lengths are: $\bar{\lambda}_0 = 0.3$ for the austenitic and duplex grades and $\bar{\lambda}_0 = 0.2$ for the ferritic grade and the imperfection parameter α is set to 0.49 for all grades, and for the CHS columns $\bar{\lambda}_0$ and α are 0.2 and 0.49, respectively for all grades. In data presented in Figure 4.8 (a)-(c) and 4.9 (a)-(c), the cross-section yield strength was taken as $k_{0.2,\theta} f_y$ and the elevated temperature member slenderness $\bar{\lambda}_\theta$ was determined using Equation (4.31).



(a) Austenitic

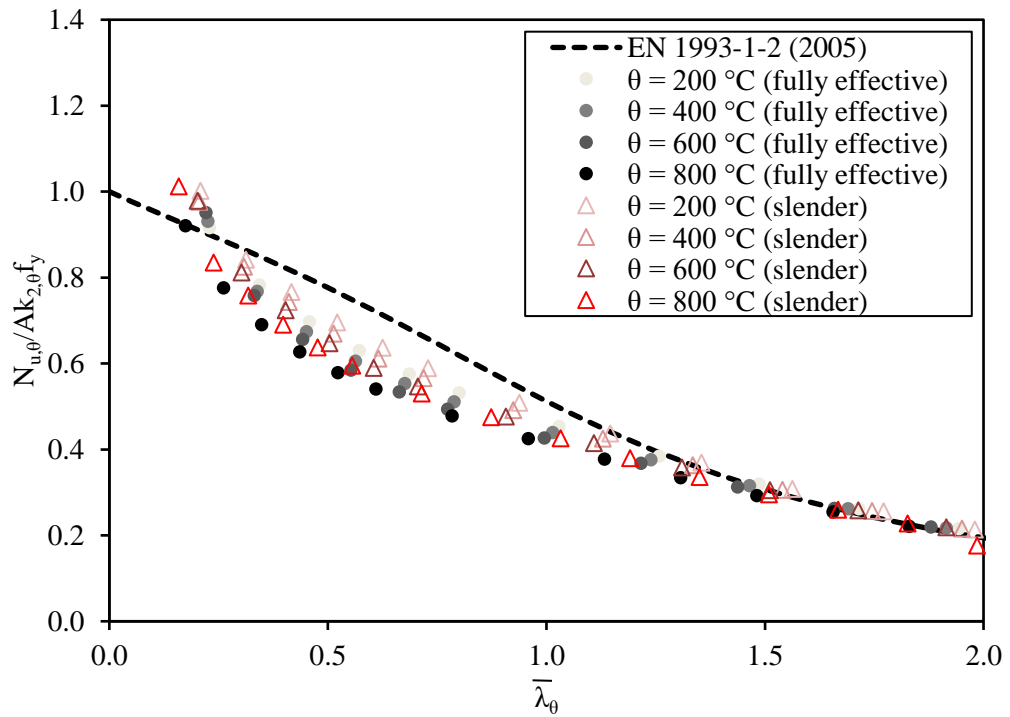


(b) Duplex

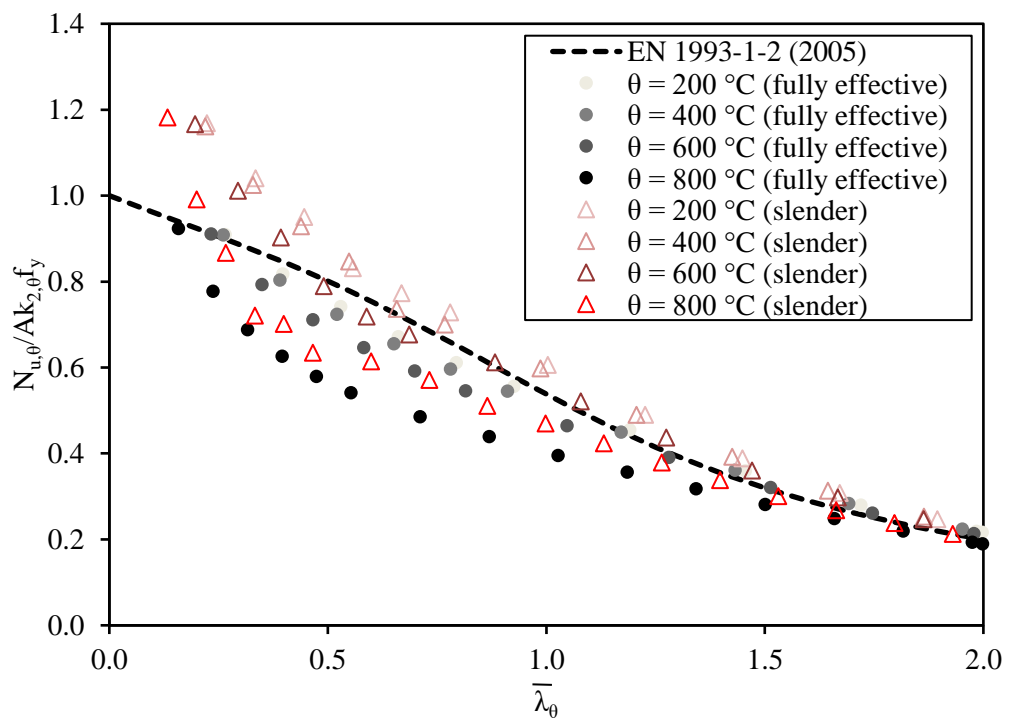


(c) Ferritic

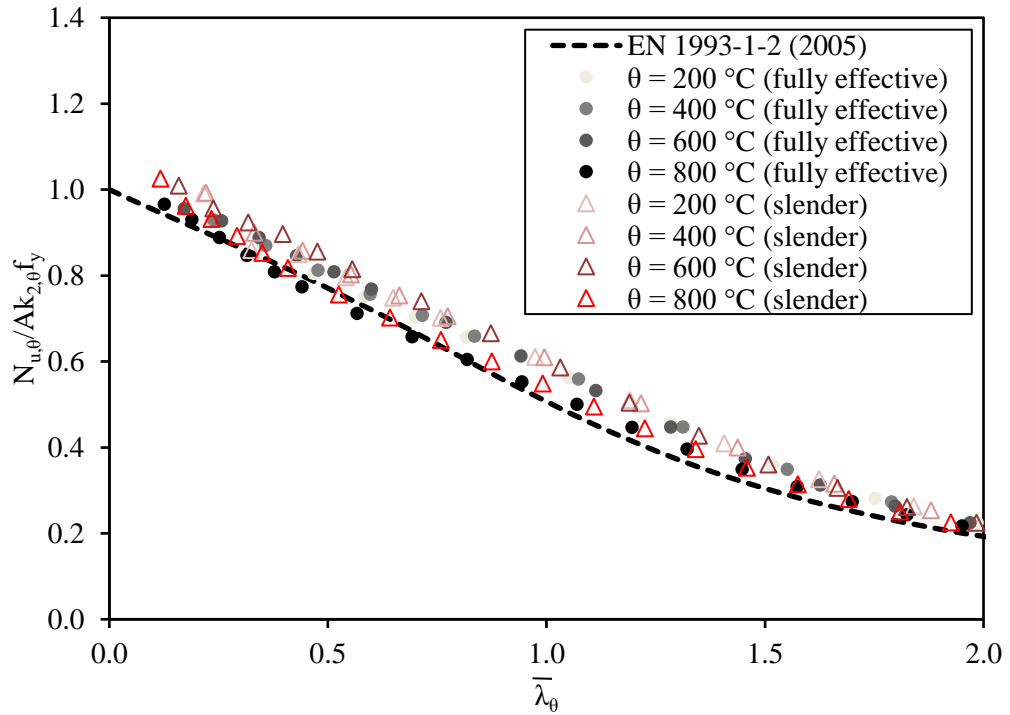
Figure 4.6: Comparison of FE results with the EN 1993-1-2 (2005) buckling curve for (a) austenitic, (b) duplex and (c) ferritic SHS and RHS columns, with fully effective and slender cross-sections.



(a) Austenitic

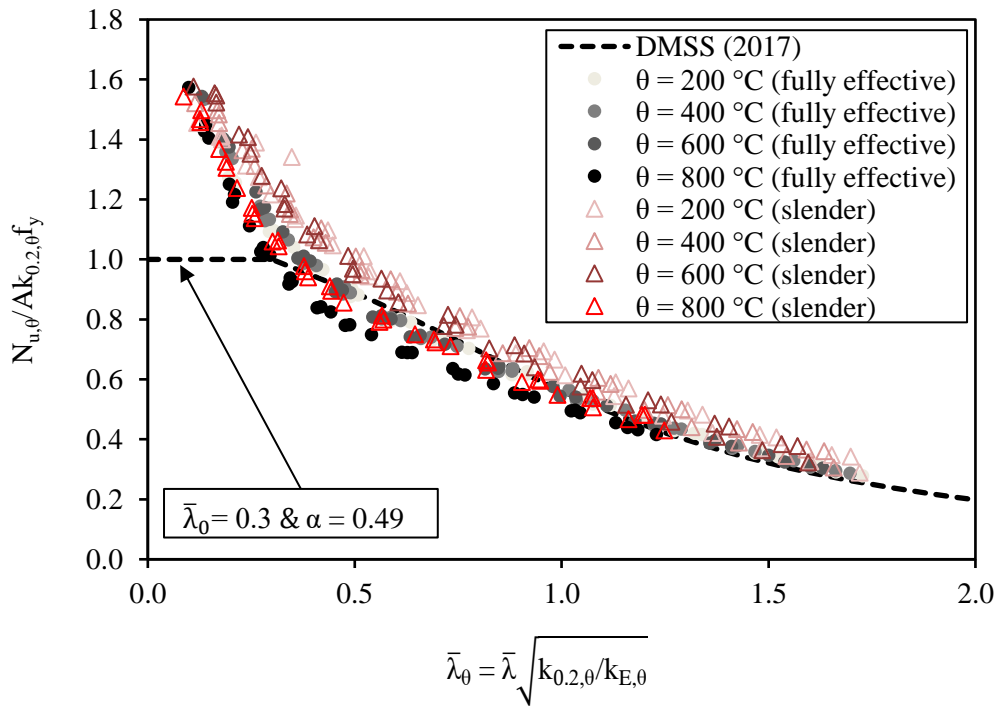


(b) Duplex

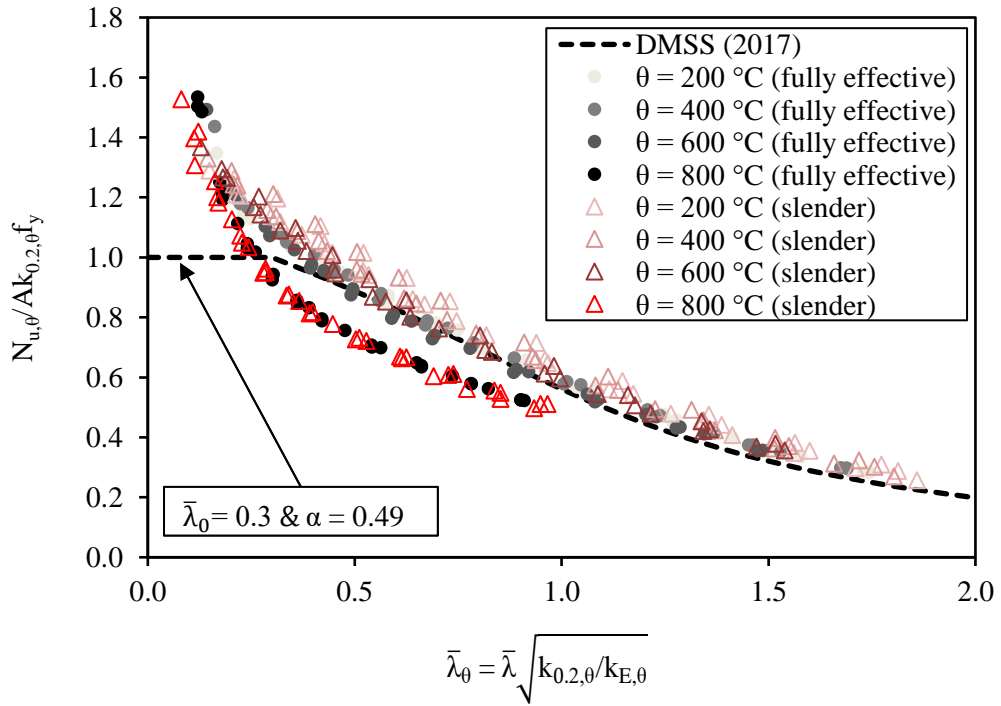


(c) Ferritic

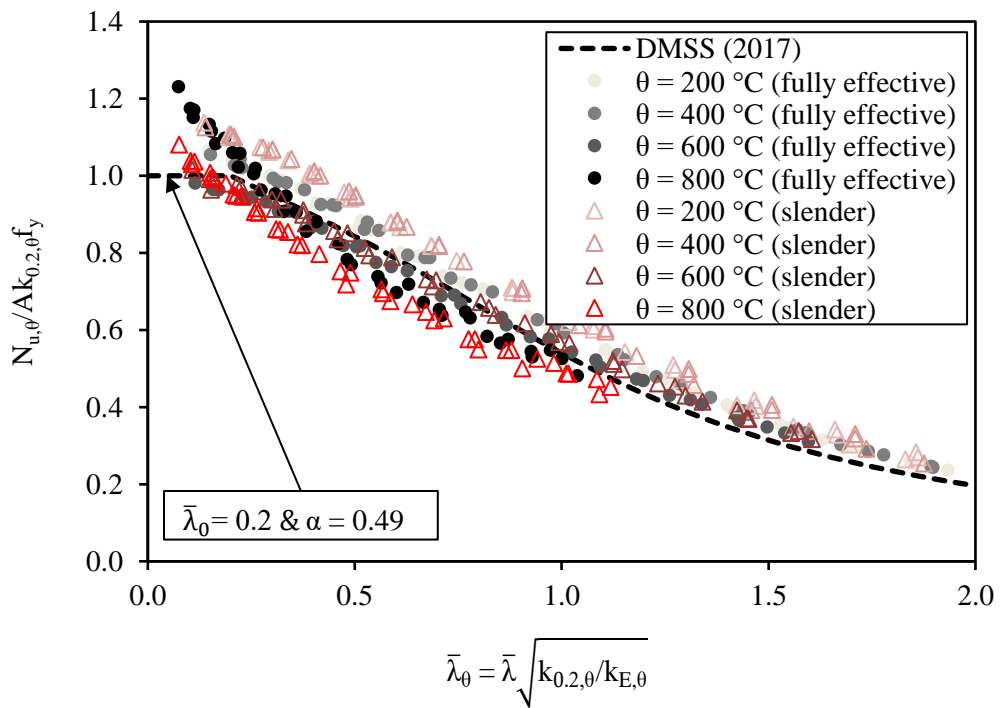
Figure 4.7: Comparison of FE results with the EN 1993-1-2 (2005) buckling curve for (a) austenitic, (b) duplex and (c) ferritic CHS columns, with fully effective and slender cross-sections.



(a) Austenitic

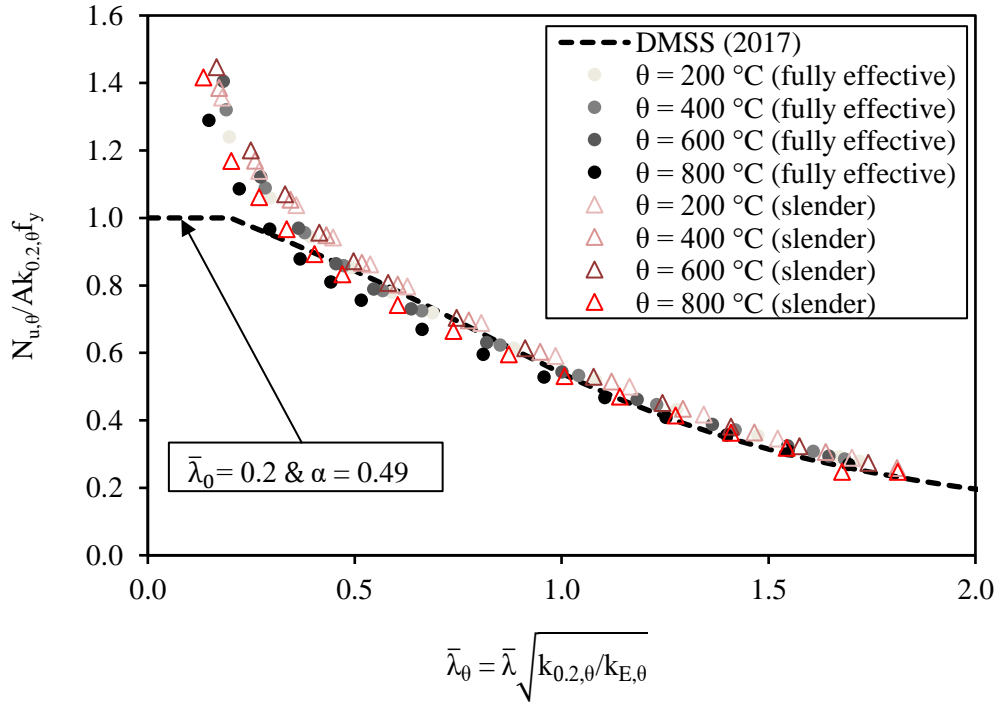


(b) Duplex

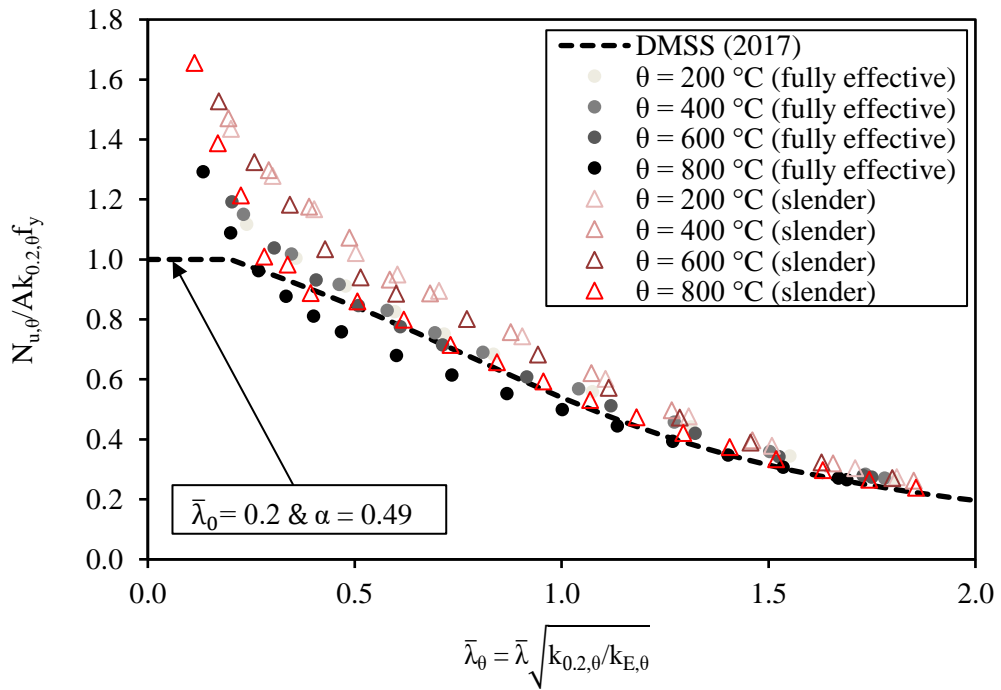


(c) Ferritic

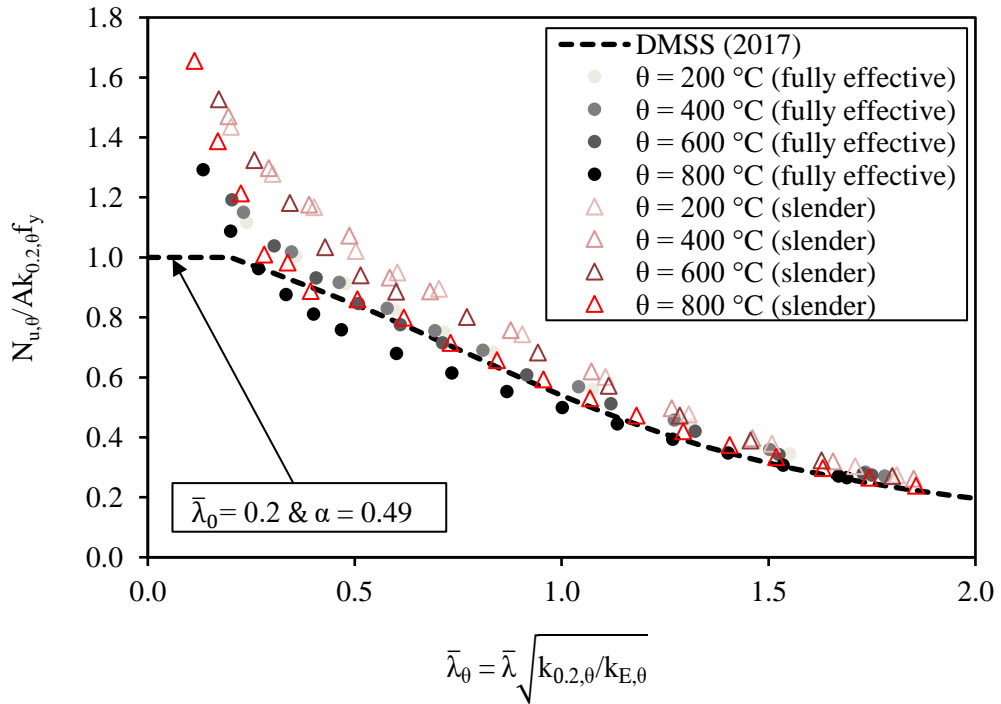
Figure 4.8: Comparison of FE results with the Design Manual for Structural Stainless Steel (DMSS) (2017) buckling curves for (a) austenitic, (b) duplex and (c) ferritic SHS and RHS columns for fully effective and slender cross-sections.



(a) Austenitic



(b) Duplex



(c) Ferritic

Figure 4.9: Comparison of FE results with the Design Manual for Structural Stainless Steel (DMSS) (2017) buckling curves for (a) austenitic, (b) duplex and (c) ferritic CHS columns for fully effective and slender cross-sections.

Table 4.4 presents a summary of the numerical comparison results including the mean, minimum, maximum and coefficient of variation (COV) values of the ratios between the ultimate loads obtained from the numerical parametric models ($N_{u,FE}$) and the predicted capacities obtained from EN 1993-1-2 ($N_{u,EC3}$) and Design Manual for Structural Stainless Steel ($N_{u,DMSS}$) methods for No. number of numerical data considered.

Table 4.4: Comparison between FE and predicted resistances.

Section	Material	FE/Predicted	$N_{u,FE}/N_{u,EC3}$	$N_{u,FE}/N_{u,DMSS}$	$N_{u,FE}/N_{u,proposed}$
SHS/RHS	Austenitic	No.	311	311	311
		Mean	0.96	1.12	1.19
		COV	0.13	0.14	0.09
		Max	1.26	1.58	1.43
		Min	0.68	0.84	0.96
	Duplex	No.	277	277	277
		Mean	0.95	1.08	1.07
		COV	0.15	0.13	0.08
		Max	1.21	1.53	1.27
		Min	0.64	0.79	0.87
Ferritic	No.	319	319	319	
	Mean	1.06	1.06	1.08	
	COV	0.11	0.10	0.06	
	Max	1.30	1.30	1.25	
	Min	0.80	0.83	0.92	
CHS	Austenitic	No.	104	104	104
		Mean	0.90	1.07	1.07
		COV	0.11	0.10	0.06
		Max	1.10	1.42	1.21
		Min	0.74	0.90	0.94
	Duplex	No.	106	106	106
		Mean	0.99	1.13	1.17
		COV	0.13	0.12	0.09
		Max	1.28	1.58	1.38
		Min	0.70	0.87	0.96
Ferritic	No.	118	118	118	
	Mean	1.10	1.06	1.10	
	COV	0.06	0.08	0.06	
	Max	1.24	1.22	1.22	
	Min	0.97	0.90	0.96	

The EN 1993-1-2 (2005) buckling curve which is common for all temperatures generally over-predicts the buckling resistance of the SHS, RHS and CHS columns for the case of austenitic and duplex stainless steels for all modelled temperatures, though it provides a better fit to the ferritic stainless steel columns for temperatures below 800 °C. This is expected as this curve was originally calibrated against carbon steel column data and inaccuracies are observed when its predicted capacities are compared with the FE obtained capacities for stainless steel columns, especially the austenitic and duplex grades

which possess comparatively different stress-strain responses at elevated temperatures to those of carbon steel. Furthermore, the EN 1993-1-2 buckling curves gives unsafe predictions for stainless steel columns as shown by the reliability analysis discussed in detail in Section 4.5.

The Design Manual for Structural Stainless Steel provisions (2017), which use the elevated temperature 0.2% proof stress rather than the elevated temperature stress at 2% total strain used in EN 1993-1-2 (2005), significantly under-predicts the resistance of the stockier columns with low elevated temperature member slenderness values as it limits the cross-section predicted resistance to the squash load based on the 0.2% proof stress, though it gives improved predictions than the EN 1993-1-2 (2005) method for higher slenderness ranges. Similar observation were made by Ng and Gardner (2007) and Uppfeldt et al. (2008) in their studies of elevated temperature resistance of stainless steel cold-formed SHS and RHS columns. Note that no comparisons have been made with the method proposed by Lopes et al. (2010) as it was developed for welded I-section columns, with distinctly different buckling performance compared with cold-formed box sections columns.

4.4.2 Extension of Lopes et al. method for tubular columns

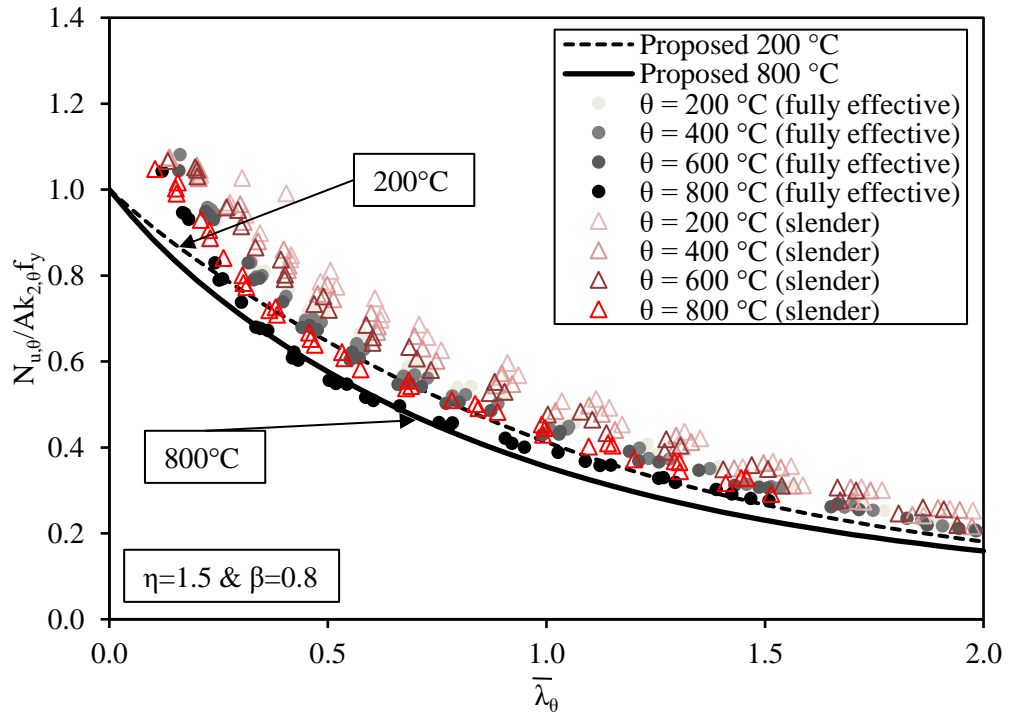
Buckling curves of the same form as the Lopes et al. (2010) formulation as presented in Section 4.3.2 were calibrated on the basis of the normalised FE data for the SHS, RHS and CHS cold-formed stainless steel columns generated herein to extend its application to these sections. The Lopes et al. method uses the 2% strength ($k_{2,\theta} f_y$) in its buckling curve formulation and in that respect allows similar coordination between the design rules provided for carbon steel and stainless steel. The use of the α parameter, as given by Equation (4.26) and (4.27), which is a function of elevated temperature strength and

stiffness reduction factors, enables different buckling curves for different temperatures, which is required for stainless steel columns as the FE data presented in Figure 4.6 to 4.9 confirm. In addition, the introduction of the β parameter in the χ_{fi} equation, which is similar to that employed in the lateral torsional buckling formulation in Clause 6.3.2.3 of EN 1993-1-1 (2014), allows the shape of the buckling curve to better represent the normalised FE data. The β and η parameters, which were fitted against data on welded I-section columns in (Lopes et al., 2010), were calibrated against the FE data for austenitic, duplex and ferritic SHS, RHS and CHS stainless steel columns generated in Section 4.2, and their proposed value are presented in Table 4.5.

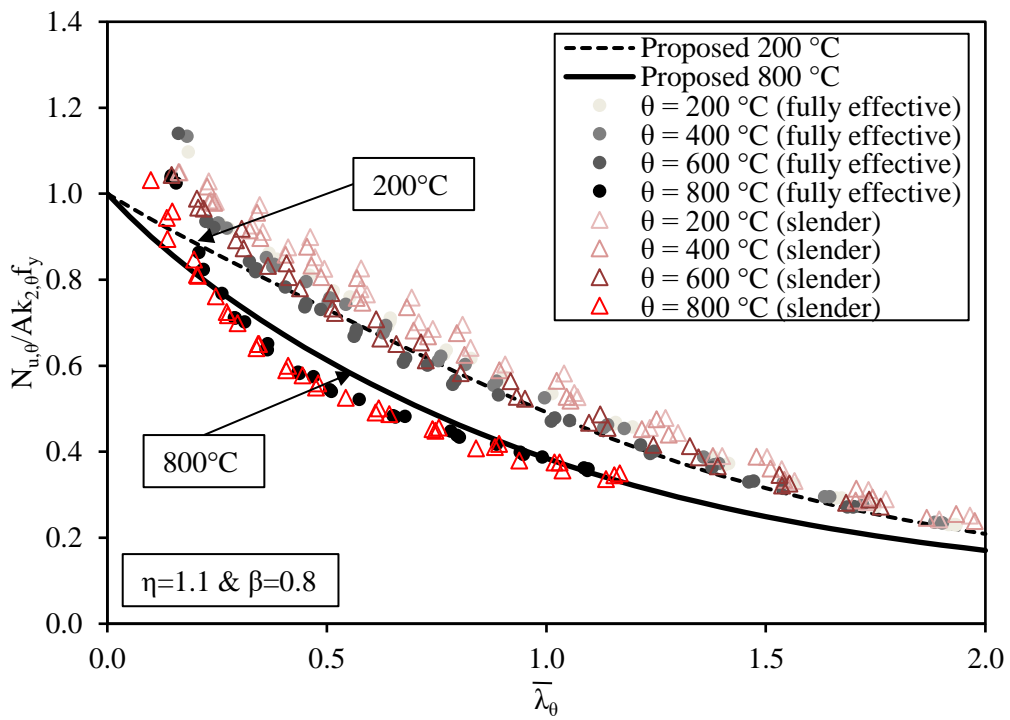
Table 4.5: Proposed β and η parameters for cold-formed SHS, RHS and CHS columns.

	SHS/RHS			CHS		
	Austenitic	Duplex	Ferritic	Austenitic	Duplex	Ferritic
β	0.8	0.8	1.0	0.7	0.8	1.0
η	1.5	1.1	0.6	1.3	1.2	0.5

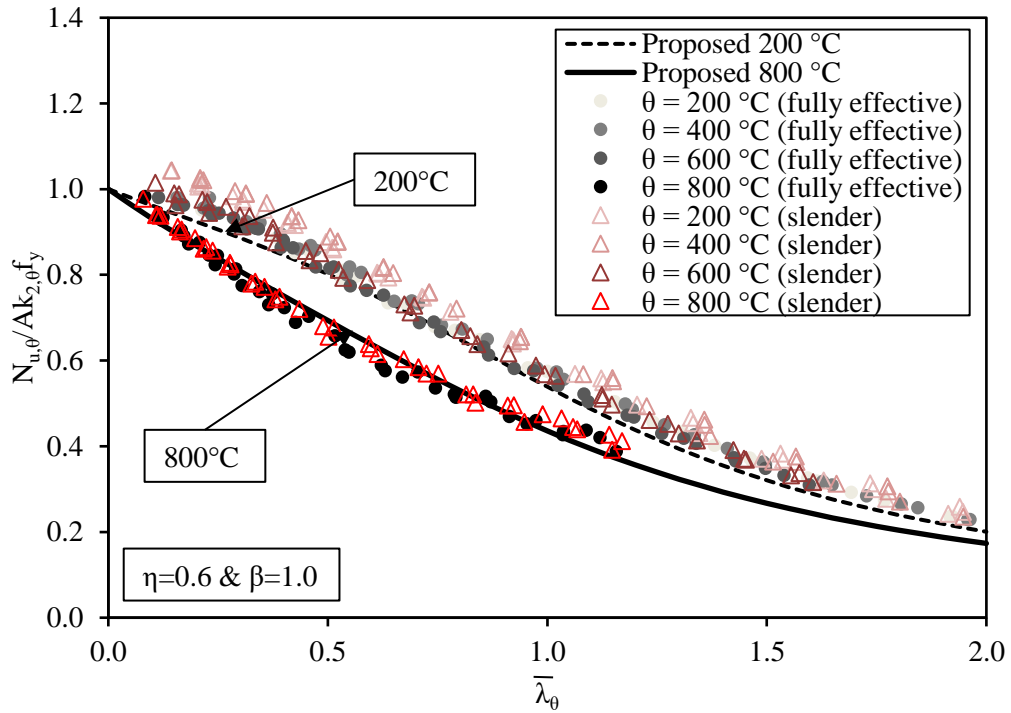
Figures 4.10 (a)-(c) and 4.11 (a)-(c) show the FE ultimate loads normalised by the cross-section elevated temperature yield loads ($Ak_{2,\theta}f_y$), plotted against the elevated temperature member slenderness $\bar{\lambda}_\theta$ from Equation (4.20) and (4.21), together with the proposed buckling curves for temperature bounds 200 °C and 800 °C also depicted for SHS/RHS and CHS columns respectively.



(a) Austenitic

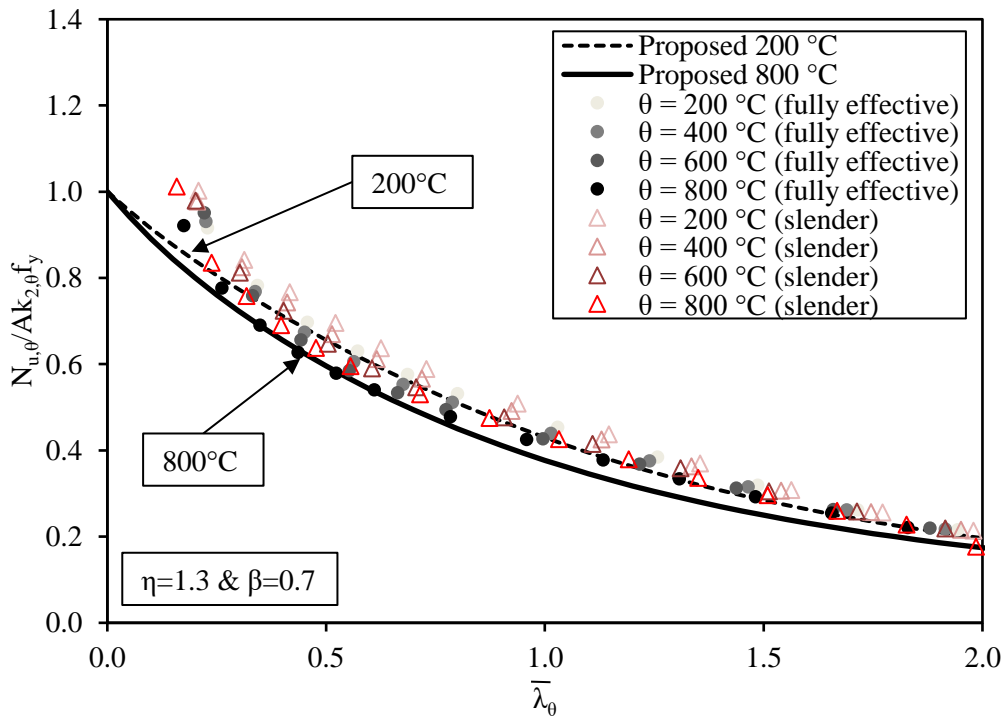


(b) Duplex

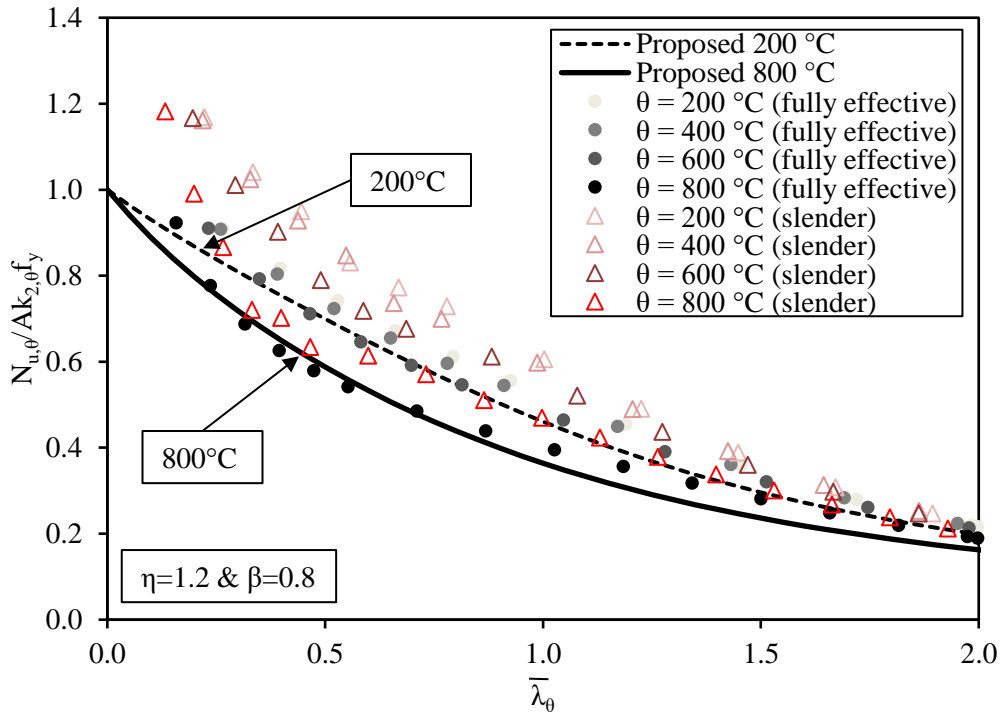


(c) Ferritic

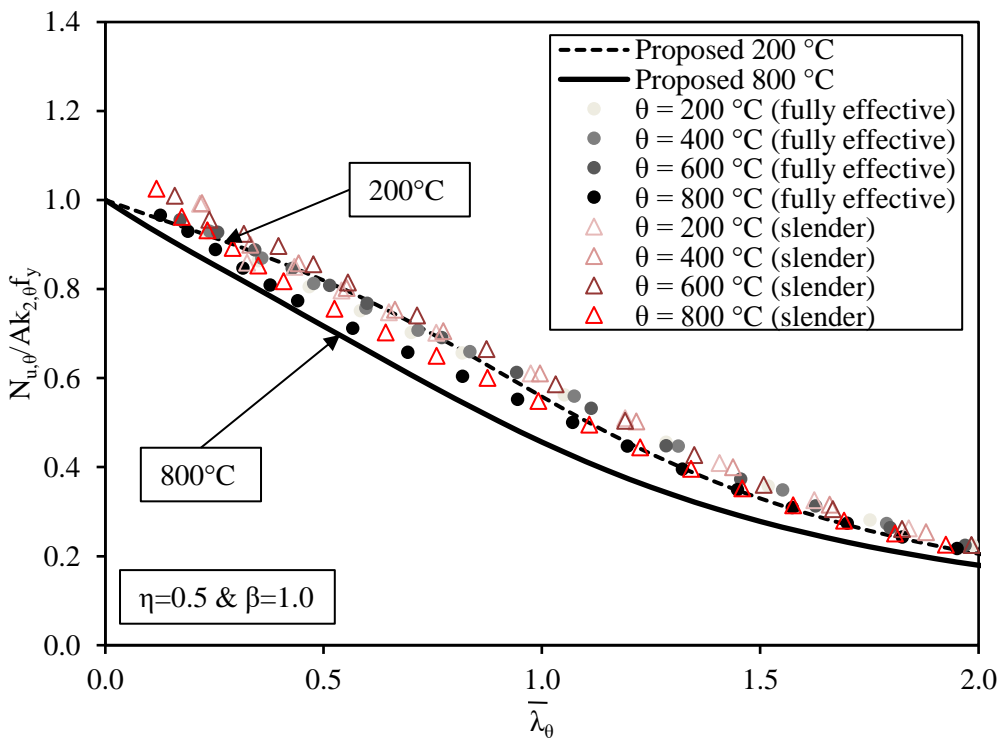
Figure 4.10: Comparison of FE results with the proposed buckling curves for (a) austenitic, (b) duplex and (c) ferritic SHS and RHS columns for fully effective and slender cross-sections.



(a) Austenitic



(b) Duplex



(c) Ferritic

Figure 4.11: Comparison of FE results with the proposed buckling curves for (a) austenitic, (b) duplex and (c) ferritic CHS columns for fully effective and slender cross-sections.

Comparisons between the FE results and the predicted resistances using the proposed new β and η parameters presented in Table 4.5 were carried out and the numerical comparisons in terms of $N_{u,FE}/N_{u,proposed}$ ratios are reported in Table 4.4 and also presented in Figure 4.12 and 4.13 for SHS/RHS and CHS columns, respectively. From the presented comparison results, it is shown that the proposed buckling curves provide an improved representation of the buckling resistance of cold-formed stainless steel SHS, RHS and CHS columns in fire and allow their flexural buckling capacity at elevated temperature to be predicted with higher degree of accuracy as well as with significantly less scatter.

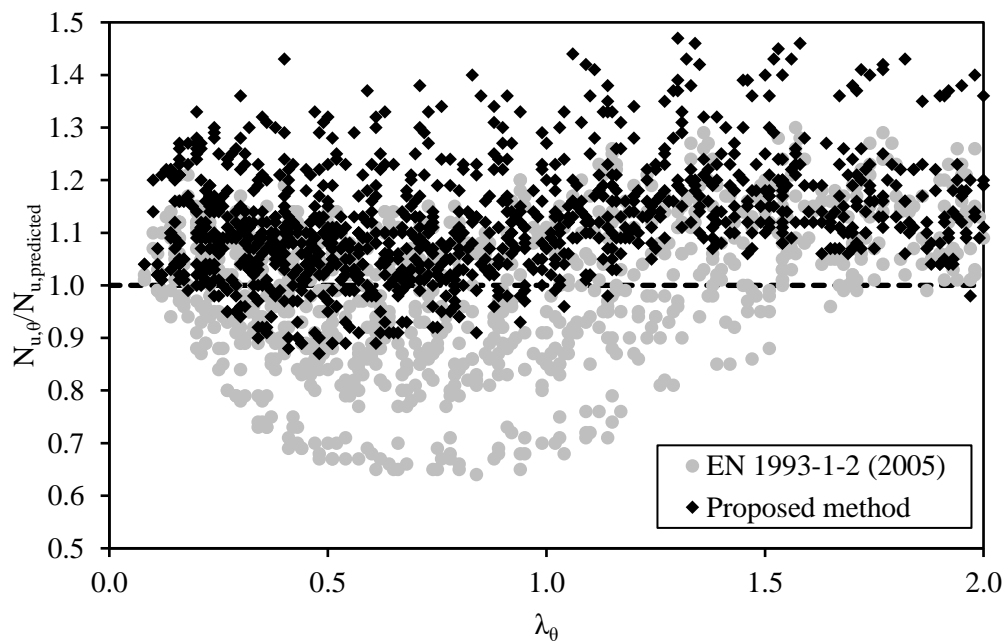


Figure 4.12: Comparisons of predicted capacities from EN 1993-1-2 (2005) and proposed methods for stainless steel SHS/RHS.

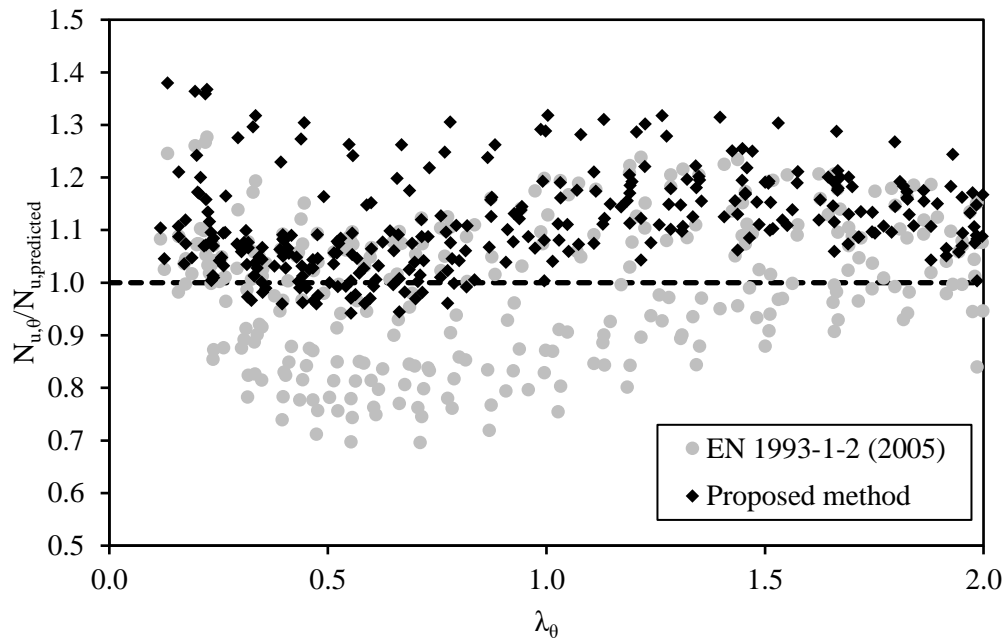


Figure 4.13: Comparisons of predicted capacities from EN 1993-1-2 (2005) and proposed methods for stainless steel CHS.

4.5 Reliability analysis

Safety assessments according to the method recommended by Kruppa (1999) for development of fire design rules were conducted to assess the reliability and accuracy of the existing and the proposed design methods for predicting the flexural buckling resistance of cold-formed austenitic, duplex and ferritic SHS/RHS and CHS stainless steel columns in fire. The method by Kruppa (1999) sets out three distinct reliability criteria to compare the theoretical resistance r_{ti} values, determined from the considered design method, with the experimental (or numerical) values r_{ei} , for each specimen as listed hereafter and further illustrated in Figure 4.14.

- Criterion 1: The percentage of the theoretical resistance values r_{ti} on the unsafe side by more than 15% of the experimental (or numerical) values r_{ei} i.e. $r_{ti} > 1.15r_{ei}$, which should be zero.
- Criterion 2: The percentage of the theoretical resistance values r_{ti} on the unsafe side i.e. $r_{ti} > 1.0r_{ei}$, which should be less than 20%.

- Criterion 3: The mean value of all percentage difference between the theoretical resistance values r_{ti} and the experimental (or numerical) values r_{ei} which should be on the safe side and less than zero.

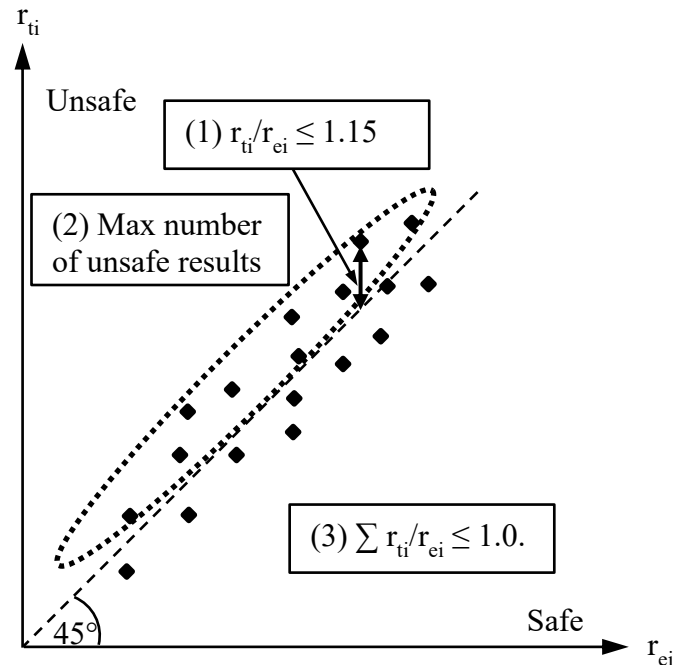


Figure 4.14: Schematic representation of the reliability criteria set out by Kruppa (1999)

Table 4.6 provides a summary of the safety assessment results for the predicted resistances from the design methods in EN 1993-1-2 (2005), Design Manual for Structural Stainless Steel (2017) and the proposed method, where it is shown that unlike to the other methods, the three reliability criteria are satisfied by the proposed method.

Table 4.6: Summary of the reliability assessment results.

Section	Material	Criterion	EN 1993-1-2 (2005)		DMSS (2017)		Proposed method	
SHS/RHS	Austenitic	Criterion 1	27.65%	Fail	2.57%	Fail	0.00%	Pass
		Criterion 2	60.45%	Fail	24.44%	Fail	3.86%	Pass
		Criterion 3	6.49%	Fail	-8.65%	Pass	-15.00%	Pass
	Duplex	Criterion 1	30.00%	Fail	11.88%	Fail	0.00%	Pass
		Criterion 2	70.00%	Fail	35.00%	Fail	15.00%	Pass
		Criterion 3	11.47%	Fail	-2.04%	Pass	-4.12%	Pass
	Ferritic	Criterion 1	9.04%	Fail	0.00%	Pass	0.00%	Pass
		Criterion 2	31.91%	Fail	30.85%	Fail	12.23%	Pass
		Criterion 3	-1.91%	Pass	-3.63%	Pass	-6.17%	Pass
CHS	Austenitic	Criterion 1	41.35%	Fail	0.00%	Pass	0.00%	Pass
		Criterion 2	82.69%	Fail	23.08%	Fail	11.54%	Pass
		Criterion 3	12.23%	Fail	-5.81%	Pass	-6.56%	Pass
	Duplex	Criterion 1	17.92%	Fail	0.94%	Fail	0.00%	Pass
		Criterion 2	50.94%	Fail	13.21%	Pass	3.77%	Pass
		Criterion 3	2.55%	Fail	-10.32%	Pass	-13.97%	Pass
	Ferritic	Criterion 1	0.00%	Pass	0.00%	Pass	0.00%	Pass
		Criterion 2	5.08%	Pass	25.42%	Fail	10.17%	Pass
		Criterion 3	-8.85%	Pass	-5.50%	Pass	-8.34%	Pass

4.6 Worked example

An example is provided in this section to demonstrate the workings of the proposed method. The minor axis buckling resistance $N_{b,z,fi,t,Rd}$ of a stainless steel RHS 100×50×6 column with a limiting design temperature of 600 °C is determined. The column length is 2.7m and has pinned support conditions. The cross-section classification is Class 1 according to DMSS (2017). The material properties used throughout this worked example are taken from the Design Manual for Stainless Steel Structures (2017). All symbols in accordance with Eurocode 3 notation and are as previously defined.

Cross-section geometric and material properties

Material properties – Austenitic grade EN 1.4301

$f_y = 230 \text{ N/mm}^2$, $f_u = 540 \text{ N/mm}^2$, $E = 200000 \text{ N/mm}^2$, $k_{2,\theta} = 0.68$ and $k_{E,\theta} = 0.76$ (at 600 °C)

Geometric properties – RHS 100×50×6

$$h = 100 \text{ mm}, b = 50 \text{ mm}, t = 6 \text{ mm}, r_i = 12 \text{ mm}, A = 1500 \text{ mm}^2, I_{zz} = 547239 \text{ mm}^4$$

Determine the non-dimensional slenderness

$$\bar{\lambda}_z = \sqrt{\frac{Af_y}{N_{cr,z}}} = \sqrt{\frac{1500 \times 230}{\pi^2 \times 200000 \times 547239 / 2700^2}} = 1.53$$

(the column effective length L_{cr} is taken as $1 \times$ column length = 2.7m)

$$\bar{\lambda}_{z,\theta} = \bar{\lambda} \left(\frac{k_{2,\theta}}{k_{E,\theta}} \right)^{0.5} = 1.53 \left(\frac{0.68}{0.76} \right)^{0.5} = 1.44$$

Determine the buckling reduction factor

$$\alpha = \eta \sqrt{\frac{235}{f_y} \times \frac{E}{210000}} \sqrt{\frac{k_{E,\theta}}{k_{2,\theta}}} = 1.5 \sqrt{\frac{235}{230} \times \frac{200000}{210000}} \sqrt{\frac{0.76}{0.68}} = 1.56$$

$$\varphi = 0.5 [1 + \alpha \bar{\lambda}_\theta + \beta \bar{\lambda}_\theta^2] = 0.5 [1 + 1.56 \times 1.44 + 0.8 \times 1.44^2] = 2.46$$

($\eta = 1.5$ and $\beta = 0.8$ for Austenitic SHS/RHS columns – from Table 4.5)

$$\chi_{fi} = \frac{1}{\varphi_\theta + \sqrt{\varphi_\theta^2 - \beta \bar{\lambda}_\theta^2}} = \frac{1}{2.46 + \sqrt{2.46^2 - 0.8 \times 1.44^2}} = 0.22$$

Determine the member buckling resistance in compression

$$N_{b,z,fi,t,Rd} = \frac{\chi_{fi} A k_{2,\theta} f_y}{\gamma_{M,fi}} = \frac{0.22 \times 1500 \times 0.68 \times 230}{1.0} = 51.6 \text{ kN}$$

4.7 Concluding remarks

The flexural buckling response of stainless steel columns of square, rectangular and circular hollow sections in fire was assessed through a numerical investigation. The developed FE models were initially validated against the room and elevated temperatures column tests reported in Chapter 3 and then adopted to conduct a systematic parametric study. The FE generated flexural buckling data were used to carry out an assessment of the design methods provided in EN 1993-1-2 (2005) and the Design Manual for Stainless Steel Structures (2017) where it was shown that inaccurate flexural buckling resistances in fire are predicted by both methods. New buckling curves for cold-formed stainless steel square, rectangular and circular hollow section columns in fire in line with the Lopes et al.'s (2010) method were proposed on the basis of the FE results, which were shown to consistently predict the flexural buckling capacities of the columns in fire with higher degree of accuracy as well as with significantly less scatter. Moreover, the predicted resistances from the proposed buckling curves were assessed in accordance with the three reliability criteria set out by Kruppa (1999) and were shown to consistently satisfy the specified safety levels required.

Chapter 5 Fire design of stainless steel hollow section beam-columns

5.1 Introduction

In this chapter, a comprehensive numerical modelling study of cold-formed stainless steel tubular beam-column members subjected to compressive axial load and uniform bending moment at elevated temperatures is carried out. Through a rigorous validation process, the accuracy of the numerical models is first established, following which extensive parametric study is carried out to generate the structural performance data required for assessment and development of design guidance rules. Improvements to the current Eurocode 3 design approach for stainless steel beam-columns are made through two key areas: (1) proposing a new flexural buckling formulation to obtain accurate predictions of the pure compression end point $N_{b,Rd}$ at elevated temperature; this was presented in Chapter 4 and (2) development of new combined loading interaction factor k for the combined axial load and bending moment interaction equations, which will be presented in this chapter. The accuracy of the proposals for predicting the load-carrying capacity of stainless steel SHS/RHS and CHS beam-columns in fire is assessed through numerical comparisons as well as reliability assessments.

5.2 Design rules for beam-column members in fire

In this section the prescribed expressions defined in EN 1993-1-4 (2006) for the design of stainless steel beam-column members at room and elevated temperatures are presented. For structural fire design of stainless steel structural components, EN 1993-1-4 refers to

EN 1993-1-2 (2005), where the design rules provided are mainly based on those developed for carbon steel structures.

5.2.1 EN 1993-1-4 - room temperature design

The current European design provision for stainless steel at room temperature in EN 1993-1-4 (2006) adopts the same design interaction curve for beam-columns that is used in EN 1993-1-1 (2005) for carbon steel. These are defined in Equations (5.1) and (5.2) for the cases of beam-column members with and without lateral torsional buckling (LTB), respectively. However, modified combined loading factors, k_y , k_z and k_{LT} , given by Equations (5.3) - (5.5), are employed to consider the effects of the material's stress-strain response on the member instability.

For axial load + major axis bending + minor axis bending (without LTB)

$$\frac{N_{Ed}}{(N_{b,Rd})_{\min}} + k_y \frac{M_{y,Ed} + N_{Ed}e_{Ny}}{\beta_{w,y}W_{pl,y}f_y/\gamma_{M1}} + k_z \frac{M_{z,Ed} + N_{Ed}e_{Nz}}{\beta_{w,z}W_{pl,z}f_y/\gamma_{M1}} \leq 1 \quad (5.1)$$

For axial load + major axis bending + minor axis bending (with LTB)

$$\frac{N_{Ed}}{(N_{b,Rd})_{\min,1}} + k_{LT} \frac{M_{y,Ed} + N_{Ed}e_{Ny}}{M_{b,Rd}} + k_z \frac{M_{z,Ed} + N_{Ed}e_{Nz}}{\beta_{w,z}W_{pl,z}f_y/\gamma_{M1}} \leq 1 \quad (5.2)$$

The definition of symbols in Equations (5.1) and (5.2) are as follow:

- N_{Ed} , $M_{y,Ed}$ and $M_{z,Ed}$ are the design values for axial load, major axis moment and minor axis moment, respectively.
- e_{Ny} and e_{Nz} are the shifts in the neutral axes when the cross-section is subject to uniform compression (i.e. for slender cross-sections).

- $(N_{b,Rd})_{\min}$ is the smallest value of the resistance buckling load $N_{b,Rd}$ for the following four buckling modes: flexural buckling about the y axis, flexural buckling about the z axis, torsional buckling and torsional-flexural buckling.
- $(N_{b,Rd})_{\min,1}$ is the smallest value of the resistance buckling load $N_{b,Rd}$ for the following three buckling modes: flexural buckling about the z axis, torsional buckling and torsional-flexural buckling.
- $M_{b,Rd}$ is the member lateral torsional buckling resistance.
- $\beta_{w,y}$ and $\beta_{w,z}$ values depend on the cross-section classification. $\beta_w = 1$ for Class 1 and 2 sections, $\beta_w = W_{el}/W_{pl}$ for Class 3 sections and $\beta_w = W_{eff}/W_{pl}$ for Class 4 sections.
- W_{el} and W_{pl} are the elastic and plastic section moduli, respectively (subscripts y and z refer to major and minor axes, respectively).
- γ_{M1} is the partial safety factor for member resistance in fire.
- f_y is the yield stress.
- k_{LT} , k_y , and k_z are the interaction factors which are defined by Equations (5.3)-(5.5), respectively according to Method 2 of EN1993-1-1 (2005), where $\bar{\lambda}_y$ and $\bar{\lambda}_z$ are the non-dimensional member slenderness for major and minor axes, respectively.

$$k_{LT} = 1.0 \quad (5.3)$$

$$k_y = 1 + 2(\bar{\lambda}_y - 0.5) \frac{N_{Ed}}{N_{b,Rd,y}} \quad \text{but} \quad 1.2 \leq k_y \leq 1.2 + 2 \frac{N_{Ed}}{N_{b,Rd,y}} \quad (5.4)$$

$$k_z = 1 + 2(\bar{\lambda}_z - 0.5) \frac{N_{Ed}}{(N_{b,Rd})_{\min,1}} \quad \text{but} \quad 1.2 \leq k_z \leq 1.2 + 2 \frac{N_{Ed}}{(N_{b,Rd})_{\min,1}} \quad (5.5)$$

5.2.2 EN 1993-1-2 - elevated temperature design

The fire design of stainless steel structures is covered in EN 1993-1-2 (2005). For beam-column members, the resistance equations are the same as those provided for carbon steels. These are given by Equations (5.6) and (5.7) for Class 1 and Class 2 cross-sections for with and without LTB, respectively and Equations (5.8) and (5.9) for Class 3 cross-sections for with and without LTB, respectively.

For axial load + major axis bending + minor axis bending (without LTB) – Class 1 and 2

$$\frac{N_{fi,Ed}}{\chi_{min,fi} A k_{y,\theta} f_y / \gamma_{M,fi}} + k_y \frac{M_{y,fi,Ed}}{W_{pl,y} k_{y,\theta} f_y / \gamma_{M,fi}} + k_z \frac{M_{z,fi,Ed}}{W_{pl,z} k_{y,\theta} f_y / \gamma_{M,fi}} \leq 1 \quad (5.6)$$

Axial load + major axis bending + minor axis bending (with LTB) – Class 1 and 2

$$\frac{N_{fi,Ed}}{\chi_{z,fi} A k_{y,\theta} f_y / \gamma_{M,fi}} + k_{LT} \frac{M_{y,fi,Ed}}{\chi_{LT,fi} W_{pl,y} k_{y,\theta} f_y / \gamma_{M,fi}} + k_z \frac{M_{z,fi,Ed}}{W_{pl,z} k_{y,\theta} f_y / \gamma_{M,fi}} \leq 1 \quad (5.7)$$

Axial load + major axis bending + minor axis bending (without LTB) – Class 3

$$\frac{N_{fi,Ed}}{\chi_{min,fi} A k_{y,\theta} f_y / \gamma_{M,fi}} + k_y \frac{M_{y,fi,Ed}}{W_{el,y} k_{y,\theta} f_y / \gamma_{M,fi}} + k_z \frac{M_{z,fi,Ed}}{W_{el,z} k_{y,\theta} f_y / \gamma_{M,fi}} \leq 1 \quad (5.8)$$

Axial load + major axis bending + minor axis bending (with LTB) – Class 3

$$\frac{N_{fi,Ed}}{\chi_{z,fi} A k_{y,\theta} f_y / \gamma_{M,fi}} + k_{LT} \frac{M_{y,fi,Ed}}{\chi_{LT,fi} W_{el,y} k_{y,\theta} f_y / \gamma_{M,fi}} + k_z \frac{M_{z,fi,Ed}}{W_{el,z} k_{y,\theta} f_y / \gamma_{M,fi}} \leq 1 \quad (5.9)$$

The definition of symbols in Equations (5.6)-(5.9) are as follows:

- $N_{fi,Ed}$, $M_{y,fi,Ed}$ and $M_{z,fi,Ed}$ are the design values for the axial load, major axis moment and minor axis moment in the fire situation, respectively.

- $\chi_{\min,fi}$ is the smallest of reduction factors for flexural, torsional and torsional-flexural buckling at elevated temperature
- $\chi_{z,fi}$ and $\chi_{LT,fi}$ are the reduction factors for minor axis flexural buckling and lateral torsional buckling at elevated temperature, respectively.
- A is the cross-sectional area.
- $k_{y,\theta}$ is the elevated temperature reduction factor for yield stress
- $\gamma_{M,fi}$ is the partial safety factor for member resistance in fire
- k_y, k_{LT}, k_z are the combined loading factors for elevated temperature.

All other symbols are as previously defined where the subscript ‘fi’ or ‘ θ ’ relates to elevated temperature. The combined loading factors at elevated temperature, k_y and k_z , are given by Equations (5.10) and (5.11) for major and minor axes bending, respectively.

$$k_y = 1 - \frac{\mu_y N_{fi,Ed}}{\chi_{y,fi} A k_{y,\theta} f_y / \gamma_{M,fi}} \leq 3 \quad (5.10)$$

$$\text{with } \mu_y = (2\beta_{M,y} - 5) \bar{\lambda}_\theta + 0.44\beta_{M,y} + 0.29 \leq 0.8 \text{ with } \bar{\lambda}_{y,20} \leq 1.1$$

$$k_z = 1 - \frac{\mu_z N_{fi,Ed}}{\chi_{z,fi} A k_{y,\theta} \frac{f_y}{\gamma_{M,fi}}} \leq 3 \quad (5.11)$$

$$\text{with } \mu_z = (1.2\beta_{M,z} - 3) \bar{\lambda}_{z,\theta} + 0.71\beta_{M,z} - 0.29 \leq 0.8$$

where $\beta_{M,y}$ and $\beta_{M,z}$ are the equivalent uniform moment factors for the major and minor axes, respectively, $\chi_{y,fi}$ and $\chi_{z,fi}$ are the flexural buckling reduction factors for major and minor axes, respectively at elevated temperature and $\bar{\lambda}_{y,\theta}$ and $\bar{\lambda}_{z,\theta}$ are the non-dimensional member slenderness for major and minor axes, respectively at elevated temperature θ , which are defined by Equations (5.12) and (5.13).

$$\bar{\lambda}_{y,\theta} = \bar{\lambda}_y \left[\frac{k_{y,\theta}}{k_{E,\theta}} \right]^{0.5} \quad (5.12)$$

$$\bar{\lambda}_{z,\theta} = \bar{\lambda}_z \left[\frac{k_{y,\theta}}{k_{E,\theta}} \right]^{0.5} \quad (5.13)$$

5.3 Proposed design method

5.3.1 Combined axial load and bending moment interaction equations

As discussed in section 5.2, the EN 1993-1-2 (2005) design rules for stainless steel beam-column members in fire were simply taken as those for carbon steel beam-columns without rigorous validation. In addition, they are based on the flexural buckling curves in EN 1993-1-2, which were shown in Chapter 4 to be given inaccurate predictions of the flexural buckling capacities of stainless steel column members in fire. Hence, to overcome these limitations, in this section new combined loading design interaction expressions as presented in Equation (5.14) for combined axial load and uniaxial major axis bending and Equation (5.15) for combined axial load and uniaxial minor axis bending are developed. The proposed design expressions are of the same form as the EN 1993-1-2 (2005) expressions, but employ the flexural buckling resistances from the buckling curves proposed in Chapter 4 and incorporate the combined loading interaction factors k_y and k_z calibrated on the basis of the numerical results of stainless steel beam-column members developed herein.

Axial load + major axis bending (no LTB)

$$\frac{N_{fi,Ed}}{N_{b,y,Rd,fi}/\gamma_{M,fi}} + k_y \frac{M_{y,fi,Ed}}{M_{c,y,Rd,fi}/\gamma_{M,fi}} \leq 1 \quad (5.14)$$

Axial load + minor axis bending (no LTB)

$$\frac{N_{fi,Ed}}{N_{b,z,Rd,fi}/\gamma_{M,fi}} + k_z \frac{M_{z,fi,Ed}}{M_{c,z,Rd,fi}/\gamma_{M,fi}} \leq 1 \quad (5.15)$$

The definition of symbols in Equations (5.14) - (5.15) are as follow:

- $N_{fi,Ed}$, $M_{y,fi,Ed}$ and $M_{z,fi,Ed}$ are the design values for the axial load, major axis moment and minor axis moment in the fire situation, respectively
- $N_{b,y,Rd,fi}$ and $N_{b,z,Rd,fi}$ are the major and minor axes flexural buckling resistances in fire situation, respectively (obtained from the proposed method in Chapter 4)
- $M_{c,y,Rd,fi}$ and $M_{c,z,Rd,fi}$ are the major and minor axes cross-section bending moment resistances in fire, respectively
- k_y and k_z are the major and minor axes combined loading interaction factors, respectively (developed in Section 5.3.2 herein)
- $\gamma_{M,fi}$ is the partial safety factor for member resistance in fire

5.3.2 Derivation of combined loading interaction factors

In this section, numerically derived interaction factors are presented and discussed for RHS and CHS members, which are subsequently altered to a simplified formula. The details of the numerical models used to generate structural performance data for the derivation of the interaction factors is presented hereafter.

5.3.2.1 Numerical modelling

The validated numerical models of steel and stainless steel beam-column members developed in Chapter 3 were employed for the numerical modelling study herein. Structural performance data for stainless steel tubular cross-section beam-column members at elevated temperature were generated for the calibration of the combined

loading interaction factors. For the purpose of this numerical study, the beam-column members were modelled under isothermal loading conditions, where the beam-column models were subjected to a given uniform temperature θ , incorporating the reduced stress-strain data corresponding to the modelled temperature θ , followed by applying a combined axial compressive load and uniform bending moment until failure.

The parametric models covered beam-column members of RHS and CHS profiles subjected to varying levels of axial load to bending ratios subjected to elevated temperatures: 200 °C, 400 °C, 600 °C and to 800 °C. Uniaxial bending about both major and minor axes were considered. Beam-columns of austenitic, duplex and ferritic stainless steel grades were modelled. For each stainless steel grade and elevated temperature considered, members with slenderness $\bar{\lambda}_\theta$ between 0.5 and 3.0 were modelled. Both modelled cross-sections were classified as fully effective in accordance with EN 1993-1-2 (2005) and EN 1993-1-4 (2015) cross-section classification limits at both room and elevated temperatures. Table 5.1 and 5.2 presents a summary of the parametric models. In total, 1134 RHS and 604 CHS parametric results were generated. The same modelling assumptions as explained in Chapter 3 were employed in the FE models of developed herein with the input parameters taken as those described hereafter.

The initial local and global geometric imperfections were introduced as eigenmodes that were scaled to a suitable magnitude. Similar to the columns modelled in Chapter 4, the beam-column members were modelled with an initial global imperfection amplitude which was set equal to the tolerance limit, which is specified in EN 1090-2 (2008) as $L/1000$, where L is the member length. The initial local imperfection amplitude for the RHS beam-column members was set to $b/200$, where b is the section width and for the CHS beam-column members, the local imperfection amplitude was $0.008D$, where D is the diameter, in accordance with recommendations in EN 1993-1-5-Annex C (2006).

The loading was simulated in two steps, firstly, a concentric compressive axial load was applied to the beam-column member, which was maintained constant, followed by an increasing equal uniaxial bending moment at the member ends until failure. The applied axial compressive load $N_{Ed,\theta}$ was taken as a portion of the member flexural buckling resistance $N_{b,y,Rd,fi}$ or $N_{b,z,Rd,fi}$ i.e. $N_{Ed,fi} = n N_{b,y, Rd,\theta}$ or $N_{b,z, Rd,\theta}$ with n (load level) values equal to 0.3, 0.4, 0.5, 0.6 and 0.7 and $N_{b,y,Rd,fi}$ or $N_{b,z,Rd,fi}$ capacities obtained from the proposed flexural buckling curves in Chapter 4. Hence, a range of axial load to bending moment ratios were considered. The load-deformation response was obtained by using a modified Riks method (ABAQUS, 2016).

Table 5.1: Summary of the parametric study variables.

Section	Grade	Cross-section	h/b	Buckling axis	Temperatures (°C)	$\bar{\lambda}_\theta$
RHS	Austenitic	RHS 150×100×14	1.5	Major and Minor	200 °C, 400 °C, 600 °C and 800 °C	0.2-3.0
	Duplex	RHS 150×100×14	1.5	Major and Minor		
	Ferritic	RHS 150×100×14	1.5	Major and Minor		
CHS	Austenitic	CHS 100×8	-	-		
	Duplex	CHS 100×8	-	-		
	Ferritic	CHS 100×8	-	-		

Table 5.2: Room temperature material properties adopted in the parametric models.

Grade	Section	E (N/mm ²)	$f_{0.2}$ (N/mm ²)	f_2 (N/mm ²)	f_u (N/mm ²)	n	m
Austenitic	SHS/RHS (F), CHS	200000	460	603	700	2.9	2.8
Duplex	SHS/RHS (F), CHS	200000	630	706	780	4.8	3.3
Ferritic	SHS/RHS (F), CHS	200000	430	490	490	4.6	3.5
Austenitic	SHS/RHS (C)	200000	640	838	830	7.1	3.2
Duplex	SHS/RHS (C)	200000	800	896	980	6.7	3.2
Ferritic	SHS/RHS (C)	200000	560	610	610	6.8	3.6

F = Flat face, C = Corner region

5.3.2.2 Derivation of interaction factor formulae

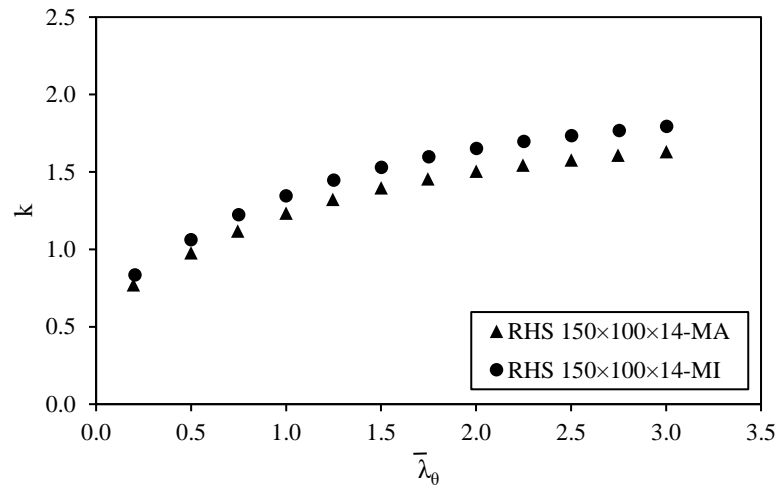
The numerically derived interaction factors, k_y and k_z , were obtained by rearranging Equations (5.14) and (5.15), as presented by Equations (5.16) and (5.17), where $N_{fi,Ed}$, $M_{y,fi,Ed}$ and $M_{z,fi,Ed}$ were set to the FE obtained values, $N_{b,y,Rd,fi}$ and $N_{b,z,Rd,fi}$ were set to

the elevated temperature flexural buckling resistances obtained from the proposed method in Chapter 4 and $M_{c,y,Rd,fi}$ and $M_{c,z,Rd,fi}$ are the elevated temperature cross-section resistances determined according to EN 1993-1-2 (2005) design provisions.

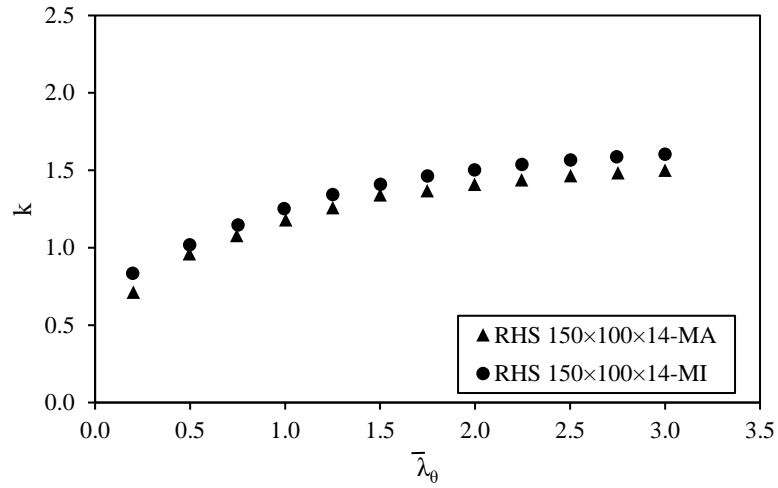
$$k_y = \left(1 - \frac{N_{fi,Ed}}{N_{b,y,Rd,fi}} \right) / \left(\frac{M_{y,fi,Ed}}{M_{c,y,Rd,fi}} \right) \quad (5.16)$$

$$k_z = \left(1 - \frac{N_{fi,Ed}}{N_{b,z,Rd,fi}} \right) / \left(\frac{M_{z,fi,Ed}}{M_{c,z,Rd,fi}} \right) \quad (5.17)$$

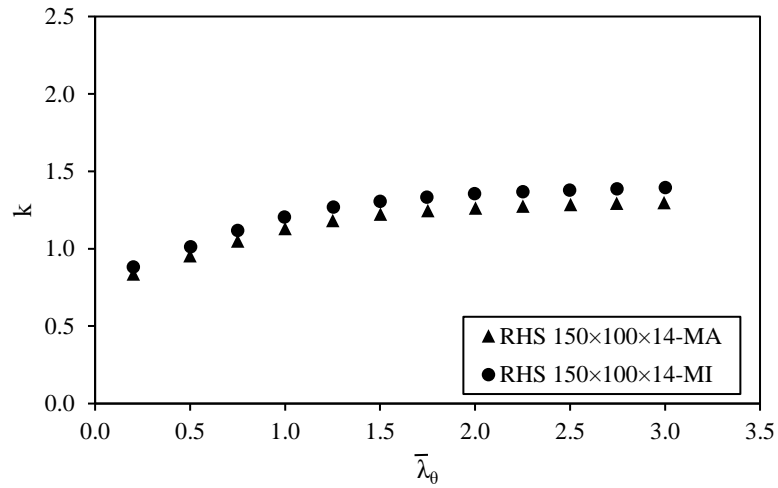
Examples of the derived interaction factors for RHS and CHS austenitic, duplex and ferritic beam-column members subjected to 200 °C temperature and with load level $n = 0.2$ are provided in Figures 5.1 and 5.2, respectively. Figures 5.1 and 5.2 demonstrate the relationship between the derived interaction factors k and non-dimensional slenderness ($\bar{\lambda}_\theta$).



(a) Austenitic stainless steel

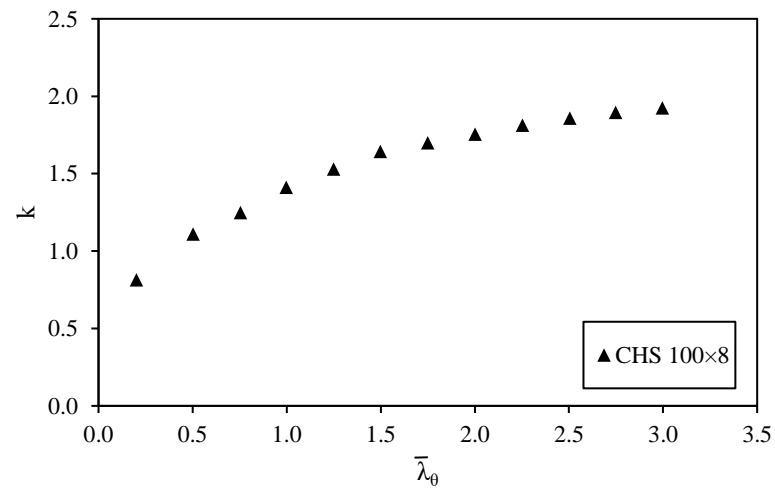


(b) Duplex stainless steel

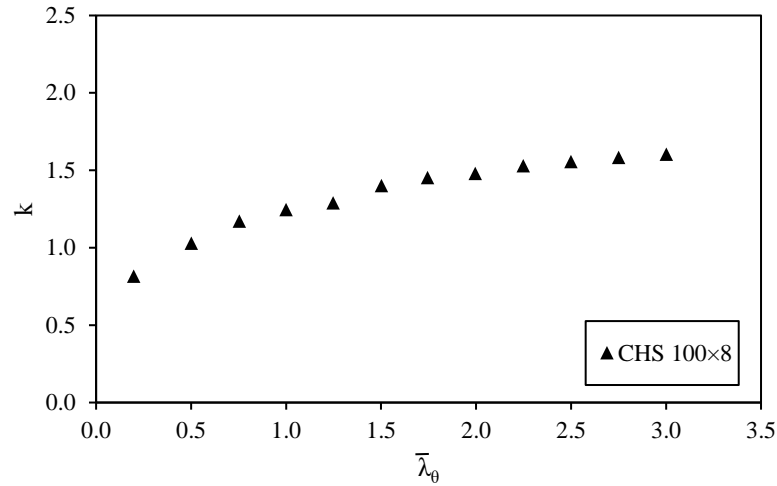


(c) Ferritic stainless steel

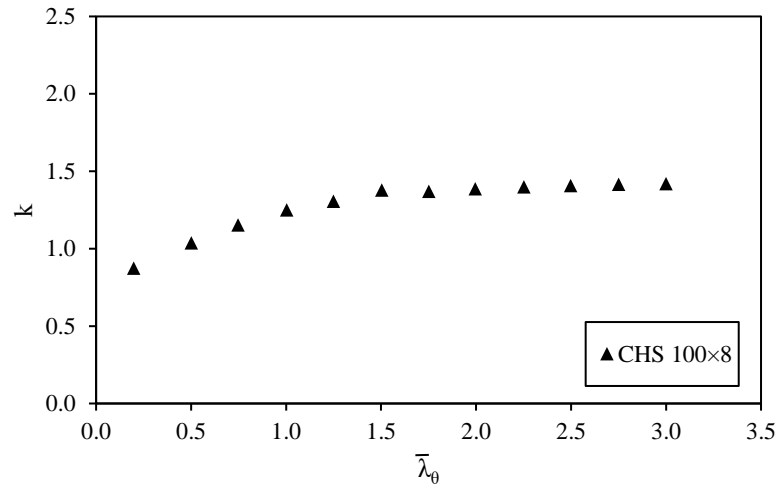
Figure 5.1: Examples of numerically derived k factors for RHS beam-columns ($n=0.2$ at $\theta=200^\circ\text{C}$).



(a) Austenitic stainless steel



(b) Duplex stainless steel



(c) Ferritic stainless steel

Figure 5.2: Examples of numerically derived k factors for CHS beam-columns ($n=0.2$ at $\theta=200^\circ\text{C}$).

It can be observed that the relationship between the non-dimensional member slenderness ($\bar{\lambda}_\theta$) and interaction factors (k) has a steep slope in the low member slenderness range but a relatively steady slope in the high member slenderness range. Hence, the design formulae for k can be assumed to be of a bi-linear form given by Equation (5.18), as used by Greiner and Linder (2006) and Boissonnade et al. (2006) for carbon steel beam-column members and more recently for stainless steel tubular member at room temperature by Zhao et al. (2016).

$$k = 1 + D_1(\bar{\lambda}_\theta - D_2)n, \text{ but } k \leq 1 + D_1(D_3 - D_2)n \quad (5.18)$$

where D_1 and D_2 are the coefficients, which define the linear relationship between member slenderness $\bar{\lambda}_\theta$ and interaction factor k in the low slenderness range i.e. when $\bar{\lambda}_\theta \leq D_3$, while D_3 is a limit value, beyond which the interaction factor k remains constant equal to $1 + D_1(D_3 - D_2)n$. D_1 and D_2 values for each individual load level were calculated from a regression fit of Equation (5.18) to the corresponding numerical dataset over a member slenderness range of 0.2 and 1.2. The values of D_1 and D_2 were averaged for all load levels (i.e. $0.2 \leq n \leq 0.7$) for each specified temperature. Then, the values of D_3 were calculated based on the fit of Equation (5.18) to the upper bound of the assembled numerical dataset for low axial compressive load level (i.e. $n \leq 0.4$). Table 5.3 reports the values of D_1 , D_2 and D_3 for each of the material grades and temperatures considered.

The calculations of D_1 , D_2 and D_3 coefficients for the CHS ferritic beam-column specimen at 200 °C with load level $n = 0.2$ is illustrated below:

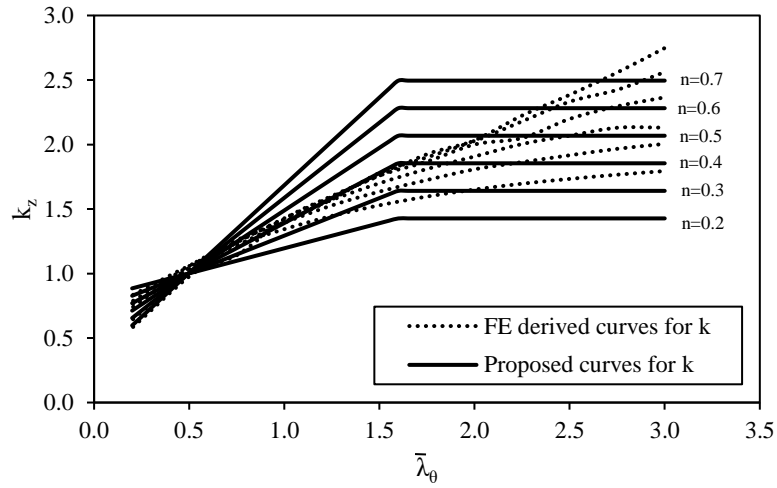
To Calculate D_1 and D_2 , a linear line is fitted between the k data in the range of $\bar{\lambda}_\theta = 0.2 - 1.2$.

- The slope of the linear line is $m = 0.42$ and the intercept is $c = 0.82$.
- $D_1 = m/n = 0.42/0.2 = 2.08 \approx 2.1$
- $D_2 = (1 - c)/(D_1 n) = (1 - 0.82)/(2.08 \times 0.2) = 0.44 \approx 0.4$

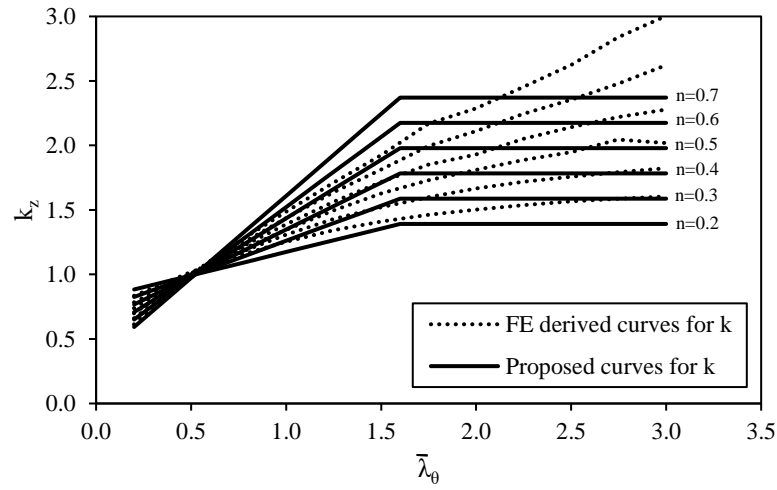
To Calculate D_3 a horizontal line is fitted between the k data in the range of $\bar{\lambda}_\theta > 1.2$.

- The value of the horizontal line is $d = 1.38$
- $D_3 = (d + D_2 D_1 n - 1)/(D_1 n) = (1.38 + 0.44 \times 2.08 \times 0.2 - 1)/(2.08 \times 0.2) = 1.35 \approx 1.4$

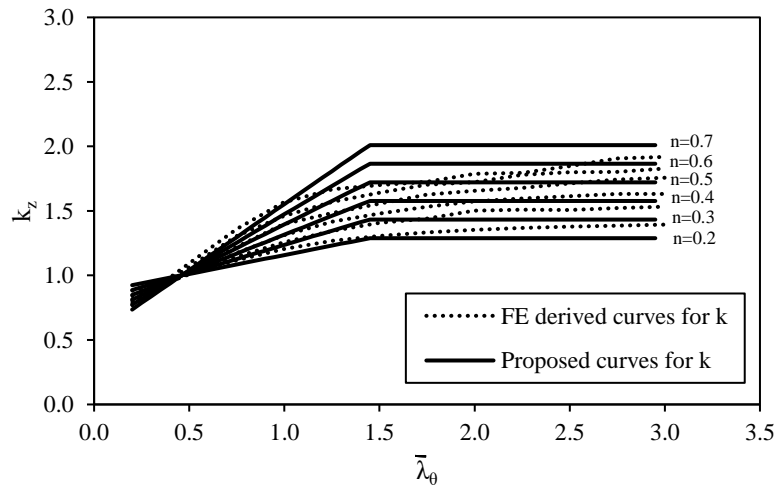
The FE derived and proposed curves for interaction factors are shown in Figure 5.3 for RHS 150×100×14 (minor axis), Figure 5.4 for RHS 150×100×14 (major axis) and Figure 5.5 for CHS 100×8.



(a) Austenitic stainless steel

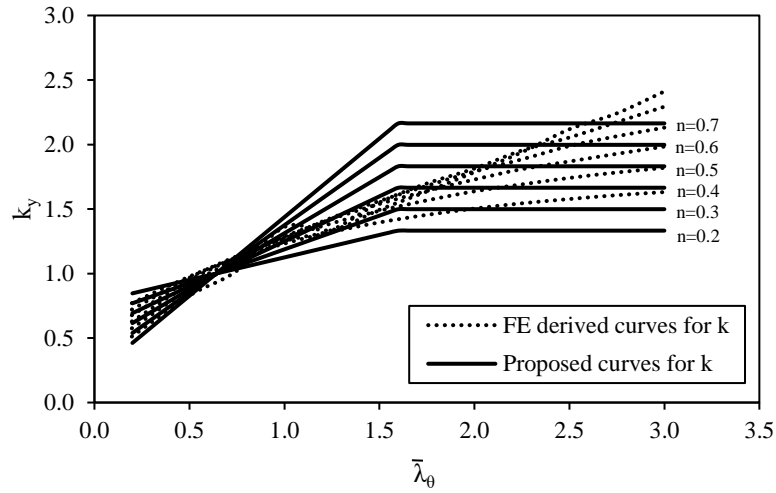


(b) Duplex stainless steel

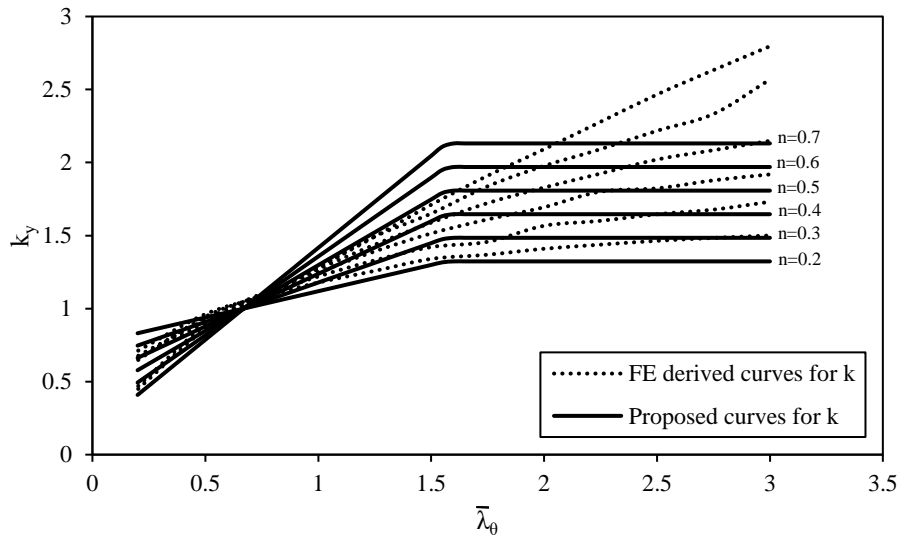


(c) Ferritic stainless steel

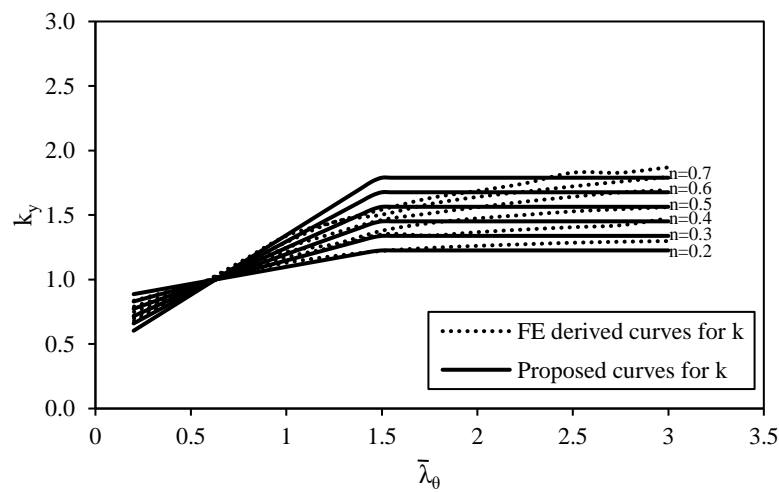
Figure 5.3: Comparison between FE and proposed derived curves for RHS minor axis at $\theta=200^{\circ}\text{C}$ interaction factors.



(a) Austenitic stainless steel

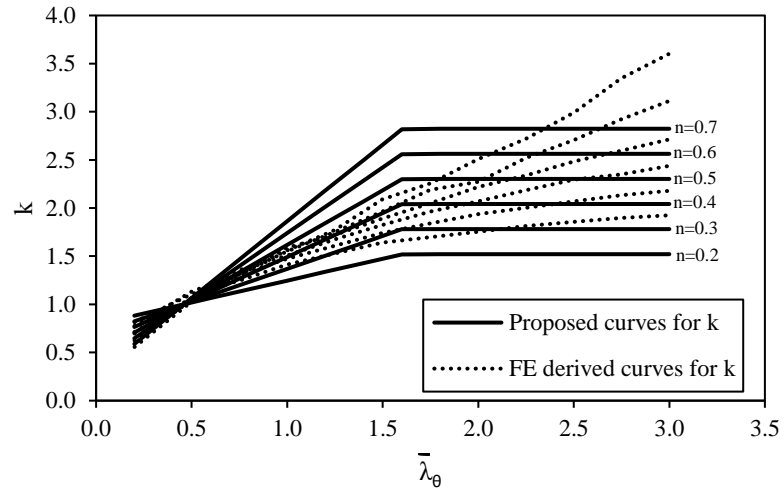


(b) Duplex stainless steel

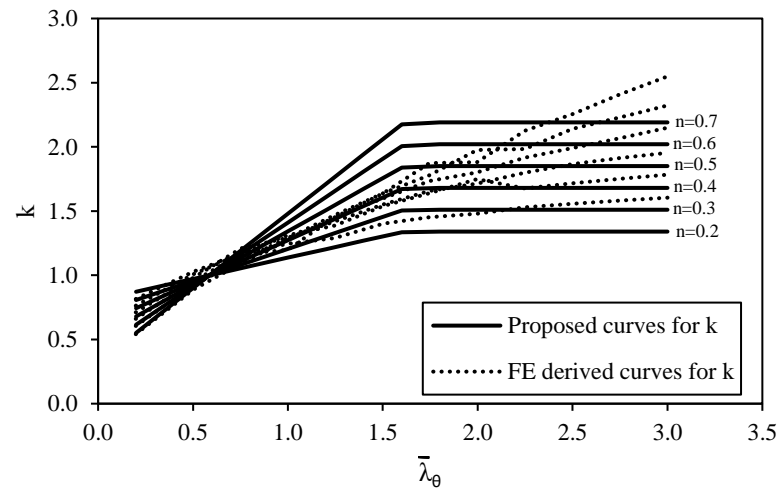


(c) Ferritic stainless steel

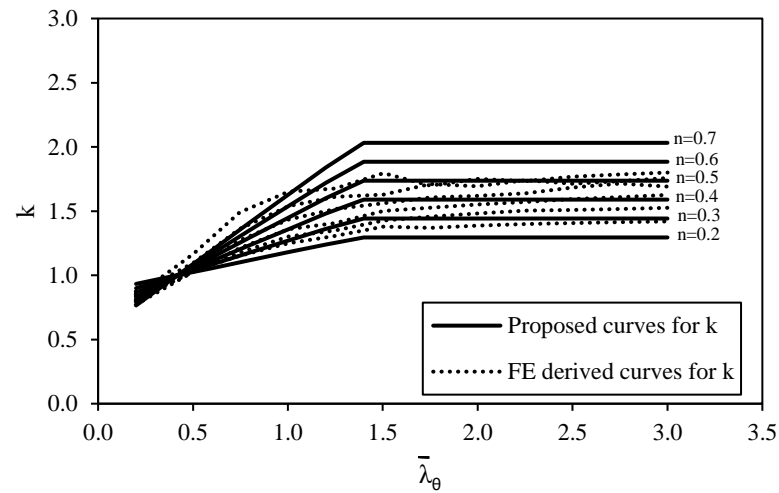
Figure 5.4: Comparison between FE and proposed derived curves for RHS major axis at $\theta=200^{\circ}\text{C}$ interaction factors.



(a) Austenitic stainless steel



(b) Duplex stainless steel



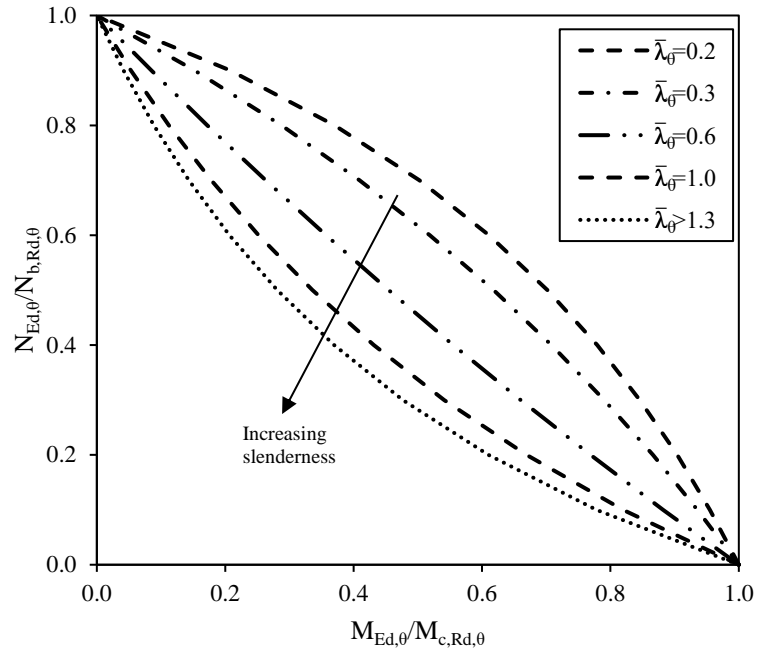
(c) Ferritic stainless steel

Figure 5.5: Comparison between FE and proposed derived curves for CHS at $\theta=200^\circ\text{C}$ interaction factors.

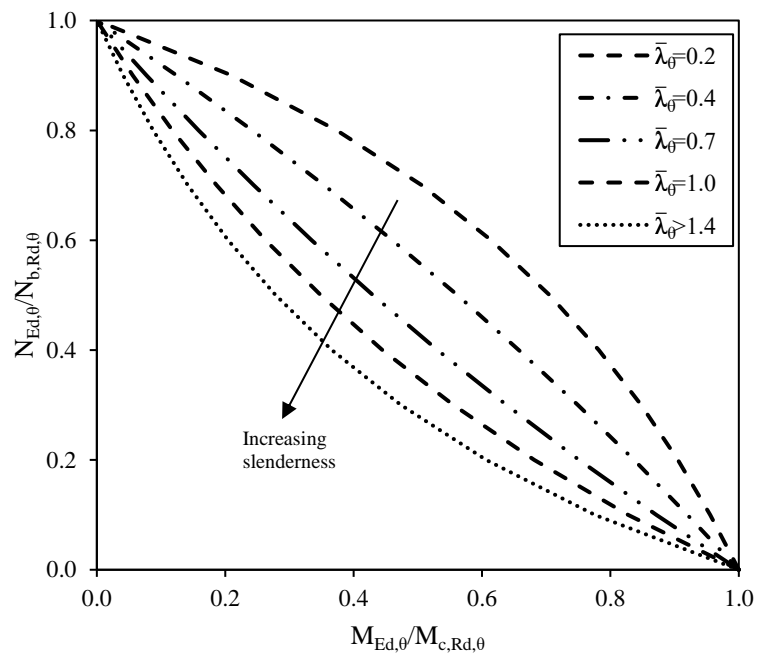
Table 5.3: Proposed interaction factors for different cross-sections, material grades and elevated temperatures.

Section	Material	k_y or k_z		Temperature ($^{\circ}\text{C}$)			
				200	400	600	800
RHS	Austenitic	k_z	D ₁	1.9	2.3	2.4	2.6
			D ₂	0.5	0.5	0.4	0.3
			D ₃	1.6	1.6	1.6	1.5
		k_y	D ₁	1.7	2.0	2.2	2.6
			D ₂	0.6	0.6	0.5	0.4
			D ₃	1.6	1.6	1.6	1.5
	Duplex	k_z	D ₁	1.8	2.1	2.3	2.4
			D ₂	0.5	0.5	0.4	0.2
			D ₃	1.6	1.6	1.6	1.6
		k_y	D ₁	1.8	2.1	2.2	2.4
			D ₂	0.7	0.6	0.6	0.4
			D ₃	1.6	1.5	1.5	1.5
	Ferritic	k_z	D ₁	1.5	1.4	1.3	1.7
			D ₂	0.5	0.5	0.5	0.2
			D ₃	1.4	1.4	1.5	1.4
		k_y	D ₁	1.3	1.3	1.2	2.0
			D ₂	0.6	0.7	0.7	0.3
			D ₃	1.5	1.5	1.5	1.5
CHS	Austenitic	k_y or k_z	D ₁	2.3	2.7	2.9	2.5
			D ₂	0.5	0.4	0.4	0.3
			D ₃	1.6	1.5	1.5	1.6
	Duplex	k_y or k_z	D ₁	1.7	1.9	2.1	2.2
			D ₂	0.6	0.6	0.5	0.3
			D ₃	1.6	1.6	1.5	1.5
	Ferritic	k_y or k_z	D ₁	1.5	1.5	1.1	1.2
			D ₂	0.4	0.4	0.6	0.5
			D ₃	1.4	1.4	1.5	1.5

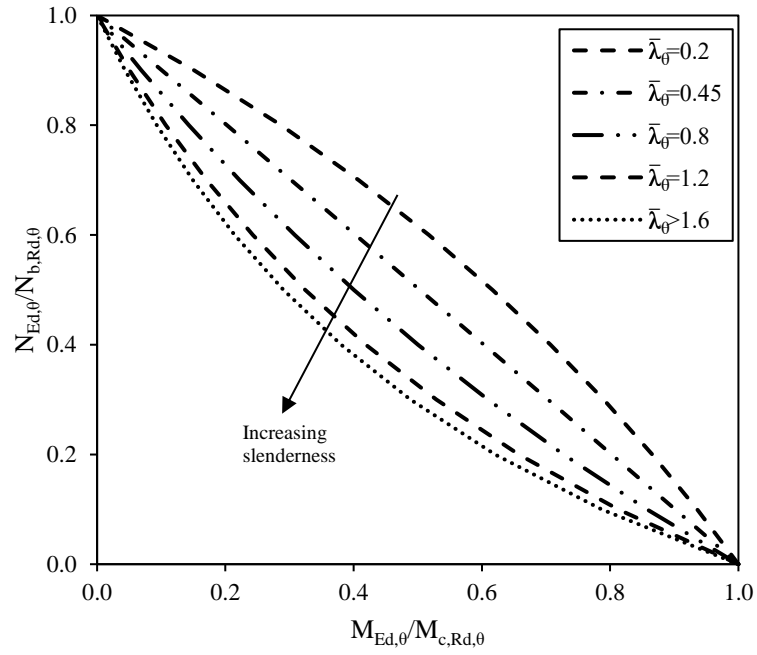
The proposed design interaction curves for austenitic, duplex and ferritic stainless steel beam-columns are plotted in Figure 5.6 and 5.7 for major and minor axes, respectively while those for CHS beam columns are shown in Figure 5.8. For austenitic, duplex and ferritic, respectively. All figures show that as the member slenderness increases, the interaction curves tends to be concave; this is due to the second order effect as the member slenderness grows.



(a) Austenitic stainless steel

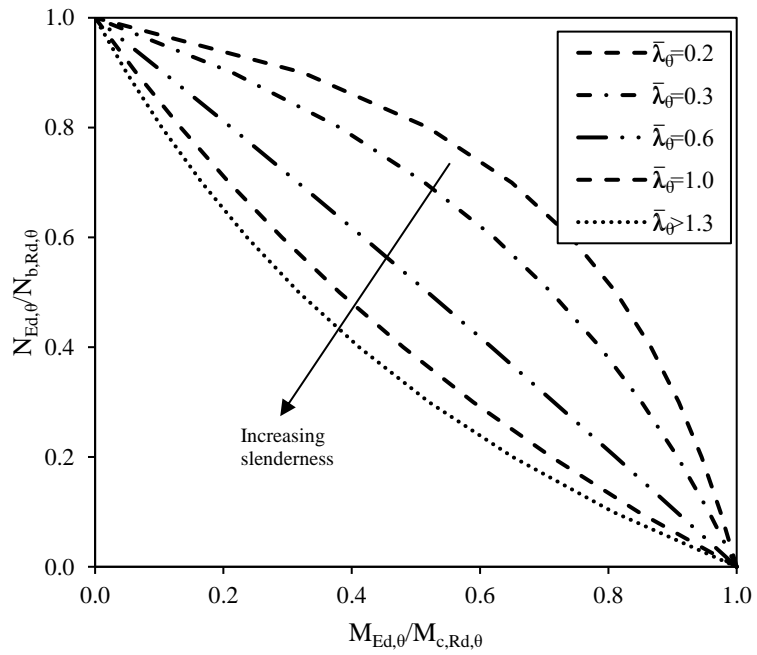


(b) Duplex stainless steel

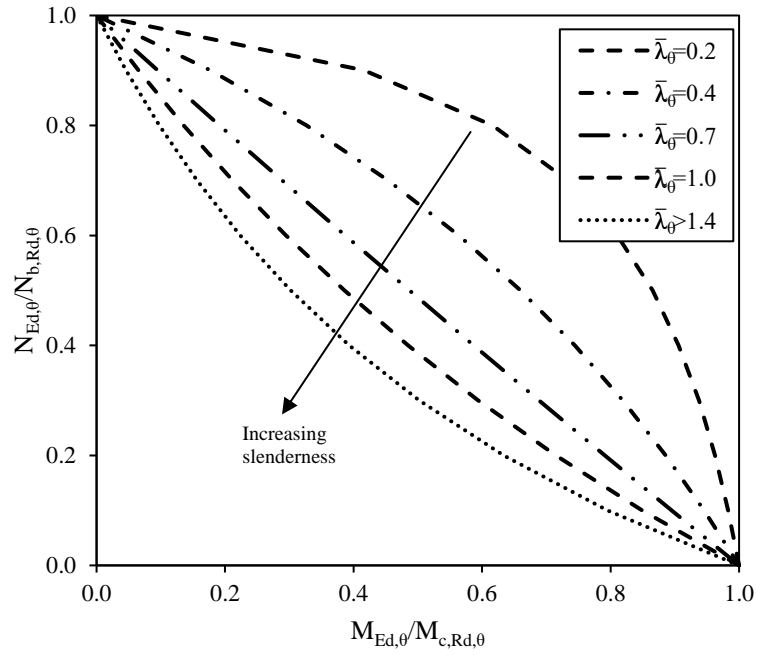


(c) Ferritic stainless steel

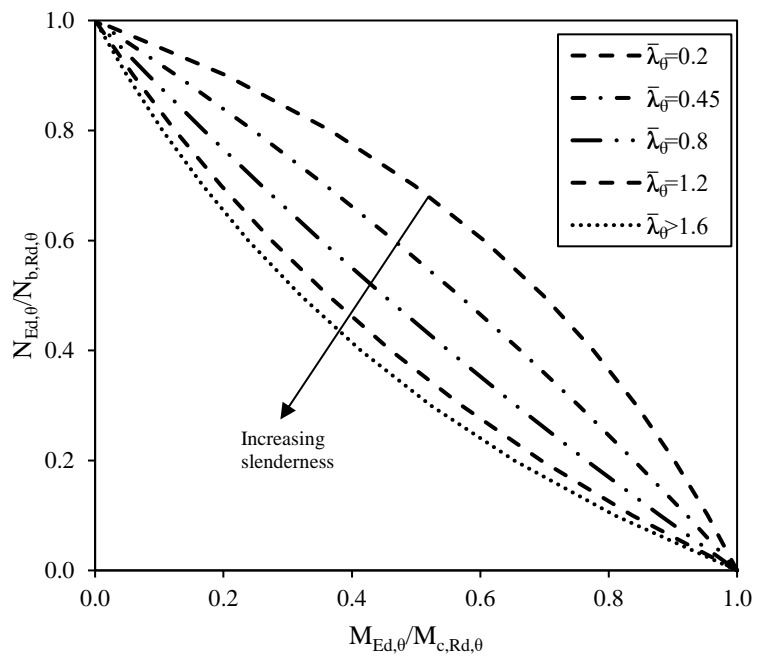
Figure 5.6: RHS minor axis beam-column design interaction curves $\theta=200^\circ\text{C}$ for varying member slenderness.



(a) Austenitic stainless steel

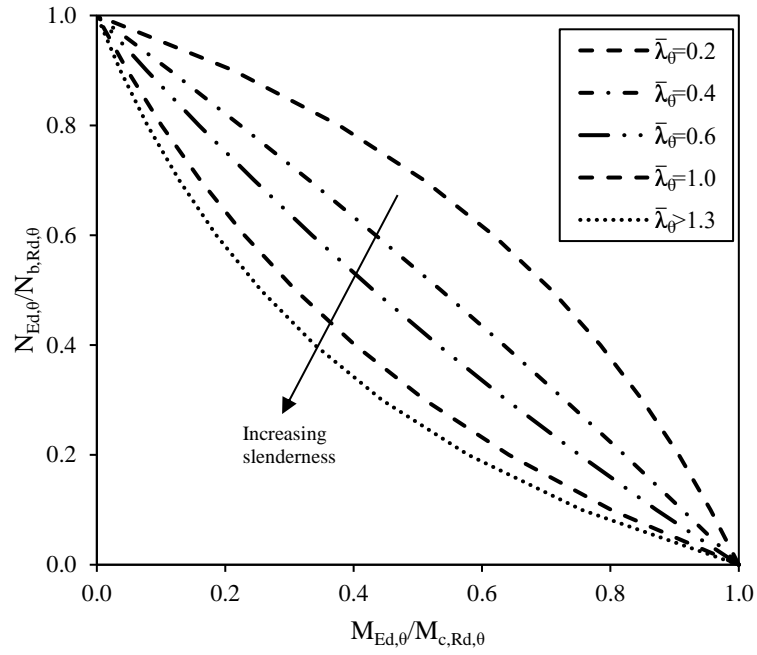


(b) Duplex stainless steel

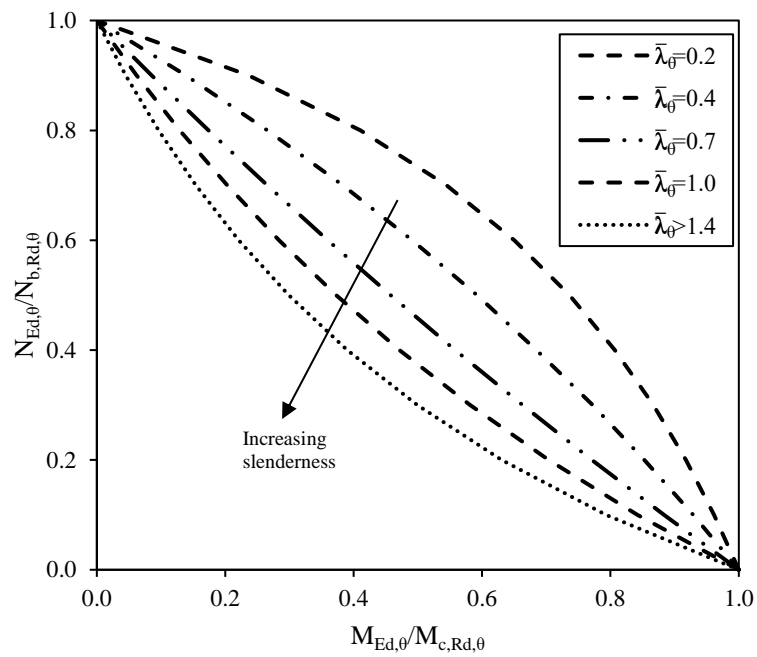


(c) Ferritic stainless steel

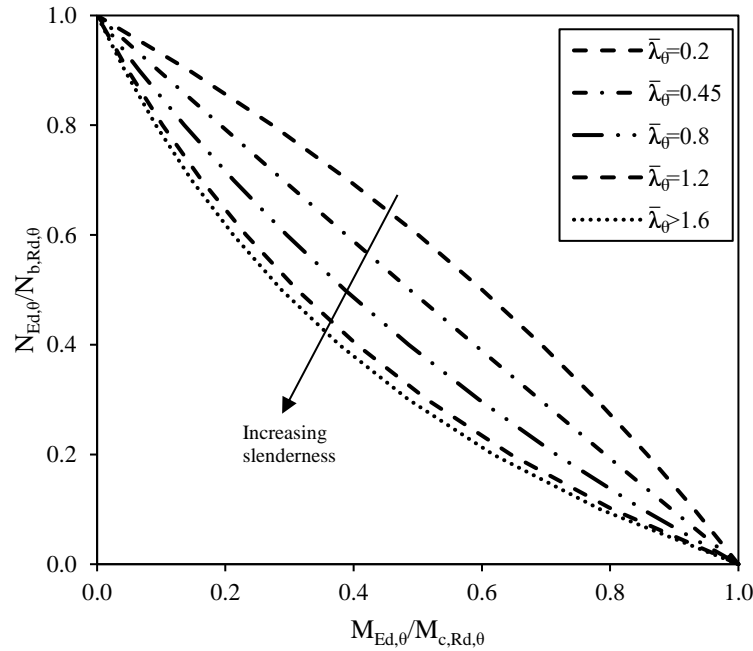
Figure 5.7: RHS major axis beam-column design interaction curves $\theta=200^\circ\text{C}$ for varying member slenderness.



(a) Austenitic stainless steel



(b) Duplex stainless steel



(c) Ferritic stainless steel

Figure 5.8: CHS beam-column design interaction curves $\theta=200^{\circ}\text{C}$ for varying member slendernesses.

5.4 Comparison of predicted resistances with proposed and codified methods

The accuracy and the reliability of the newly proposed design approach was assessed through a comparison against a large number of FE results, which were generated through parametric study. In the parametric study, beam-column performance data for RHS and CHS stainless steel members were generated.

5.4.1 Analysis and Discussion of results

For the modelled RHS, the outer depth and width of the cross-section were set equal to 200 mm and 100 mm, respectively, leading to a cross-section aspect ratio of 2.0. For the CHS, the outer diameter was set 100 mm. The values for the internal corner of the RHS was set equal to the thickness, which was 15 mm, resulting in a range of cross-section plate slenderness for the austenitic, duplex and ferritic ($\bar{\lambda}_p$) between 0.37 and 0.44, and for the CHS, the thickness was set to 6mm having a local slenderness ($\bar{\lambda}_c$) of 0.19 and

0.22 for stainless steel hollow sections. The lengths of the beam-column members were varied to cover a wide spectrum of member slenderness between 0.2 and 2.0. The axial compressive load applied concentrically ranged from load levels of 0 to 1, increasing in steps of 0.1, followed by applying a moment concentrically. This provided a broad range of axial to bending moment ratios to be considered. In total, 1980 parametric study results were generated, including 1320 for the RHS (major and minor axes) and 660 for CHS. The numerical results were compared with the strength predictions from the European code EN 1993-1-2 (2005) and the proposed approach. This is presented in Figures 5.10 to 5.13 for the austenitic, duplex and ferritic stainless steel grades, respectively, where the FE to predicted failure load ratio $N_{u,FE,\theta}/N_{u,pred,\theta}$ is plotted against the angle parameter ϕ . A $N_{u,FE,\theta}/N_{u,pred,\theta}$ ratio of value greater than unity indicates that the FE data point lies on the safe side of the design interaction curve. The predicted failure load ($N_{u,pred,\theta}$) was determined assuming proportional loading, as defined in Figure 5.9 (Zhao et al. e, 2016), where axial load ratio $N_{\theta}/N_{R,\theta}$ is plotted against the bending moment ratio $M_{\theta}/M_{R,\theta}$. In Figures 5.19, N_{θ} and M_{θ} are the FE ($N_{u,FE,\theta}$ and $M_{u,FE,\theta}$) or predicted ($N_{u,pred,\theta}$ and $M_{u,FE,\theta}$) axial compressive load and bending moment capacities of the beam-column members under consideration, while $N_{R,\theta}$ and $M_{R,\theta}$ are the corresponding flexural buckling load and bending moment resistances at elevated temperature. The angle parameter ϕ is defined by Equation (5.19). Note that $\theta = 0^{\circ}$ corresponds to pure bending while $\theta = 90^{\circ}$ represents pure compression. The measured geometric and material properties have been used in all comparisons and all partial safety factors have been set equal to unity.

Table 5.4 reports the ratios of FE beam-column failure loads to predicted failure loads for austenitic, duplex and ferritic stainless steel beam-columns, respectively. The ratios greater than unity indicate that the FE data points lie on the safe side (outside) of the design interaction curve.

$$\phi = \tan^{-1} \left[\frac{N_{u,FE,\theta}/N_{R,\theta}}{M_{u,FE,\theta}/M_{R,\theta}} \right] \quad (5.19)$$

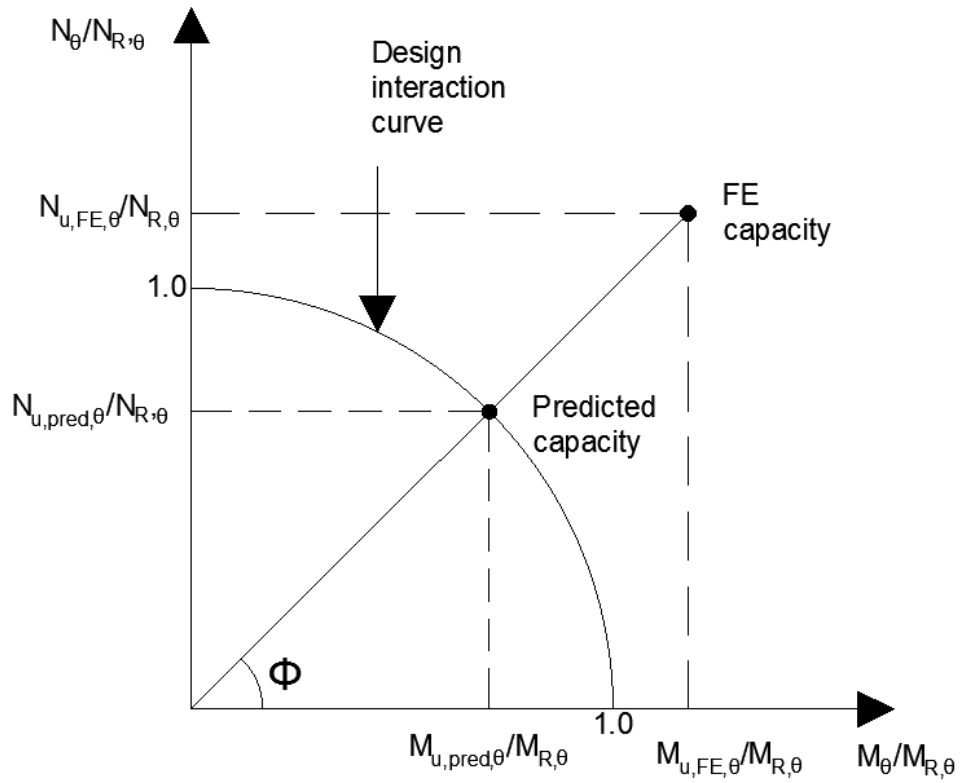
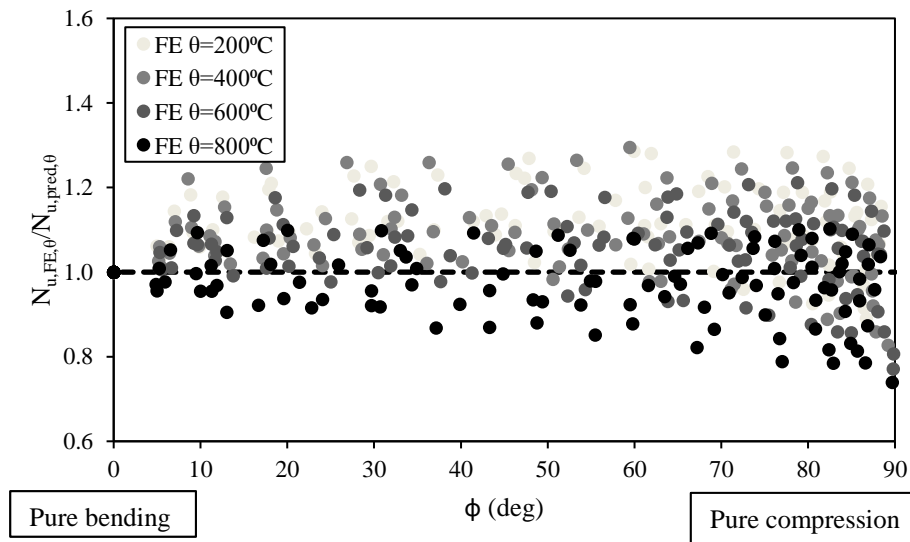
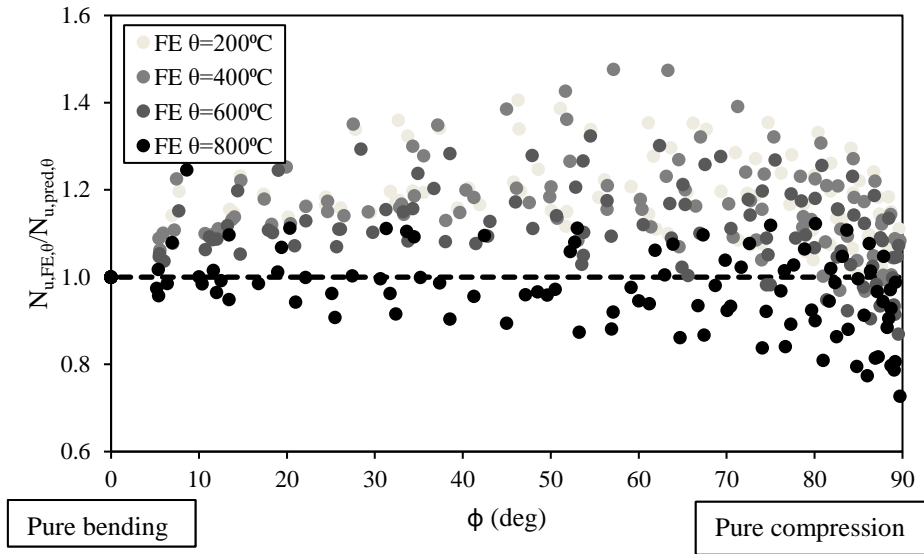


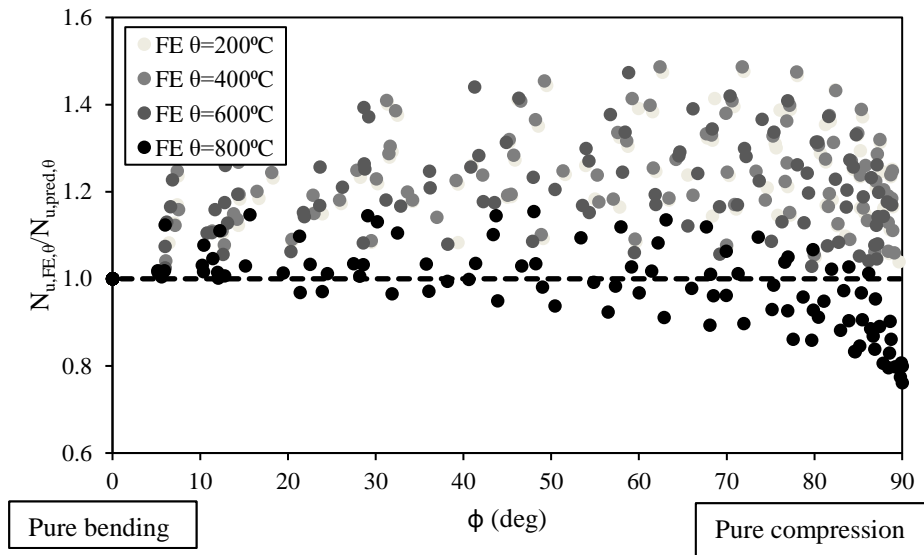
Figure 5.9: Axial load and moment interaction diagram for θ



(a) Austenitic stainless steel

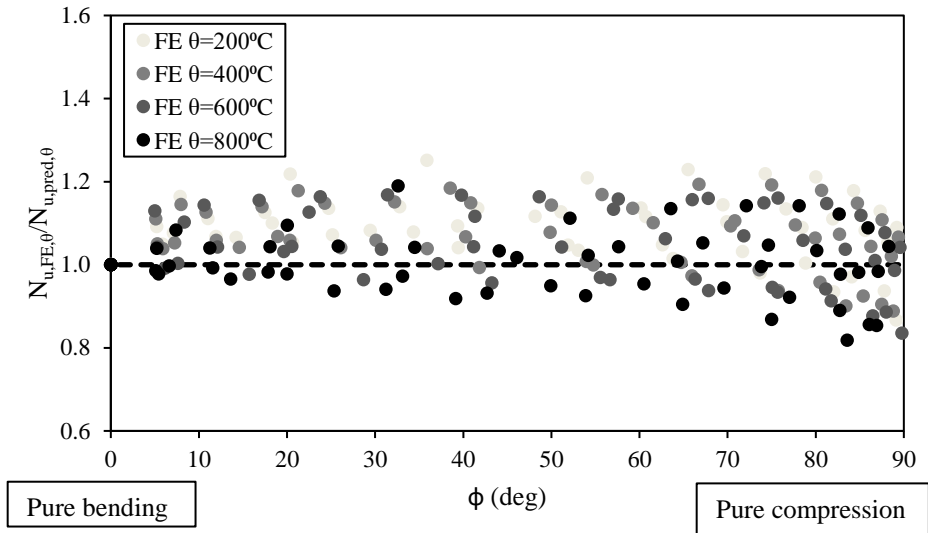


(b) Duplex stainless steel

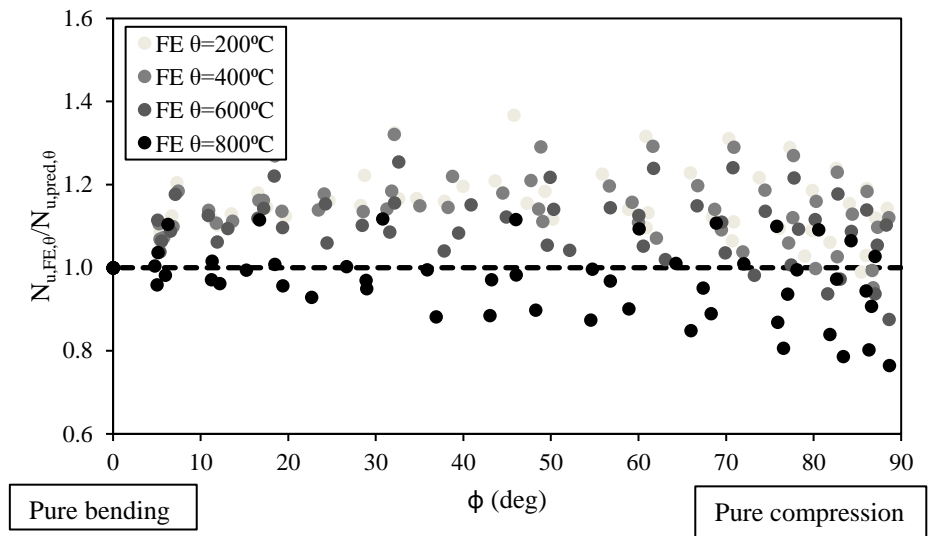


(c) Ferritic stainless steel

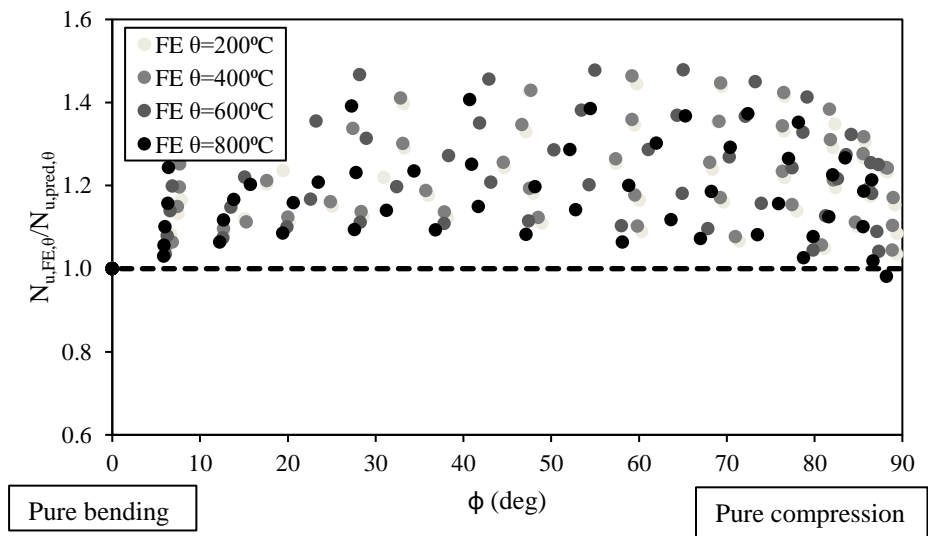
Figure 5.10: Comparison of RHS FE results ($N_{u,FE,\theta}$) with EN 1993-1-2 (2005) predicted strength ($N_{u,pred,\theta}$) for (a) Austenitic, (b) Duplex and (c) Ferritic.



(a) Austenitic stainless steel

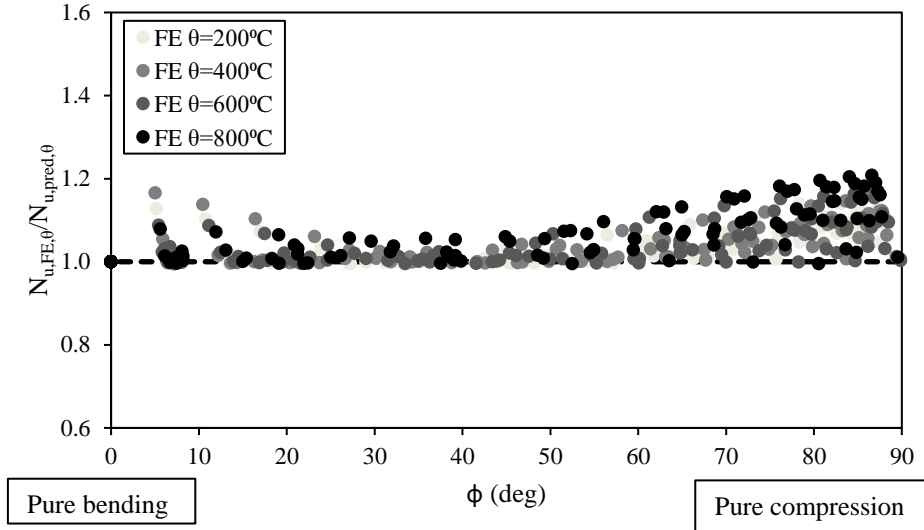


(b) Duplex stainless steel

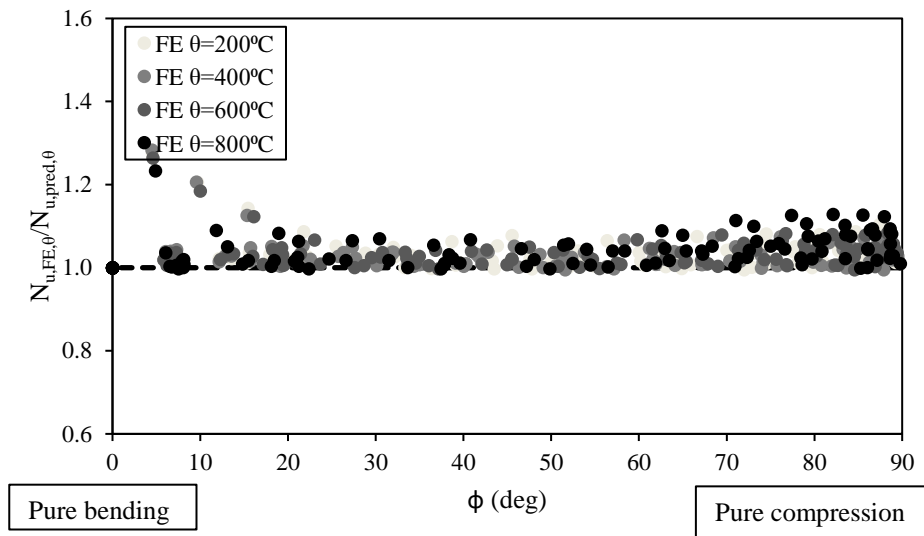


(c) Ferritic stainless steel

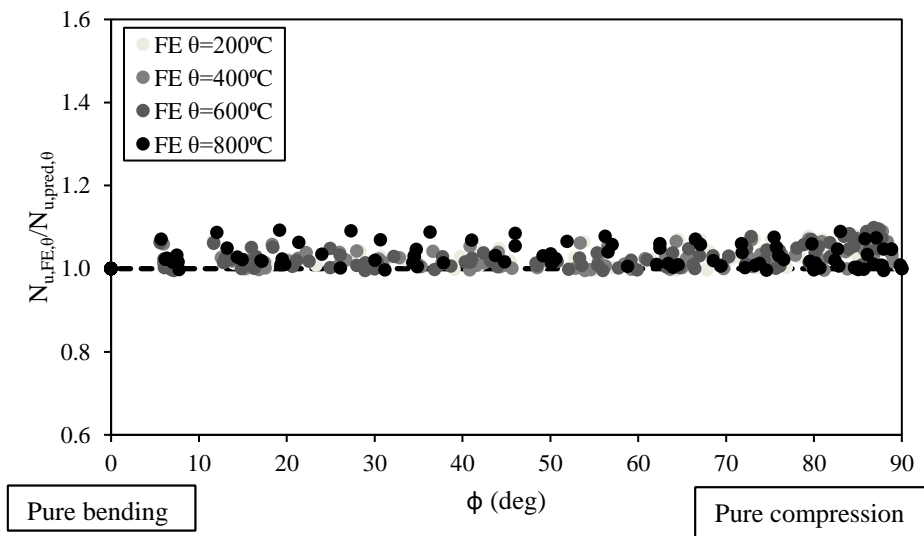
Figure 5.11: Comparison of CHS FE results ($N_{u,FE,\theta}$) with EN 1993-1-2 (2005) predicted strength ($N_{u,pred,\theta}$) for (a) Austenitic, (b) Duplex and (c) Ferritic.



(a) Austenitic stainless steel

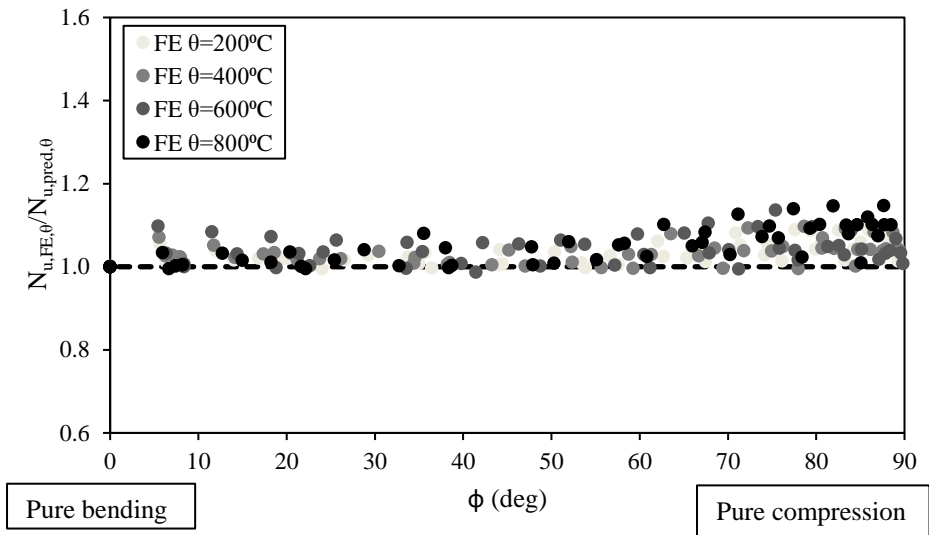


(b) Duplex stainless steel

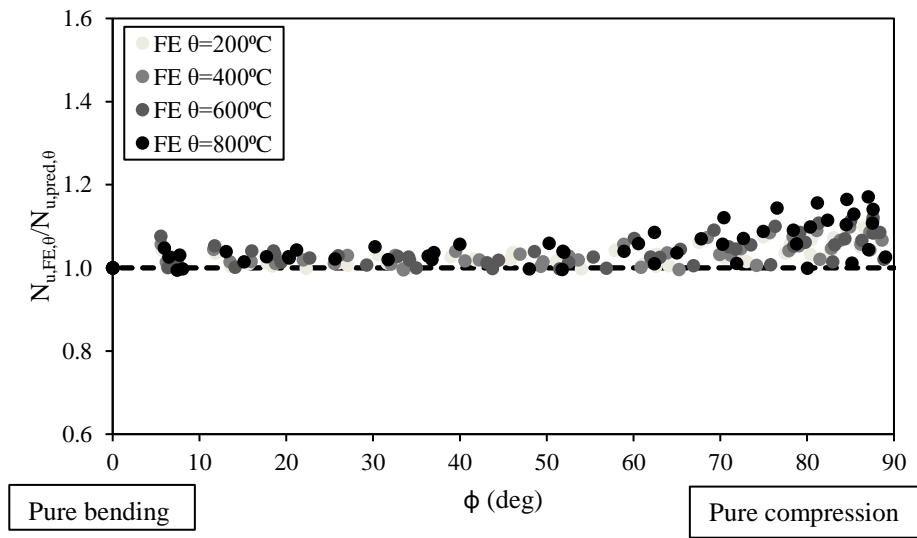


(c) Ferritic stainless steel

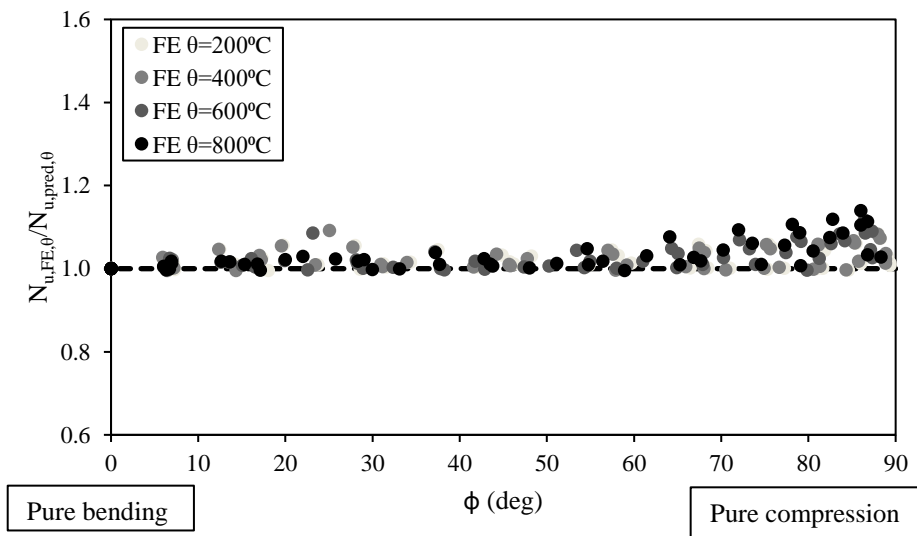
Figure 5.12: Comparison of RHS FE results ($N_{u,FE,\theta}$) with proposed predicted strength ($N_{u,pred,\theta}$) for (a) Austenitic, (b) Duplex and (c) Ferritic.



(a) Austenitic stainless steel



(b) Duplex stainless steel



(c) Ferritic stainless steel

Figure 5.13: Comparison of CHS FE results ($N_{u,FE,\theta}$) with proposed predicted strength ($N_{u,pred,\theta}$) for (a) Austenitic, (b) Duplex and (c) Ferritic.

Table 5.4: Comparison of stainless steel RHS and CHS beam-column FE results with predicted resistances.

				EN 1993-1-2	Proposed
Section	Material	Buckling axis		$N_{u,0}/N_{u,pred,0}$	$N_{u,0}/N_{u,pred,0}$
RHS	Austenitic	Major	Mean	1.08	1.05
			COV	0.08	0.06
		Minor	Mean	1.01	1.03
			COV	0.08	0.05
	Duplex	Major	Mean	1.12	1.03
			COV	0.09	0.05
	Minor	Mean	1.04	1.00	
		COV	0.08	0.03	
Ferritic	Major	Mean	1.16	1.02	
		COV	0.10	0.03	
	Minor	Mean	1.11	1.01	
		COV	0.10	0.03	
CHS	Austenitic	-	Mean	1.04	1.03
			COV	0.08	0.04
	Duplex	-	Mean	1.07	1.03
			COV	0.08	0.04
	Ferritic	-	Mean	1.19	1.02
			COV	0.10	0.03

For each stainless steel grade, comparisons are made between the EN 1993-1-2 (2005) and the proposed methods and the FE beam-column resistances. In general, the current EN 1993-1-2 (2005) displays scattered results with inaccurate prediction of the column buckling loads, as the applied loading varies from pure compression to pure bending. The proposed approach yields the improved degree of accuracy and consistency in the prediction of beam-column strength for all loading combinations.

5.4.2 Reliability analysis

In this subsection, the reliability analysis for the beam-column fire design approach is performed on the existing structural fire design method (EN 1993-1-2, 2005) and proposed method. Statistical analyses according to Kruppa (1999), has been utilised to assess the resistance of the beam-column members at elevated temperatures, which

includes the three distinctive criteria. Further information is provided in Chapter 4 sub-section 4.5.

Table 5.5 provides a summary of the safety assessment results for the predicted resistances for the existing design EN 1993-1-2 (2005) codified method and proposed method for stainless steel beam-columns. It is shown that proposed method satisfies the reliability criteria set out by Kruppa (1999), whereas EN 1993-1-2 (2005) fails to satisfy the criteria, except for CHS Ferritic.

Table 5.5: Summary of reliability assessment results.

Section	Material	Criterion	EN 1993-1-2 (2005)		Proposed method	
RHS	Austenitic	Criterion 1	4.55%	Fail	0.00%	Pass
		Criterion 2	33.41%	Fail	19.55%	Pass
		Criterion 3	-4.08%	Pass	-4.05%	Pass
	Duplex	Criterion 1	3.18%	Fail	0.00%	Pass
		Criterion 2	28.18%	Fail	13.18%	Pass
		Criterion 3	-7.76%	Pass	-3.05%	Pass
	Ferritic	Criterion 1	3.64%	Fail	0.00%	Pass
		Criterion 2	20.68%	Fail	16.14%	Pass
		Criterion 3	-11.44%	Pass	-2.47%	Pass
CHS	Austenitic	Criterion 1	2.73%	Fail	0.00%	Pass
		Criterion 2	35.45%	Fail	15.91%	Pass
		Criterion 3	-3.81%	Pass	-3.53%	Pass
	Duplex	Criterion 1	3.18%	Fail	0.00%	Pass
		Criterion 2	28.18%	Fail	16.36%	Pass
		Criterion 3	-6.79%	Pass	-3.48%	Pass
	Ferritic	Criterion 1	0.00%	Pass	0.00%	Pass
		Criterion 2	9.55%	Pass	20.00%	Pass
		Criterion 3	-15.47%	Pass	-2.42%	Pass

5.5 Concluding remarks

The current design interaction curves for stainless steel beam-column elements in fire conditions under in-plane bending and axial compression were developed on inaccurate end points (i.e. under-predicted column buckling strength in compression). This led to the

derivation of interaction factors that accounts for inaccurate end points. In order to overcome these inadequacies, new beam-column interaction factors have been developed in this chapter, based on using more accurate end points (i.e. the revised buckling curve from Chapter 4). The accuracy of the proposed beam-column design interaction curve were assessed against 1980 FE data. The comparison revealed that the proposed method provided more accurate predictions for stainless steel beam-column members in fire than the current EN 1993-1-2 (2005). Moreover, statistical analysis according a method provided by Kruppa (1999) was performed on the proposed method beam-column design method and was shown to satisfy the specified levels of requirement.

Chapter 6 Conclusion and suggestion for further work

The aim and objective of this thesis is to advance the fundamental knowledge of the stability and design of stainless steel element in fire conditions, with a particular emphasis on providing safe, reliable and efficient design. This was performed through comprehensive numerical modelling programme and analytical assessments. Specific conclusions pertinent to each section of the work have been given within the frame of this thesis. The subsequent sections provide a brief overview of the research performed and outlines the main conclusions that have been concluded. In light of these suggestions and points, recommendations for further research are made thereafter.

6.1 Conclusion

This research study investigated the stability and design of stainless steel elements in fire conditions. The focus was placed upon cold-formed stainless steel square, rectangular and circular hollow sections in fire. Chapter 3 focused on the numerical modelling of compression members and beam-column members at cross-sectional and member level in fire conditions. Chapter 4 studied the flexural compressive behaviour and fire design at member level. In Chapter 5, the behaviour and fire design under combined in-plane bending and compression was examined.

6.1.1 Numerical modelling and validation of elements

In order to achieve the accuracy of the numerical results, the developed numerical models were validated against test data. Chapter 3 examined existing test results extracted from literature and presented the results of numerical models, using ABAQUS (2016) on

stainless steel hollow section columns and beam-columns in fire conditions. The following conclusion were made:

- Twenty-three column flexural buckling tests and thirty-seven stub and member beam-column tests have been replicated numerically and were compared with their corresponding experimental test results. The aim of this investigation was to develop finite element models which included element type, mesh material modelling, strength enhancement in the corner regions for SHS and RHS, initial geometric imperfection (global and local) and amplitudes, residual stresses, boundary conditions, heat transfer analysis and analysis technique.
- The global and local initial geometric imperfection were initiated in the form of the elastic buckling mode shapes equivalent to the relevant failure modes.
- The numerical models were proven to be able to replicate accurately the nonlinear response of stainless steel members in fire conditions.
- Similar behaviour and failure modes were obtained throughout the numerical modelling programme.
- The validated FE models in Chapter 3 were employed for conducting parametric studies on stainless steel columns and beam-columns at elevated temperature in Chapters 4 and 5, the results of which form the basis for the development of the design guidance in Chapters 4 and 5.

6.1.2 Fire design of stainless steel hollow section columns

The proposed design method for stainless steel hollow section columns was developed in Chapter 4. The flexural buckling response was assessed through a comprehensive numerical simulation programme. The following conclusion were made:

- The developed FE models from Chapter 3, with the additional parametric studies performed in Chapter 4 were compared against with the codified design rules from EN 1993-1-2 (2005) and Design Manual for Structural Stainless Steel (2017), where it was shown that inaccurate flexural buckling resistances in fire are predicted by both methods.
- Based on the comparison, a number of revised buckling curves for stainless steel hollow sections at various temperature in fire were proposed on the basis of FE results, in line with Lopes et al. (2010) method, which were shown to consistently predict the flexural buckling capacities of the columns in fire with higher degree of accuracy as well as with significantly less scatter.
- These revisions led to a more efficient and consistent treatment of buckling of stainless steel tubular column in fire.
- The predicted resistances from the proposed buckling curves were assessed in accordance with the three reliability criteria set out by Kruppa (1999) and were shown to consistently satisfy the specified safety levels required. Improvement to the fire design of stainless steel hollow section column should increase and prevail the use of stainless steel as a construction material.

6.1.3 Fire design of stainless steel hollow section beam-columns

Combined in-plane bending and axial compression at member level and their subsequent fire design was the focus of Chapter 5. The following conclusion were made:

- The developed FE models from Chapter 3 were utilised to perform parametric studies under various parameters to compare against existing European design guidance for structural fire design EN 1993-1-2 (2005).

- The ultimate loads of the specimens were employed to evaluate the accuracy of the current beam-column fire design method (EN 1993-1-2, 2005). It was observed that the existing method provided inaccurate predictions, leading to an inexact beam-column strength prediction.
- These existing inaccuracies coming from inaccurate predictions of the bending and column buckling end points of the design interaction curves and the adopted inaccurate interaction factors (which have been based upon carbon steel design), which in general does not capture the behaviour response of stainless steel member under combined loading at elevated temperature.
- A previous method was made to stainless steel beam-column design at room temperature and was suggested to improve the current European guidance. In the design proposal, the existing bending moment capacity at temperature has been utilised and the revised buckling curves and method provided in Chapter 4 for the compression was used for the end point of the interaction curves. Subsequently, based on these more accurate end points, new beam-column interaction factors were derived, following a comprehensive numerical modelling programme.
- The accuracy of the proposed design approach for stainless steel hollow sections beam-column under combined in-plane bending and compression was assessed through parametric studies. The comparison revealed that the proposals provided more consistent and more accurate beam-column capacity.
- This simplified design proposal was also found to yield significantly less scattered and more accurate strength predictions than the European code as shown in Chapter 5. Finally, a reliability analysis was performed on the proposed design method and was shown that the specified level of safety were satisfactory.

The limitation of the research has been performed on column and beam-columns members under pinned-ended conditions, however there are additional boundary condition such as fixed-fixed, pinned-fixed. In addition, there are also additional stainless steel material which is prevailing such as lean duplex which is a cheaper alternative than duplex. Overall, the aims and objective set out in this thesis, of assessing and improving the current design guidance for stainless steel hollow section elements in fire was met. The corresponding codified fire design rules for each element type of column and beam-column have been discussed and assessed, and their inadequacies have been highlighted. Improved design methods for stainless steel member level under axial compression and under in-plane bending, and axial compression have been proposed and shown to provide a higher level of accuracy and consistency in the strength predictions. The reliability of the hollow section columns and beam-column has been confirmed through statistical analyses to Kruppa (1999). It is therefore recommended that the proposed approaches for stainless steel hollow section column and beam-columns elements be considered into future revisions of stainless steel structural design standards for fire conditions.

6.2 Suggestion for further work

The relatively high material cost of stainless steel supports the attempts for enhancing the efficiency of its usage in the construction industry. The flexural buckling of hollow section columns and beam-column for the three different grades of stainless steel members at elevated temperature have been successfully dealt with, while other aspects of design still need further research.

The essential research could, in the author's opinion, shadow two distinct paths, since improvement to current design provisions of EN 1993-1-2 (2005) can be achieved either by optimising the design equations according to test and FE results within the current

design format, or by deriving novel design approaches in accordance with the actual material response. As demonstrated in Chapter 4, where existing design format was followed, maintaining current design format ensures consistency with carbon steel design, but at the expense of design efficiency, new addition modification leads to more efficient design at the expense of simplicity. Clearly, an acceptable trade-off between simplicity and design efficiency is sought, and design rules of different levels of complexity could be made available to the designer.

The scope of the work presented in Chapter 4 could be expanded to more complex load cases, involving other tubular cross-sections such as elliptical and channel cross-sections. Additionally, the derivation of accurate interaction formulae for members subjected to compression and biaxial bending with the design format of EN 1993-1-2 (2005) is necessary for the development of an integrated design approach for stainless steel. An interesting research area also concerns stainless steel frames subjected to elevated temperatures. A series of experimental and numerical work on stainless steel frames would be required.

The material grades utilised for stainless steel are expected to affect the capacity and deformation of stainless steel structures. The execution of experiments and numerical studies on different types of material grades e.g. lean duplex at elevated temperatures is recommended.

Research into stainless steel in fire conditions is relatively scarce and limited. Further research could be extended on the structural behaviour and design of concrete filled stainless steel columns and beam-column elements at elevated temperatures. The influence of the composite behaviour and fire design of stainless steel non-linearities could be investigated.

Finally, investigation into stainless steel beams at cross-sectional and member level instabilities in fire conditions are required. Comprehensive data from experiments and numerical studies is required to support accurate design rules to be derived, which then can be implemented in future design revision, in order to take advantage of the stainless steel members.

References

ABAQUS. 2016. Version 6.14. Dassault Systmes Simulia Corp. USA.

Afshan, S. Zhao, O., Gardner, L. 2019. Standardised material properties for numerical parametric studies of stainless steel structures and buckling curves for tubular columns. *Journal of Constructional Steel Research*, **152**, 2-11.

Afshan, S., and Gardner, L. 2013. The continuous strength method for structural stainless steel design. *Thin-Walled Structures*, **68**(0), 42-49.

AISI. 1974. Stainless Steel Cold-Formed Structural Design Manual. American Iron and Steel Institute. Washington, D.C.

Ala-Outinen, T. 2007. Stainless steel in fire (SSIF). Work package 3: Members with class 4 cross-sections in fire. Tech. rept. RFS-CR-04048. The Steel Construction Institute, UK.

Ala-Outinen, T. and Oksanen, T. 1997. Stainless steel compression members exposed to fire. VTT research notes 1864. Espoo (Finland).

Allen, H.G., Bulson, P.S. 1980. *Background to buckling*. McGraw-Hill Book Company.

Anderberg, Y. 1988. Modelling steel behaviour. *Fire Safety Journal*, **13**(1), 17-26.

Ashraf, M., Gardner, L. and Nethercot, D. A. 2005. Strength enhancement of the corner regions of stainless steel cross-sections. *Journal of Constructional Steel Research*, **61**(1), 37-52.

Ashraf, M., Gardner, L., and Nethercot, D. A. 2006. Finite element modelling of structural stainless steel cross-sections. *Thin-Walled Structures*, **44**(10), 1048-1062.

B. Uppfeldt, T. Ala Outinen, M. Veljkovic. 2008. A design model for stainless steel box columns in fire. *Journal of Constructional Steel Research*, **64** (4), 1294-1301.

Baddoo, N. R. 2013. 100 years of stainless steel: A review of structural applications and the development of design rules. *The Structural Engineer*, **91**, 10-18.

- Baddoo, N.R., Gardner L. 2000. Member behaviour at elevated temperatures. ECSC project - Development of the use of stainless steel in construction, Contract No. 7210 SA/842. The Steel Construction Institute, UK, WP5.2.
- Beer, H., Sculz, G. 1970. Bases théoriques des courbes européennes de flambement. *Construction métallique*, **3**, 37-57.
- Bleich, F. 1952. *Buckling strength of metal structures* (McGraw-Hill Book Company, ed.). New York.
- Boissonnade, N., Greiner, R., Jaspart, J. P. and Lindner, J. 2006. Rules for Member Stability in EN 1993-1-1: Background documentation and design guidelines. ECCS European Convention for Constructional Steelwork.
- Boissonnade, N., Jaspart, J. P., Muzeau, J. P. and Villette, M. 2002. Improvement of the interaction formulae for beam columns in Eurocode 3. *Computers & structures*, **80** (27), 2375-2385.
- Boissonnade, N., Jaspart, J. P., Muzeau, J. P. and Villette, M. 2004. New interaction formulae for beam-columns in Eurocode 3: The French–Belgian approach. *Journal of Constructional Steel Research*, **60**, 421-431.
- Bryan, G.H. 1890. On the stability of a plane plate under thrusts in its own plane, with applications to the buckling of the sides of a ship. *Proceedings of the London Mathematical Society*. **S1-22**(1), 54–67.
- Buchanan, A.H. 2001. Structural design for fire safety.
- Buchanan, C. 2017. *Testing and design of conventional and novel stainless steel hollow structural sections*. Ph.D. thesis. Imperial College London, UK.
- Buchanan, C., Real, E., Gardner, L. 2018. Testing, simulation and design of cold-formed stainless steel CHS columns. *Thin-Walled Structures*, **130**, 297-312.
- Case, J., Lord, C., Ross, C.T.F. 1992. Strength and materials and Structures. 3, edition.
- Chen, J., and Young, B. 2006. Stress-strain curves for stainless steel at elevated temperatures. *Engineering Structures*, **28**(2), 229-239.

- Chen, W. F., Atsuta, T. 1976. *Theory of beam-columns, Vol. 1 In-plane behaviour and design*. McGraw-Hill, New York.
- Chen, W. F., Atsuta, T. 1977. *Theory of beam-columns, Vol. 2 In-plane behaviour and design*. McGraw-Hill, New York.
- Cheong Siat Moy, F. 1974a. A method of analysis of laterally loaded columns. *Journal of the Structural Division, ACSE*, **100:ST5**, 953–970.
- Cheong Siat Moy, F. 1974b. General analysis of laterally loaded beam columns. *Journal of the Structural Division, ASCE*, **100:ST6**, 1263–1278.
- China Association for Engineering Construction Standardisation. 2015. CECS 410:2015. Technical specification for stainless steel structures.
- Cruise, R. B. 2007. *The influence of production routes on the behaviour of stainless steel structural members*. Ph.D. thesis. Imperial College London, UK.
- Cruise, R. B., and Gardner, L. 2008a. Residual stress analysis of structural stainless steel sections. *Journal of Constructional Steel Research*, **64**(3), 352 - 366.
- Cruise, R. B., and Gardner, L. 2008b. Strength enhancements induced during cold forming of stainless steel sections. *Journal of Constructional Steel Research*, **64**(11), 1310-1316.
- Dawson, R.G. and Walker, A.C. 1972. Post-Buckling of Geometrically Imperfect Plates. *Journal of the Structural Division*, **98**(1), 75–94.
- Deng, D. and Murakawa, H. 2006. Numerical simulation of temperature field and residual stress in multi-pass welds in stainless steel pipe and comparison with experimental measurements. *Computational Materials Science*, **37**(3), 269–277.
- EN 1090-2. 2008. *Execution of steel structures and aluminium structures - Part 2: Technical requirements for steel structures*. Brussels: European Committee for Standardization.
- EN 1363-1. 2012. *Fire resistance tests - Part 1: General requirements*. Brussels: European Committee for Standardization.

EN 1990. 2002. *Eurocode - Basis of structural design*. Brussels: European Committee for Standardization.

EN 1991-1-2. 2002. *Eurocode 1: Actions on structures - Part 1-2: General actions - Actions on structures exposed to fire*. Brussels: European Committee for Standardization.

EN 1993-1-1. 2005. *Eurocode 3: Design of steel structures - Part 1-1: General rules and rules for buildings*. Brussels: European Committee for Standardization.

EN 1993-1-2. 2005. *Eurocode 3: Design of steel structures - Part 1-2: General rules – Structural fire design*. Brussels: European Committee for Standardization.

EN 1993-1-4. 2006. *Eurocode 3: Design of steel structures - Part 1-4: General rules – Supplementary rules for stainless steels*. Brussels: European Committee for Standardization.

EN 1993-1-5. 2006. *Eurocode 3 - Design of steel structures - Part 1-5: Plated structural elements*. Brussels: European Committee for Standardization.

EN 1999-1-1. 2007. *Eurocode 9: Design of aluminium structures - Part 1-1: General structural rules*. Brussels: European Committee for Standardization.

EN ISO 6892-1. 2009. *Metallic materials - Tensile testing - Part 1: Method of test at room temperature*. Brussels: European Committee for Standardisation.

Euro Inox 1993. *Design manual for structural stainless steel* 1st edition.

Fan, S., Ding, X., Sun, W., Zhang, L. Liu, M. 2016. Experimental investigation on fire resistance of stainless steel columns with square hollow section. *Thin-Walled Structures*, **98**, 196-211.

Foster, A. 2014. *Stability and design of steel beams in the strain-hardening range*. Ph.D. thesis. Imperial College London. UK.

Galambos, T. V. 1998. *Guide to stability design criteria for metal structures*. John Wiley & Sons.

Gardner, L. 2002. *A new approach to structural stainless steel design*. Ph.D. thesis, Imperial College London, UK.

- Gardner, L. 2005. The use of stainless steel in structures. *Progress in Structural Engineering and Materials*, **7**(2), 45-55.
- Gardner, L. 2007. Stainless steel structures in fire. *Proceedings of the ICE - Structures and Buildings*, **160**(3), 129-138.
- Gardner, L. 2008. Aesthetics, economics and design of stainless steel structures. *Advanced Steel Construction*, **4**(2), 113–122.
- Gardner, L. 2008. The continuous strength method. *Proceedings of the ICE - Structures and Buildings*, **161**(3), 127-133.
- Gardner, L. 2019. Stability and design of stainless steel structures- Review and outlook. *Thin-walled Structures*, **141**, 208-216.
- Gardner, L. and Ashraf, M. 2006. Structural design for non-linear metallic materials. *Engineering Structures*, **28**(6), 926–934.
- Gardner, L. and Baddoo, N.R. 2006. Fire testing and design of stainless steel structures. *Journal of Constructional Steel Research*, **62**(6), 532–543.
- Gardner, L. and Cruise, R. B. 2009. Modelling of Residual Stresses in Structural Stainless Steel Sections. *Journal of Structural Engineering (ASCE)*, **135**(1), 42–53.
- Gardner, L. and Ng, K.T. 2006. Temperature development in structural stainless steel sections exposed to fire. *Fire Safety Journal*, **41**(3), 185-203.
- Gardner, L. and Theofanous, M. 2008. Discrete and continuous treatment of local buckling in stainless steel elements. *Journal of Constructional Steel Research*, **64**(11), 1207–1216.
- Gardner, L., and Baddoo, N. R. 2006. Fire testing and design of stainless steel structures. *Journal of Constructional Steel Research*, **62**(6), 532-543.
- Gardner, L., and Nethercot, D. A. 2004a. Experiments on stainless steel hollow sections -Part 1: Material and cross-sectional behaviour. *Journal of Constructional Steel Research*, **60**(9), 1291-1318.

- Gardner, L., and Nethercot, D. A. 2004b. Experiments on stainless steel hollow sections – Part 2: Member behaviour of columns and beams. *Journal of Constructional Steel Research*, **60**(9), 1319-1332.
- Gardner, L., and Nethercot, D.A. 2004c. Numerical modeling of stainless steel structural components-a consistent approach. *Journal of structural Engineering*, **130**(10), 1586-1601.
- Gardner, L., and Ng, K. T. 2006. Temperature development in structural stainless steel sections exposed to fire. *Fire Safety Journal*, **41**(3), 185-203.
- Gardner, L., Insausti, A., Ng, K. T., and Ashraf, M. 2010. Elevated temperature material properties of stainless steel alloys. *Journal of Constructional Steel Research*, **66**(5), 634-647.
- Greiner, R. and Lindner, J. (2006). Interaction formulae for members subjected to bending and axial compression in EUROCODE 3 – the Method 2 approach. *Journal of Constructional Steel Research*, **62**(8), 757–770.
- Hill, H. 1944. Determination of stress-strain relations from offset yield strength values. Tech. rept. 927. National Advisory Committee for Aeronautics. Washington, D.C.
- Hoke, J. H. 1977. Handbook of Stainless Steels. McGraw-Hill.
- Huang, Y. and Young, B. 2018. Structural performance of cold-formed lean duplex stainless steel beams at elevated temperatures. *Thin-Walled Structures*, **129**, 20-27.
- Huang, Y., and Young, B. 2014. Stress-strain relationship of cold-formed lean duplex stainless steel at elevated temperatures. *Journal of Constructional Steel Research*, **92**, 103-113.
- J. Chen, B. Young. 2006. Stress-strain curves for stainless steel at elevated temperatures. *Engineering Structures*, **28**(2), 229-239.
- J. Kruppa. 1999. Eurocodes Fire parts: Proposal for a methodology to check the accuracy of assessment methods. CEN TC 250, Horizontal Group Fire, Document no: 99/130.
- Jacquet, J. 1970. Essais de flambement et exploitation statistique. *Construction métallique*. **3**,13–36.

- Knobloch, M. and Fontana, M. 2006. Strain-based approach to local buckling of steel sections subjected to fire. *Journal of Constructional Steel Research*, **62**(1-2), 44–67.
- Knobloch, M., Pauli, M., and Fontana, M. 2013. Influence of the strain-rate on the mechanical properties of mild carbon steel at elevated temperatures. *Materials and Design*, **49**(0), 553-565.
- Kruppa, J., Newman, G., Schleich, J-B. and Twilt, L. 1999. *ECCS model code on fire engineering*.
- Lennon, T. and Moore, D. 2003. The natural fire safety concept-Full scale tests at Cardington. *Fire Safety Journal* **28**(7), 623-643.
- Lennon, T., Moore, D., Wang, Y.C., and Bailey, C.G. 2007. Designer guide to EN 1991-1-2, EN 1992-1-2, EN 1993-1-2 and EN 1994-1-2.
- Lopes, N., Vila Real, P., Silva, L. S., and Franssen, J. M. 2010. Axially loaded stainless steel columns in case of fire. *Journal of Structural Fire Engineering*, **1**(1), 43-59.
- Mazzolani, F.M. 1995. *Aluminium alloy structures* 2nd edition.
- Mirambell, E., and Real, E. 2000. On the calculation of deflections in structural stainless steel beams: an experimental and numerical investigation. *Journal of Constructional Steel Research*, **54**(1), 109-133.
- N. Lopes, P. Vila Real, L. da Silva, J.M. Franssen. 2010. Axially Loaded Stainless Steel Columns in Case of Fire. *Journal of Structural Fire Engineering*, **1**(1), 43-60.
- Navier, L.M.H. 1826. *Résumé des Leçons données à l'école des ponts et chaussées sur l'application de la Mécanique à l'établissement des constructions et des machines*.
- Nethercot, D.A. 2001. *Limit States Design of Structural Steelwork*. Third edition.
- Ng, K. T., and Gardner, L. 2007. Buckling of stainless steel columns and beams in fire. *Engineering Structures*, **29**(5), 717-730.
- Pauli, J., Somaini, D., Knobloch, M. and Fontana, M. (2012) Experiments on steel columns under fire conditions.

- Pi, Y.L. and Trahair, N.S. 1995. Lateral buckling strengths of cold-formed rectangular hollow sections. *Thin-Walled Structures*, **22**(2), pp.71–95
- Pournaghshband, A., Afshan, S. Foster, A. (2019). Structural fire performance of axially and rotationally restrained stainless steel columns. *Thin-Walled Structures*, **137**. 561-572.
- Ramberg, W. and Osgood, W.R. 1943. Description of stress-strain curves by three parameters. Technical Notes 902. *National Advisory Committee for Aeronautics, Technical Notes 902.*, p.29
- Rasmussen, K. J. R. 2000. The Development of an Australian Standard for Stainless Steel Structures. Proceedings of the Fifteenth International Speciality Conference on Cold-formed Steel Structures. St. Louis, Missouri, USA. 659-671.
- Rasmussen, K. J. R. 2003. Full-range stress-strain curves for stainless steel alloys. *Journal of Constructional Steel Research*, **59**(1), 47-61.
- Rasmussen, KJR and Hancock, G. 1993. Design of cold-formed stainless steel tubular members. II: Beams. *Journal of structural Engineering*, **119**(8), 2368–2386.
- Rhodes, J. 1991. Design of cold formed steel members. *Elsevier Applied Science, London*.
- Rossi, B., Afshan, S. and Gardner, L. 2012. Predictive models for strength enhancements in cold-formed structural sections *In: Tubular Structures XIV - Proceedings of the 14th International Symposium on Tubular Structures, ISTS 201*, 391–398.
- Schafer, B. W. 2008. Review: The direct strength method of cold-formed steel member design. *Journal of Constructional Steel Research*, **64**(78), 766-778.
- Sfintesco, D. 1970. Fondement expérimental des courbes européennes de flambement. *Construction métallique*. **3**, 5–12.
- Shanley, F.R. 1947. Inelastic Column Theory. *Journal of the Aeronautical Sciences*. **14**(5), 261–268.
- Stainless Steel Design Manual 2017. *Steel Construction Institute (SCI) Fourth Edition*.
- Theofanous, M., Chan, T.M. and Gardner, L. 2009. Structural response of stainless steel oval hollow section compression members. *Engineering Structures*, **31**(4), 922–934.

- Theofanous, M., Gardner L. 2009. Testing and numerical modelling of lean duplex stainless steel hollow section columns. *Engineering Structures*, **31**(12), 3047-3058.
- Timoshenko, S.P. 1930. Strength of materials. *D. Van Nostrand Company*.
- Timoshenko, S.P. and Gere, J.M. 1989. *Theory of elastic stability*.
- Tondini, N., Rossi, B. and Franssen, J.M. 2013. Experimental investigation on ferritic stainless steel columns in fire. *Fire Safety Journal*, **62** (2013), 238-248.
- Trahair, N.S., Bradford, M.A., Nethercot, D.A. and Gardner, L. 2008. The behaviour and design of steel structures to EC3.
- Twilit, L. 1988. Strength and deformations properties of steel at elevated temperatures: some practical implications. *Fire Safety Journal*, **13**(1), 9-15.
- Uppfeldt, B., Ala Outinen, T., and Veljkovic, M. 2008. A design model for stainless steel box columns in fire. *Journal of Constructional Steel Research*, **64**(11), 1294-1301.
- Van Musschenbroek, P. 1729. *Introductio ad cohaerentiam corporum firmorum. Lugduni*.
- von Kármán, T. 1908. Untersuchungen über Knickfestigkeit. *Mitteilungen über Forschungsarbeiten auf dem Gebiete des Ingenieurwesens*. **81**.
- von Kármán, T. 1910. Die Knickfestigkeit gerader Stäbe. *Physikalische Zeitschrift*. **9**, 136.
- Von Karman, T.; Sechler, E.E.; Donnel, L.H. 1932. *Strength of thin plates in compression* Trans ASME.
- Wang, S. T. and Errara, S. J. 1971. Behaviour of cold rolled stainless steel members. Proceedings of the First Speciality Conference on Cold-formed Steel Structures. University of Missouri-Rolla, Rolla, Mo.
- Wang, Y. 2005. Steel and composite structures: Behaviour and design for fire safety.
- Wang, Y.C. 1998. Composite beam with partial fire protection. *Fire safety Journal*, **30**(4), 315-332.
- Winter G., Lansing W., M.R.B. 1950. Four papers on the performance of thin walled steel structures. Cornell University, Ithaca, New York.

Winter, G. 1947. Strength of thin walled flanges.

Young B. and Lui WM. 2005. Behaviour of cold-formed high strength stainless steel sections. *Journal of Structural Engineering, ASCE*; **131**(11):1738–45.

Zhao, B. (2000). Material behaviour at elevated temperatures: Work package 5.1. ECSC.

Zhao, O., Gardner, L. and Young, B. 2016a. Testing and numerical modelling of austenitic stainless steel CHS beam-columns', *Engineering Structures*, **111**, 263-274.

Zhao, O., Gardner, L. and Young, B. 2016b. Buckling of ferritic stainless steel members under combined axial compression and bending. *Journal of Constructional Steel Research*, **117**, 35-48.

Zhao, O., Gardner, L. and Young, B. 2016c. Structural performance of stainless steel circular hollow sections under combined axial load and bending – Part 1: Experiments and numerical modelling. *Thin-Walled Structures*, **101**, 231–239.

Zhao, O., Gardner, L. and Young, B. 2016d. Structural performance of stainless steel circular hollow sections under combined axial load and bending – Part 2: Parametric studies and design. *Thin-Walled Structures*, **101**, 240–248.

Zhao, O., Gardner, L. and Young, B. 2016e. Behaviour and design of stainless steel SHS and RHS beam-columns. *Journal of Constructional Steel Research*, **106**, 330-345.

Zhao, O., Rossi, B., Gardner, L. and Young, B. 2015a, 'Behaviour of structural stainless steel cross-sections under combined loading - Part I: Experimental study', *Engineering Structures*, **89**, 236-246.

Zhao, O., Rossi, B., Gardner, L. and Young, B. 2015b. Behaviour of structural stainless steel cross-sections under combined loading – Part II: Numerical modelling and design. *Engineering Structures*, **89**, 247–259.

Zhao, O., Rossi, B., Gardner, L. and Young, B. 2016. Experimental and numerical studies of ferritic stainless steel tubular cross-sections under combined compression and bending. *Journal of Structural Engineering, (ASCE)*, **142**(2), 04015110.

Zhao, X-L, Hancock, GJ. And Trahair, N.S. 1995. Lateral buckling tests of cold-formed RHS beams. *Journal of Structural Engineering*, **121**(11), 1565-1573.

